

Ragnar Stefánsson, Françoise Bergerat, Maurizio Bonafede, Reynir Böðvarsson, Stuart Crampin, Páll Einarsson, Kurt L. Feigl, Christian Goltz, Ágúst Guðmundsson, Frank Roth, Ragnar Sigbjörnsson, Freysteinn Sigmundsson, Peter Suhadolc, Max Wyss, Jacques Angelier, Þóra Árnadóttir, Maria Elina Belardinelli, Grímur Björnsson, Amy Clifton, Loïc Dubois, Gunnar B. Guðmundsson, Páll Halldórsson, Sigurlaug Hjaltadóttir, Ásta Rut Hjartadóttir, Gísli Jónsson, Maryam Khodayar, Björn Lund, Benedikt Ófeigsson, Símon Ólafsson, Sandra Richwalski, Ragnar Slunga, Páll Theodórsson, Kristín S. Vogfjörð, Bergþóra S. Þorbjarnadóttir, Barði Þorkelsson

## **PREPARED – third periodic report**

February 1, 2005 – July 31, 2005

<b>WP 1 Overall coordination of the project .....</b>	<b>5</b>
<b>WP 2 Analysis of multiparameter geophysical data approaching the June 2000 earthquakes, assessing state of stress .....</b>	<b>6</b>
WP 2.1 Pattern search in multiparameter seismic data .....	7
WP 2.2 Possible precursory seismic quiescence and b-value changes .....	8
WP 2.3 Long-term deformation in the South Iceland seismic zone (SISZ) inferred by joint interpretation of GPS, InSAR and borehole strain data .....	11
WP 2.4 Space and time variations in crustal stress using microearthquake source information from the South Iceland seismic zone .....	20
WP 2.5 Using shear-wave splitting above small earthquakes to monitor stress in SISZ .....	25
<b>WP 3 Short-term changes/precursors.....</b>	<b>31</b>
WP 3.1 Foreshocks and development of warning algorithms .....	32
WP 3.2 Radon anomalies .....	47
<b>WP 4 A model of the release of the two June 2000 earthquakes based on all available observations .....</b>	<b>50</b>
WP 4.1 Source mechanism and fault dimensions of the June 17 and June 21 earthquakes determined from mapping of aftershocks .....	52
WP 4.2 Fault slip distribution of two June 2000 Mw 6.5 earthquake in South Iceland estimated by strong motion inversion .....	56
WP 4.3 Surface fractures in the source region of the June 2000 events .....	67
WP 4.4 Deformation model for the June 2000 earthquakes from joint interpretation of GPS, InSAR and borehole strain data .....	71
<b>WP 5 New hazard assessment/New methods for improving assessment of probable earthquake effects .....</b>	<b>78</b>
WP 5.1 Mapping subsurface faults in southwestern Iceland with the microearthquakes induced by the June 17th and June 21st earthquakes.....	80
WP 5.2 Mapping and interpretation of earthquake rupture in the Reykjanes peninsula and other surface effects there and in the SISZ.....	85
WP 5.3 Study of the strong ground motion, acceleration and intensities of the two large earthquakes.....	86
WP 5.4 Reevaluation of the historical earthquakes in light of the new observations .....	88
WP 5.5 Hydrogeological changes associated with the June 2000 earthquakes .....	89

WP 5.6 Paleo-stress fields and mechanics of faulting .....	92
<b>WP 6 Modelling and parameterizing the SW Iceland earthquake release and deformation process .....</b>	<b>97</b>
WP 6.1 Earthquake probability changes due to stress transfer .....	98
WP 6.2 Model stress in the solid matrix and pressure in fluids permeating the crust.....	113
<b>Appendix 1 .....</b>	<b>117</b>
<b>Appendix 2 .....</b>	<b>124</b>
<b>Appendix 3 .....</b>	<b>127</b>

## **WP 1 Overall coordination of the project**

### **Objectives**

Scientific coordination and management of the PREPARED-project.

### **Methodology and scientific achievements related to workpackages including contribution from partners**

This last 6 months period of the project was an extension period. Delays in preparation of some basic data and some workpackages made it necessary to apply for a 6 months extension, which was accepted.

This last period has been a period of fusion work in this multidisciplinary project and also a period for enhancing the Early Information and Warning System of Iceland (EWIS) where most of the results obtained will be introduced.

A special session was organized at the EGU General Assembly in Vienna, April 24-29, 2005, about the project. The latest results of the PREPARED project were presented within the Natural Hazards program of the assembly.

After the EGU meeting a special PREPARED meeting was held in Vienna for discussing and fusing results of individual partners of the project.

Another result fusion meeting was held on July 12 for some of the participants that could attend that day and another such meeting was held on July 21. Both of these meetings were held in Iceland, attended by a significant part of the project partners, Icelandic and not Icelandic.

The coordinator attended a meeting on Seismic Early Warning in Zürich, Switzerland, June 15-16, 2005, and on European Tsunami Warnings in Bologna on October 3. He and co-workers at IMO have participated in discussion about such projects during last summer and autumn.

### **Socio-economic relevance and policy implications**

There have been discussions since last spring between the coordinator and scientists and governmental responsible in India about cooperation in building an earthquake prediction research and a warning system in India in cooperation with Iceland.

### **Discussion and conclusions**

The project as a whole has progressed well towards a final outcome in accordance with the objectives that were set at the beginning of it.

### **Plan and objectives for the future**

The project is finished. But for the coordinator, IMO, which also is an end user of the project results, enormous work remains in further consolidation of the significant outcome of the project as well as in statistically testing the alerts and other warning procedures which this project has delivered.

## **WP 2 Analysis of multiparameter geophysical data approaching the June 2000 earthquakes, assessing state of stress**

### **Objectives**

Analyze and link together multiparameter geophysical observations expressing stress or strain induced variations with time approaching the June 2000 earthquakes and after these. Explain the possibly common source for these variations. Explain them physically. Formulate procedures to assess increase or decrease in probability of earthquake hazard on basis of observable multiparameter observations.

### **Methodology and scientific achievements related to workpackages including contribution from partners**

The input were observations and results of evaluations in WP2.1-2.5, and evolving models and evolving crustal parameters in various other workpackages.

An intensive work has been carried out in this workpackage in the last period, fusing together the various results.

The partners met at the Vienna meeting both for presenting results as well as for fusing them together at the Iceland meeting on July 12.

The work results are detailed in the reports cited below and in the Final Report.

### **Socio-economic relevance and policy implications**

Among the results emerging through the fusion work of the last 6 months are significant new clues to the problem of forecasting the place, size and even the time of large earthquakes. This is reported in the Final Report, in the reference below and in individual WP's and references cited there.

The prospects of possibly being able to forecast earthquakes has socio-economic relevance all over the world. We have already felt it by interest in studying our methods, especially from developing countries.

### **Discussion, conclusions and plans for the future**

It has been found that high pore fluid pressures near the bottom of the seismogenic crust are a central element for building up conditions for the release of earthquakes. This is the result of theoretical modelling, and long- and short-term patterns of geophysical observations support this. The possibility for median-term and short-term predictions rely on observing these changes in real time.

It remains to test statistically the significance of the patterns demonstrated here, introduce them into the Icelandic warning system, EWIS, and study how these findings apply in other conditions than Iceland.

### **Deliverable**

Stefánsson, R. & G.B. Guðmundsson 2005a. Long-term and short-term earthquake warnings based on seismic information in the SISZ. *Icelandic Meteorological Office – Report*. In press.

## **WP 2.1 Pattern search in multiparameter seismic data**

The work in this workpackage was finished before the extension of the project. See PREPARED First and Second Periodic Reports.

## WP 2.2 Possible precursory seismic quiescence and b-value changes

**Author: Max Wyss**

### Objectives

- (1) We set out to determine whether or not the nucleation points of the two magnitude 6.6 earthquakes of June 2000 in southern Iceland can be mapped by minima in the local recurrence time,  $TL$ .
- (2) We evaluated the seismicity rate as a function of time to determine whether or not possible precursory seismic quiescence preceded the Icelandic main shocks of 2000.

### Method and scientific achievements

The ratio of the occurrence of small to large earthquakes in a seismogenic volume is measured by the  $b$ -value of the frequency-magnitude distribution (FMD)

$$\log N = a - bM \quad (1)$$

( $N$  is the cumulative number,  $a$  and  $b$  are constants, and  $M$  is the magnitude. This power law is closely approximated by the observations in the vast majority of volumes other authors and we have investigated, regardless of size. If enough events are available (usually, we use 100 events for  $b$ -estimates), even the data from the smallest volumes resolvable (approximately 1 km dimensions) obey equation (1).

Using the above parameters, we can derive the local recurrence time,  $TL$ , can be estimated by applying the standard probabilistic approach to each node of the grid used to map the  $b$ -values.

$$TL(M) = dT(10^{(a-bM)}) \quad (2)$$

where  $a$  and  $b$  are the local parameters,  $dT$  is the time during which the observations were gathered, and  $M$  is the magnitude of the expected main shock. This calculation is based on the standard assumption that the Ishimoto-Iida or Gutenberg-Richter law can be extrapolated to large events that have not occurred during the period of observation. Based on correlation of low  $TL$ -volumes (usually equivalent to volumes with low  $b$ ) with known asperities, we have proposed that the state of stress in major asperities may control the timing of major ruptures.

Mapping the parameters  $b$  and  $TL$  in map view, in cross sections and in three dimensions, we were able to show that the main shock hypocenters correlate with low  $TL$ -values and that the bottom of the seismogenic zone shows characteristics typical for environments with high pore pressure.

## Socio-economic relevance and policy implication

The relevance of our results is that the size distribution of earthquakes can be used to approximately map the locations in which earthquake nucleations are most and least likely by calculating the local recurrence time. This means that dense seismograph networks, like the ones in Iceland, deliver useful data to map locations of likely future earthquakes, and should therefore be financially supported and improved.

## Discussion and conclusion

The earthquake catalog in southern Iceland between 20.25°W and 21.3°W is complete down to approximately  $M_w = 0$  and shows no evidence for magnitude shifts as a function of time since 1991. This means that 6902 earthquakes ( $M \geq -0.1$ , depth  $\leq 20$  km) are available for studies of seismicity patterns before the two  $M_s 6.6$  main shocks in 2000, in their source volumes and vicinity (20.25°W and 20.9°W). The power law of the frequency-magnitude relationship holds down to  $M_0$  (Fig. 1).

Detailed mapping (including 3D mapping) of the  $b$ -value of the frequency-magnitude distribution shows that variations from  $b = 0.6$  to 1.4 exist over distances of about 2 km. This suggests that the tectonic fabric in southern Iceland is heterogeneous on a small scale (Fig. 2).

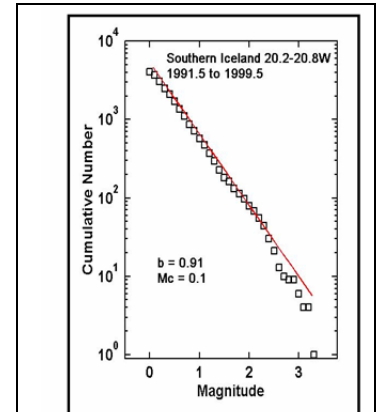


Figure 1: *The power law of earthquake size distribution holds down to  $M_0$ , at least.*

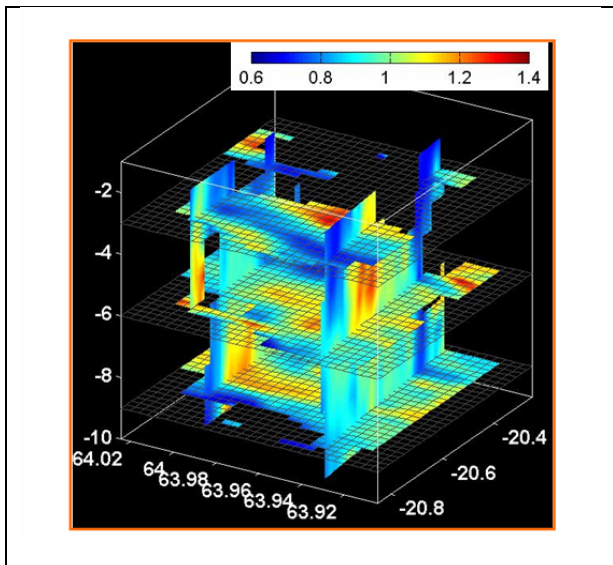


Figure 2: *Three dimensional mapping of the frequency-magnitude distribution of earthquakes shows heterogeneity of the tectonic fabric at the 2 km level.*

The hypocenters of the two  $M_s 6.6$  and one additional  $M 4.5$  main shocks are associated with low  $b$ -values (0.6 to 0.8), statistically significantly different from volumes in their vicinity. Therefore, one can expect future main shocks in southern Iceland to also emanate from volumes characterized by low  $b$ -values. However, the small dimensions of these asperities may render it difficult to identify them before the main shocks occur. Low values of estimated local recurrence times (500 to 2000 years) map the two fault zones that ruptured in 2000 against a background of local recurrence times longer than 5000 years. The first of the two  $M 6.6$  main shocks emanated from a volume of short estimated local recurrence time (Fig. 3). This supports the hypothesis that asperities with short local recurrence times control locations of major ruptures. Mapping of  $b$ -values in cross sections shows anomalies of high  $b$  at the bottom of the seismogenic crust, correlating with the change of its thickness in the middle of the

study area. These high  $b$ -value anomalies, and other pockets of such anomalies at shallower depths, are best interpreted as due to high pore pressure because evidence of fluids under high pressure is ubiquitous in this area.

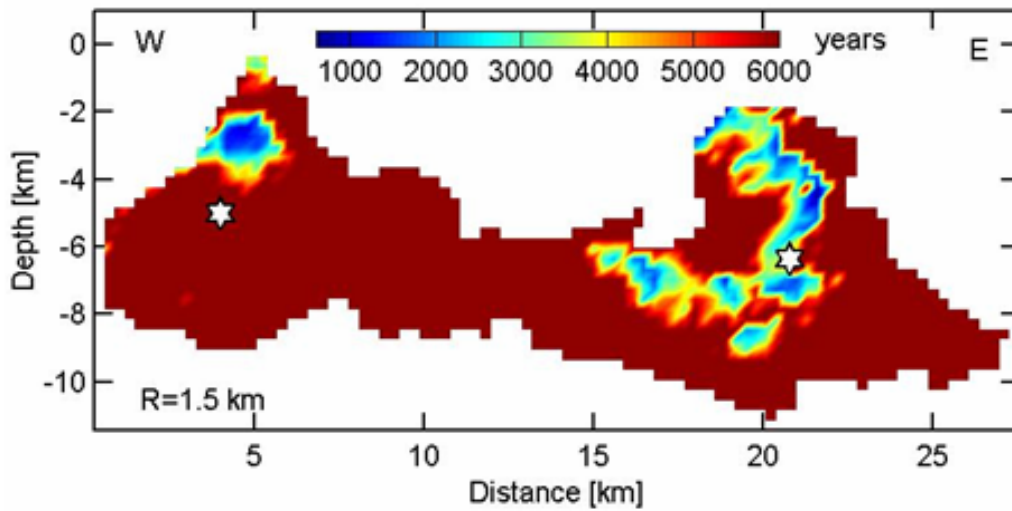


Figure 3: *Cross section of local recurrence time, TL in southern Iceland. Hypocenters of main shocks (stars) are located within and near to the volumes of minima in TL. The two fault zones that broke in 2000 are characterized as the locations of the lowest TL values.*

### **Plan and objectives for the next period**

There is no next period.

## **WP 2.3 Long-term deformation in the South Iceland seismic zone (SISZ) inferred by joint interpretation of GPS, InSAR and borehole strain data**

**Author: Thóra Árnadóttir**

### **Background**

The crustal deformation in south Iceland has been monitored by Global Positioning System (GPS) measurements since 1986. The June 2000 earthquake sequence caused significant surface deformation that was observed by GPS and InSAR (Árnadóttir *et al.*, 2001; Pedersen *et al.*, 2001; Pedersen *et al.*, 2003). Following the June 17, 2000 main shock the GPS network in the South Iceland seismic zone (SISZ) and on the Reykjanes Peninsula have been observed yearly, providing a detailed map of post-seismic deformation. The first months of post-seismic deformation contain signals due to post-seismic ground water movements inferred from InSAR measurements (Jónsson *et al.*, 2003), which are also evident in the GPS observations during the first year following the earthquakes. The June 2000 earthquake sequence provides the first opportunity to study post-seismic deformation in Iceland. The deformation signal prior to June 2000 is difficult to decipher as it is influenced by local volcano deformation near Hengill (Sigmundsson *et al.*, 1997; Feigl *et al.*, 2000) and Hekla in addition to the plate spreading signal. In our work we have tried to separate the sources of the pre- and post-seismic signals and determine the strain field during the pre-seismic time interval in order to look for anomalies in the deformation field that could be considered precursors to the June 2000 earthquake sequence.

### **Scientific/technological and socio-economic objectives**

The objective of the work package is to evaluate the long term 3D deformation in south Iceland prior to the June 2000 earthquakes, using existing geodetic data. The 3D deformation map will be used to derive a strain map for S Iceland prior to the June 2000 earthquakes, and to search for long-term precursors in the geodetic signal. The velocity field during the pre-seismic time interval has been used to estimate the pre-seismic strain field as well as a 3D kinematic model for the plate boundary in SW Iceland. The post-seismic velocity field in the SISZ has been used to estimate source of post seismic deformation and estimate stress changes due to the post seismic deformation. These results provide important information when evaluating the seismic hazard in the area.

### **Applied methodology, scientific achievements and main deliverables**

The work in this work package has exceeded the original work plan, which originally focused on analysing GPS data prior to the June 2000 earthquake sequence, since we have also included GPS data for the post-seismic time period (until mid 2004). The following is a short description of the work conducted and the main results and deliverables.

We analysed all campaign and continuous GPS data collected on Reykjanes Peninsula and in the South Iceland Seismic Zone from 1992-2004, using the GAMIT/GLOBK software (King and Bock, 2003; Herring, 2003), in the ITRF2000 reference frame. The data have also been processed using V4.2 of the Bernese software (Hugentobler *et al.*, 2001). We estimated GPS station velocities and offsets during the time spanned by the data. Firstly, we estimated the average “pre-seismic” (1992-2000) and “post-seismic” (2000-2004) velocity field in SW Iceland, as well as co-seismic offsets in position for the June 2000 earthquake sequence, as described in section 3.1 below, and by Árnadóttir *et al.* (2005a). Secondly, we divided the post-seismic time series into two intervals 2000-2001 and 2001-2004. During the first year following the June 2000 earthquakes the velocities appear larger than during the latter 3 year interval. The main results from this work are reported in section 3.2 below and by Árnadóttir *et al.* (2005b). Thirdly, we processed all continuous GPS data

collected in Iceland (ISGPS data) and generated a velocity field for stations in Iceland in the ITRF2000 reference frame. For a detailed description of this work see *Geirsson et al.* (2005).

## The GPS velocity field for SW Iceland

We use data from GPS campaign and continuous measurements from 1992 to 2004 in SW Iceland to generate surface velocity field maps from the Reykjanes Peninsula to the Eastern Volcanic Zone. We divide the time series into pre-seismic (July 1992-June 2000), and post-seismic (June 2000-May 2004) time intervals, and estimate GPS station velocities for each interval as well as coseismic offsets due to the the June 2000 earthquake sequence in the South Iceland Seismic Zone (SISZ). In addition to the plate spreading, the pre-seismic velocity field is affected by inflation at Hengill and Hekla volcanoes, whereas the post-seismic velocities show deformation following to the June 2000 earthquakes.

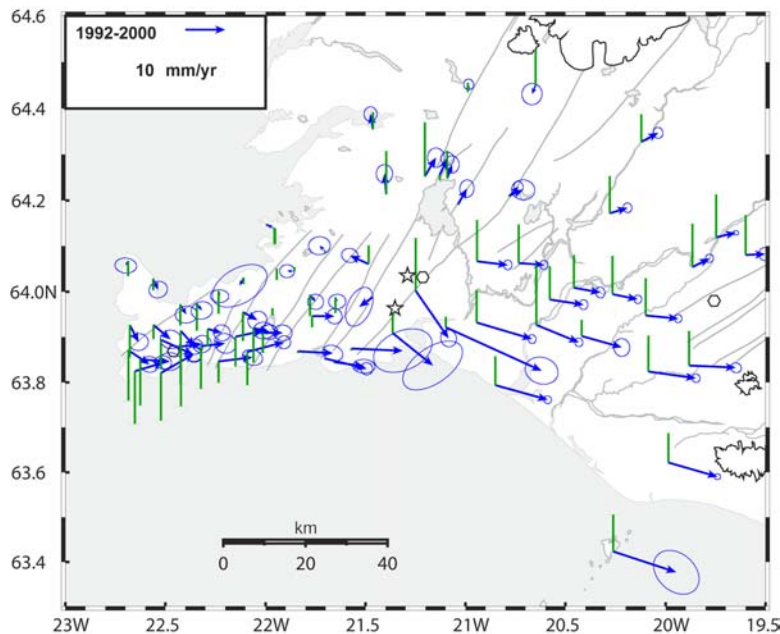


Figure 1. Pre-seismic GPS station velocities (D20). The blue arrows with 95% confidence ellipses, show horizontal velocities relative to stable North America, and the green bars show vertical velocities. The stars show epicentral locations of earthquakes during the time interval spanned by the GPS data, and hexagons indicate pressure sources at Svartsengi, Hengill and Hekla. The stations on the North American plate have small horizontal velocities, whereas stations on the Eurasian plate move southeastward. The GPS station in the Westman Island is moving with a velocity close to the full plate rate predicted by plate motion models (e.g. NUVEL1A). The vertical velocities are in the ITRF2000 reference frame, and show absolute vertical motion. In this frame Reykjavik is subsiding at a rate of about 4 mm/yr. All the stations on the Reykjanes Peninsula are subsiding, whereas stations in the Hengill area and the SISZ show uplift.

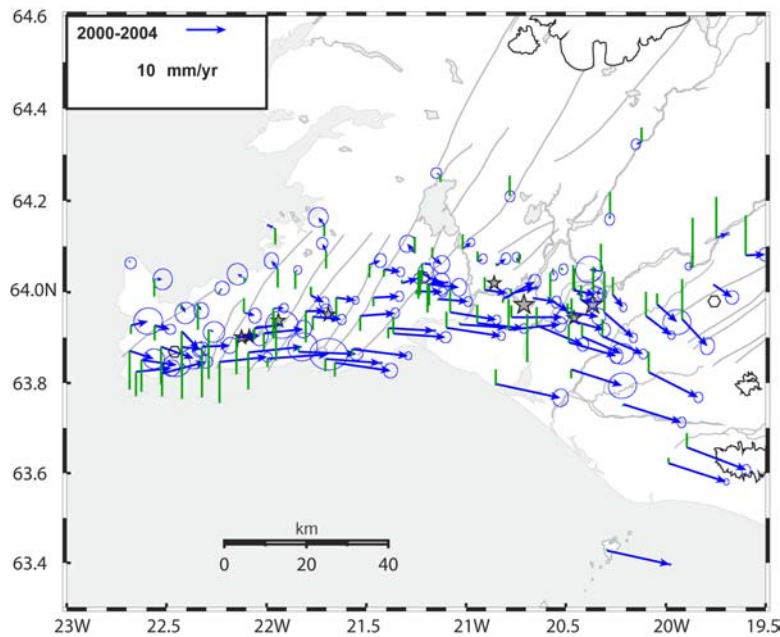


Figure 2. Post-seismic GPS station velocities (D20). The blue arrows with 95% confidence ellipses, show horizontal velocities relative to stable North America. The green bars show vertical velocities in the ITRF2000 reference frame. The stars show epicentral locations of  $M > 5$  earthquakes during the time interval spanned by the GPS data, and hexagons indicate pressure sources at Svartsengi, Hengill and Hekla.

We use the GAMIT/GLOBK solution shown in Figure 1 to calculate the strain field in South Iceland in the pre-seismic period 1992-2000. The shear strain rate is composed of several components of the gradient of the velocity field in different directions. We find that the northward gradient of the eastward velocity component, i.e.  $dV_e/dN$  is most indicative of left-lateral motion on an E-W transform, or right-lateral motion on an N-S fault, as observed in the SISZ. Figure 3 shows this component of the strain tensor. We see that the strain rate is high in the center of the SISZ, and decreases as we move north or south from 64N. This pattern demonstrates that strain was concentrated in the SISZ prior to the June 2000 earthquakes. The black color around the Hengill area indicates very high negative strain rates, due to the high rate of deformation due to inflation from 1993 to 1999. The strain rates are generally high along the plate boundary on the Reykjanes Peninsula and through the SISZ, with strain rates up to about  $0.5 \mu\text{strain/yr}$ . A large variation in strain rates in adjacent triangles around one station (e.g. station STRY on the south coast of Iceland) indicate an unstable station and the results are therefore unreliable for triangles influenced by that station.

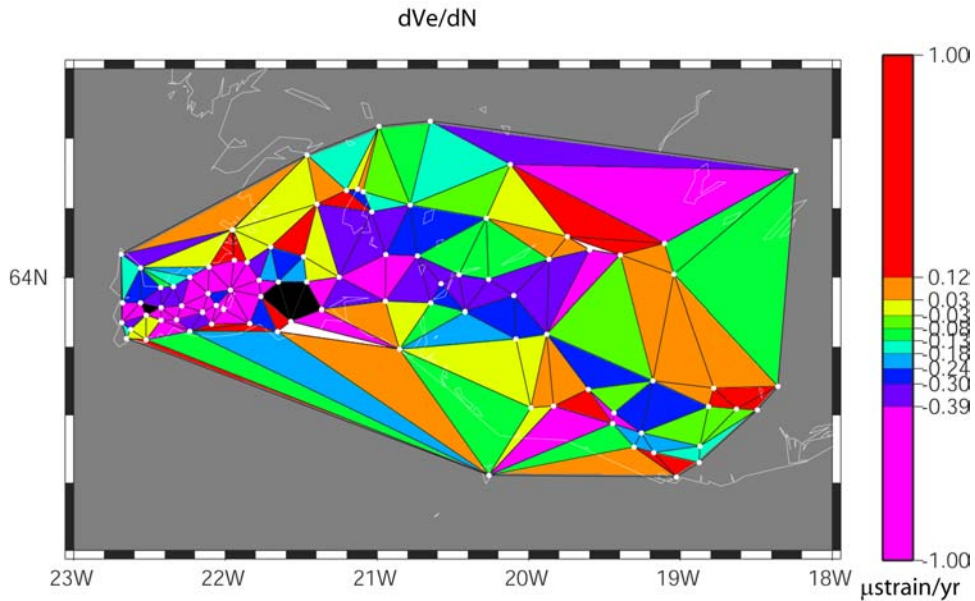


Figure 3. The strain field in the pre-seismic period (D21 and D22). The northward gradient of the eastward velocity component showing left-lateral motion on a E-W faults, or right-lateral motion on N-S faults.

We model the pre-seismic velocity field shown in Figure 1 with screw dislocation models as well as more complex 3D dislocation and point source models, to explain the plate boundary deformation (Árnadóttir *et al.*, 2005a). Our preferred model is a 3D dislocation and point source model with left-lateral slip along the plate boundary on the Reykjanes Peninsula and below the SISZ, and opening across the Western and Eastern Volcanic Zones. We can not uniquely determine all our model parameters from the GPS data. In particular, there is a trade-off between the locking depth and the deep slip rate. For constant deep slip rates in the range 16-20 mm/yr, we find a 5-7 km locking depth on the Reykjanes Peninsula, and 8-11 km depth below the SISZ. These locking depths show reasonable agreement with the thickness of the seismogenic layer in southwest Iceland, which appears to vary between 8 and 10 km.

Using our preferred plate boundary model we can estimate the rate of Coulomb failure stress change during the pre-seismic time interval, using standard methods (e.g. Harris, 1998). Figure 4 shows that the inflation in Hengill and left-lateral slip below 7 km depth along the plate boundary on Reykjanes Peninsula combine to increase the Coulomb failure stress on N-S, right-lateral strike-slip faults on the Reykjanes Peninsula, such as ruptured in the triggered earthquakes on June 17, 2000. The stress change pattern is very similar for E-W oriented, left-lateral receiver faults. The Hengill inflation appears to have acted to decrease the Coulomb failure stress on N-S faults east of Hengill, possibly explaining why the June 2000 earthquake sequence did not progress further west following the June 21, 2000 main shock.

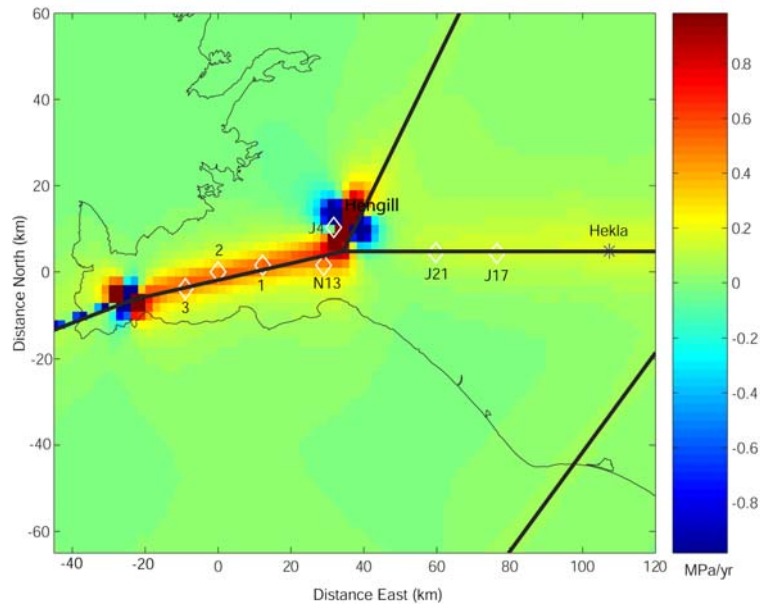


Figure 4. The rate of Coulomb failure stress change at 5 km depth, on N-S right-lateral strike-slip faults, caused by plate boundary deformation. Our model assumes left-lateral slip of 20 mm/yr along the Reykjanes Peninsula and the SISZ, below 7 and 11 km depth, respectively. The model also includes opening across the Western and Eastern Volcanic Zones as well as inflation at Hengill and Hekla volcanoes and subsidence at Svartsengi. The diamonds denote earthquake locations, where the June 17 and 21 main shocks are labelled J17 and J21 respectively, the numbers 1, 2, 3 refer to the June 17 triggered earthquakes. The  $M=5$  1998 earthquakes in the Hengill and Ölfus are labelled J4 (June 4) and N13 (November 13). Warm colors (yellow to red) indicate an increase in Coulomb failure stress. Small changes in Coulomb failure stress (0.001 MPa) have been shown to correlate with areas of increased seismicity following a mainshock (e.g. Harris, 1998).

### Post-seismic deformation in the SISZ

The post-seismic deformation in the SISZ following the June 2000 main shocks appears on two spatio-temporal scales. We observe a rapidly decaying deformation transient lasting no more than 2 months and extending about 5 km away from the two mainshock ruptures. This local, month-scale transient is captured by several radar interferograms (InSAR) and is also observed at a few campaign GPS sites located near the faults. A longer-scale transient with a characteristic time scale of about a year is only detected by GPS measurements. The month-scale deformation pattern has been explained by poro-elastic rebound due to post-earthquake pore-pressure changes (Jónsson *et al.*, 2003). In contrast, the year-scale deformation can be explained by either viscoelastic relaxation of the lower crust and upper mantle in response to the coseismic stress changes or afterslip at 8-14 km depth. The optimal viscoelastic models have lower crustal viscosities of about  $0.5 - 1 \times 10^{19}$  Pa s and a less well constrained upper mantle viscosity about  $3 \times 10^{18}$  Pa s. Due to the limitations of our GPS campaign data we consider both afterslip and viscoelastic relaxation as plausible mechanism explaining the deformation field. Both types of post-seismic deformation models suggest that the areas of large co-seismic stress increase east of the June 17 and west of the June 21 ruptures, continue to be loaded by the post-seismic deformation.

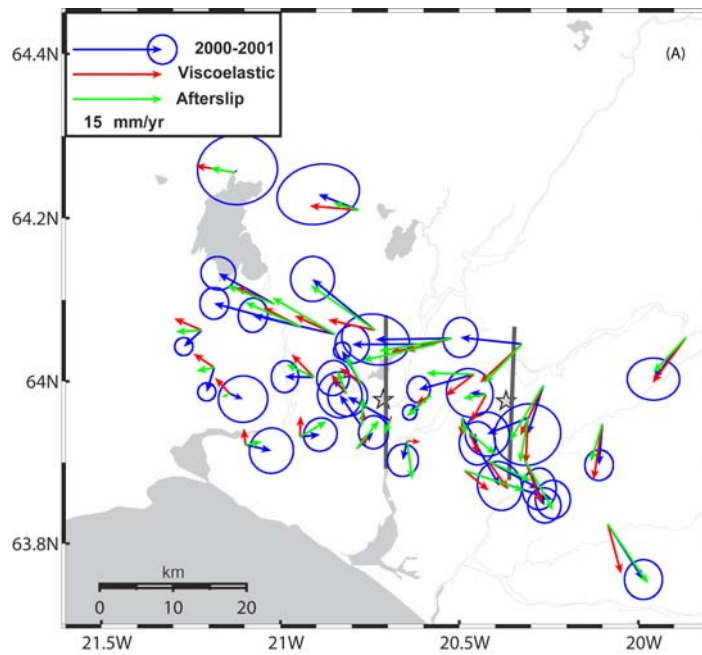


Figure 5. Post-seismic GPS station velocities from 2000 to 2001 (blue arrows with 68% confidence ellipses) corrected for interseismic plate motion (Figure 1). The calculated velocity field for the preferred viscoelastic model is shown with red vectors. The velocities predicted by the optimal afterslip model are shown with green vectors. The bold gray lines denote the up-dip surface projection of the afterslip fault models.

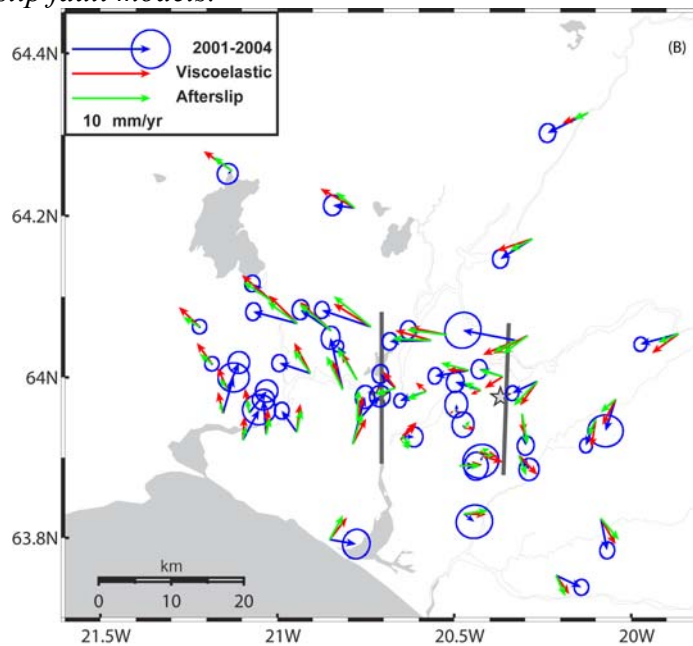


Figure 6. Post-seismic GPS station velocities from 2001 to 2004 (blue arrows with 68% confidence ellipses) corrected for interseismic plate motion. The calculated velocity field for the preferred viscoelastic model is shown with red vectors. The velocities predicted by the best fit afterslip models are shown with green vectors. The bold gray lines denote the up-dip surface projection of the afterslip fault models.

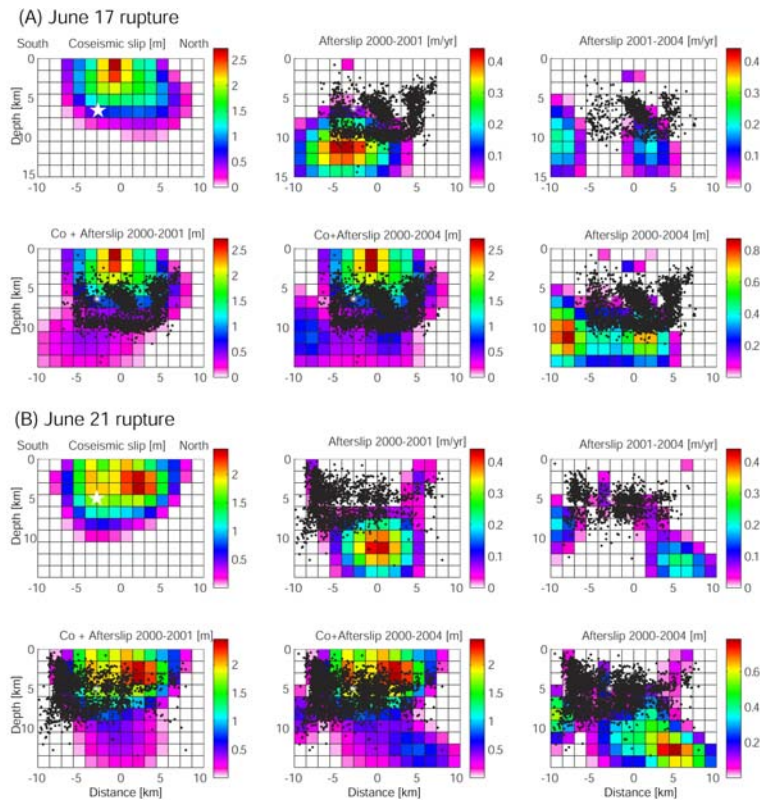


Figure 7. Distributed slip models for the (a) June 17 rupture and (b) June 21 rupture. Afterslip models for the different intervals (2000-2001 and 2001-2004) are shown in the top middle and right panels respectively. The coseismic slip distribution is shown in the top left panel. The lower three panels show the cumulative slip for the different time intervals, i.e. coseismic and first year of post-seismic slip (left), coseismic and first four years of post-seismic slip (middle) and total afterslip (right). The black dots are earthquake hypocenters recorded by the SIL seismic network during the two time intervals.

### Socio-economic relevance and policy implication

The velocity field during the pre-seismic time interval has been used to estimate the pre-seismic strain field as well as a 3D kinematic model for the plate boundary in SW Iceland. The post-seismic velocity field in the SISZ has been used to estimate source of post seismic deformation and estimate stress changes due to the post seismic deformation. These results are important information when evaluating the seismic hazard in the area.

### Conclusions including socio-economic relevance, strategic aspects and policy implications

We do not observe any evidence of anomalous velocities in the epicentral areas of the June 2000 main shocks, that could be used as an indication of their locations in hindsight. The network density has been increased in the SISZ and on the Reykjanes peninsula giving a more detailed velocity field than was available for the pre-seismic period. We have observed the GPS network once a year, and installed two continuous GPS stations in the SISZ after the earthquakes. It is however clear that the density of continuous stations needs to be increased further in order to more fully understand the post-seismic deformation field and possibly detect anomalous deformation prior to the next SISZ earthquake.

## Main literature produced

Árnadóttir, Th., W. Jiang, K. L. Feigl, H. Geirsson and E. Sturkell (2005a), Kinematic models of plate boundary deformation in southwest Iceland derived from GPS observations, submitted to *J. Geophys. Res.*, June 2005.

Árnadóttir, Th., S. Jónsson, F.F. Pollitz, W. Jiang and K.L. Feigl (2005b), Post-seismic deformation following the June 2000 earthquake sequence in the south Iceland seismic zone, submitted to *J. Geophys. Res.*, February 2005.

Geirsson, H., Th. Árnadóttir, C. Völksen, W. Jiang, E. Sturkell, T. Villemin, P. Einarsson, F. Sigmundsson, and R. Stefánsson (2005), Current plate movements across the Mid-Atlantic ridge determined from 5 years of continuous GPS measurements in Iceland, submitted to *J. Geophys. Res.*, 2005.

## References

Árnadóttir, Th., W. Jiang, K. L. Feigl, H. Geirsson and E. Sturkell (2005a), Kinematic models of plate boundary deformation in southwest Iceland derived from GPS observations, submitted to *J. Geophys. Res.*, June 2005

Árnadóttir, Th., S. Jónsson, F. Pollitz, W. Jiang, and K. L. Feigl (2005b), Post-seismic deformation following the June 2000 earthquake sequence in the south Iceland seismic zone, submitted to *J. Geophys. Res.*, February 2005.

Árnadóttir, Th., S. Hreinsdóttir, G. Guðmundsson, P. Einarsson, M. Heinert, and C. Völksen (2001), Crustal deformation measured by GPS in the South Iceland Seismic Zone due to two large earthquakes in June 2000, *Geophysical Research Letters*, 4031-4033, 2001.

Feigl, K.L., J. Gasperi, F. Sigmundsson, and A. Rigo (2000), Crustal deformation near Hengill volcano, Iceland 1993-1998: Coupling between magmatic activity and faulting inferred from elastic modeling of satellite radar interferograms, *J. Geophys. Res.*, 105, 25655-25670.

Harris, R.A. (1998), Introduction to special section: Stress triggers, stress shadows, and implications for seismic hazard, *J. Geophys. Res.*, 103, 24,347--24,358.

Herring, T.A. (2003), GLOBK: Global Kalman filter VLBI and GPS analysis program version 4.1, Mass. Inst. Technol., Cambridge.

Hugentobler, U., S. Schaer, and P. Friedez (2001), Bernese GPS software, Version 4.2, Astronomical Institute, University of Berne, Berne, Switzerland.

Jónsson, S., P. Segall, R. Pedersen, G. Björnsson (2003), Post-earthquake ground movements correlated to pore-pressure transients, *Nature*, 424, 179-183.

King, R.W., and Y. Bock (2003), Documentation for the GAMIT Analysis Software release 10.1, Mass. Inst. Technol., Cambridge.

Pedersen, R., S. Jónsson, Th. Árnadóttir, F. Sigmundsson, and K.L. Feigl (2003), Fault slip distribution of two Mw=6.5 earthquakes in South Iceland estimated from joint inversion of InSAR and GPS measurements, *Earth and Planetary Science Letters* 213, 487-502.

Pedersen, R., F. Sigmundsson, K.L. Feigl and Th. Árnadóttir (2001), Coseismic interferograms of two  $M_s = 6.6$  earthquakes in the South Iceland Seismic Zone, June 2000, *Geophysical Research Letters*, 28 , 3341-3344.

Sigmundsson, F., P. Einarsson, S. Th. Rögnvaldsson, G. Foulger, K. Hodgkinson, and G. Thorbergsson (1997), The 1994-1995 seismicity and deformation at the Hengill triple junction, Iceland: Triggering of earthquakes by minor magma injection in a zone of horizontal shear stress, *J. Geophys. Res.*, 102, 15151-15161.

## **WP 2.4 Space and time variations in crustal stress using microearthquake source information from the South Iceland seismic zone**

**Authors: Reynir Bödvarsson and Björn Lund**

### **1 Objectives**

The main purpose of the WP 2.4 is to utilize the unique data set provided by the SIL-network to analyze the SISZ using various type methods and algorithms. In this report we will only show results from the type of methods that has been further worked on since the last report.

### **2 Methodology and scientific achievements**

#### **2.1 Spectral amplitude correlation and grouping**

The Spectral Amplitude Grouping (SAG) algorithm (Lund and Bödvarsson, 2002) has now been implemented at the SIL center in Reykjavik, Iceland. The algorithm will be used as an additional tool to monitor the character of ongoing seismic activity. Currently, region specific SAG analyses are carried out in order to form a background database for comparison with future seismicity. Although there are significant variations in the SAG patterns at times associated with seismic and/or volcanic events, there is of yet no simple relationship between the SAG response and the seismicity. This is an issue where continued research is necessary.

We have initiated research on the next improvement of the algorithm, where we intend to better separate the influence of spatial variability in the seismicity from the variation in focal mechanisms. This work has just begun but as progress is being made the improvements will be incorporated into the SIL center software.

#### **2.2 Stress tensor inversion of earthquake focal mechanisms**

The temporal stress investigations, using the algorithm of Lund and Slunga, 1999, reported earlier in the project have been continued and augmented by improved models for the variance in the estimates. Generally, however, the spatial averaging involved in these estimates adds to the formal methodological uncertainty, which makes most of the temporal variability observed in the results rather uncertain. There are notable exceptions, such as the stress variations in the aftershock activity of larger earthquakes. Also, as reported earlier, there are significant variations during 1996 to 1997.

In the latter part of the project, we have concentrated on spatial investigations of stress variation. Similar to the investigations of e.g. Townend and Zoback, 2001, we have used a quadtree algorithm to divide the data into spatial bins with similar number of events. This provides very detailed spatial stress resolution in areas of large seismic activity, see Fig. 1. We have also studied the evolution of the regional stress field, by inverting large numbers of events in the source areas of the two June 2000 earthquakes and the 1998 Ölfus earthquake.

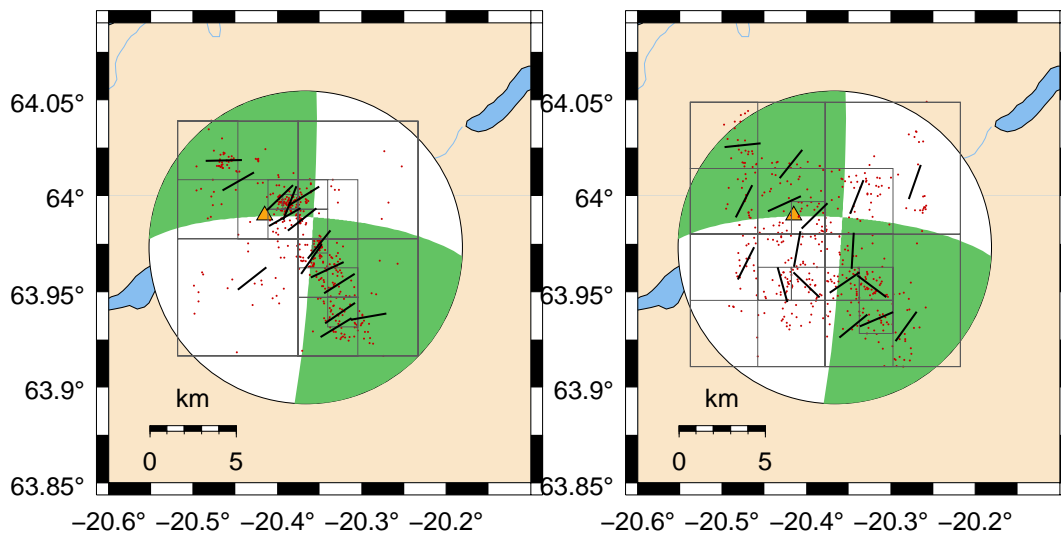


Figure 1: Epicentral region of the June 17, 2000, M 6.5 earthquake. The focal mechanism is for the large event, from the Harvard data base but centered on the SIL location. The red dots are earthquakes from the SIL catalogue from January, 1996, to June 17, 2000. The squares show the partitioning of the events using the quadtree algorithm. The black lines are the directions of the maximum horizontal stress. A) Above 7.5 km. B) Below 7.5 km.

## Regional scale stress estimates

We defined the following areas around three notable earthquakes in the studied time period:

The Ölfus November 1998 earthquake, lat. 63.9 to 63.9857, lon. -21.47 to -21.0

The June 17 2000 earthquake (J17), lat. 63.9 to 64.05, lon. -20.5 to -21.25

The June 21 2000 earthquak (J21)e, lat. 63.88 to 64.07, lon. -20.9 to -21.63

In these areas we divided the seismicity into three temporal intervals, 1991 - 1995, 1996 - 17/6 2000 (the first M 6.5 event), 17/6 2000 - 2003, and inverted the focal mechanisms for the stress field. The results for the maximum principal stress axis and the maximum horizontal stress are:

J17 area: 1991-1995 S1 N51E, plunge 30 SH N52E  
 1996-2000 N54E, 20 N54E  
 2000-2003 N58E, 20 N57E

J21 area: 1991-1995 S1 N50E, plunge 5 SH N51E  
 1996-2000 N43E, 20 N44E  
 2000-2003 N34E, 35 N31E

Ölfus area: 1991-1995 S1 N37E, plunge 45 SH N37E  
 1996-2000 N35E, 30 N36E  
 2000-2003 N28E, 30 N28E

We see that in the June 17 area, the average stress direction is very stable. In the June 21 area there appears to be a northward rotation of the maximum stress. In the case of the two first time periods, this difference is well within the confidence limits. For the aftershocks, as we will see below, there are indications that there are inhomogeneities in the stress field which causes the apparent rotation

of the average stress northwards. The estimates in the two areas agree well with the large scale results of Angelier et al., 2004. In the Ölfus area, stress directions are rather stable all through the time periods, we observe however that the Ölfus area, which is located west of the core SIL area, has a more north-southerly direction of the maximum stress. This is in agreement with Lund and Slunga, 1999.

### Local scale stress estimation

We used the areal definitions given above for the two June 2000 earthquakes to estimate as many stress tensors as possible in the areas, using a quadtree algorithm to divide the data into spatial bins. The procedure requires significant amounts of data, implying that we could only study four different time periods, 1991-1995, 1996 - 17/6 2000, 17/6 2000 - 17/6 2001 and 18/6 2001 - 31/12 2003. In Fig. 1 we show some of the results for the J17 area. We discovered that if the data is subdivided in depth, at 7.5 km, the stress state in the lower part of the seismogenic crust is significantly different from that in the upper part of the crust in the time period 1996 to just before the J17 earthquake. We see in Fig. 1 that during 1991 - 1995, although there is some scarcity of data, the direction of the maximum horizontal stress, SH, in the entire seismogenic crust agrees well with the previously estimated average for the area. During 1996 - 17/6 2000, however, the seismicity below 7.5 km shows great inhomogeneity in the SH direction, whereas the seismicity above 7.5 km is still very well ordered. We have performed the depth division at various depths in order to estimate at which depth the change in stress regime occurs, and 7.5 km is our best estimate. Extracting the stress state from the inversions indicate that around 7.5 km there is a transition from a predominately strike-slip regime into a normal faulting regime. These are however still preliminary results.

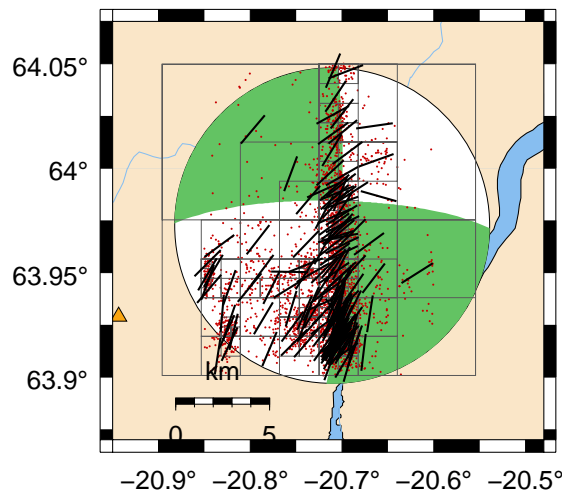


*Figure 2: Epicentral region of the June 21, 2000, M 6.5 earthquake. The focal mechanism is for the large event, from the Harvard data base but centered on the SIL location. The red dots are earthquakes from the SIL catalogue from June 17, 2000, to June 17, 2001. The squares show the partitioning of the events using the quadtree algorithm. The black lines are the directions of the maximum horizontal stress.*

The June 21 earthquake area show no signs of such variation of stress with depth. In the aftershocks, however, there is a very interesting spatial variation in the direction of SH, see Fig. 2. There is a large amount of data in Fig. 2, due to the aftershock activity during the first year after the event. If studied carefully, there is a clear division in the Figure between the northern and southern sections of the fault area. North of 63.95 deg. SH has an east-westerly direction while south of 63.95 there is more of a north-south direction in SH. This becomes clearer if the SH directions are

plotted in a rose diagram, see Fig. 3. We see that the average SH direction north of 63.95 is approximately N45E while south of 63.95 it is approximately N30E.

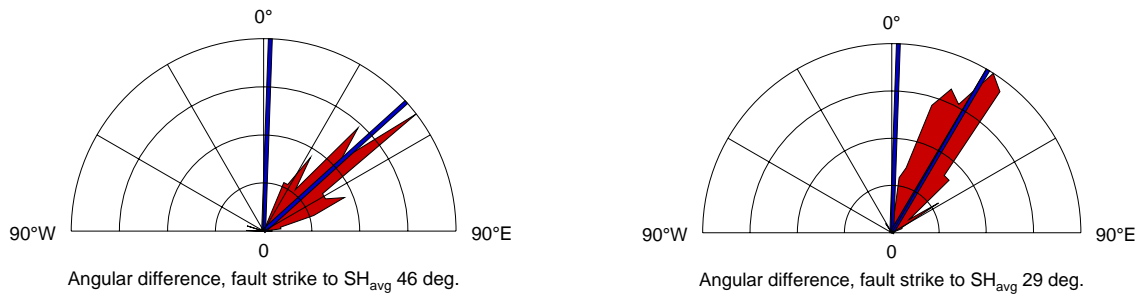


*Fig 3: Rose diagrams of maximum horizontal stress directions inferred from the aftershocks of the June 21, 2000 event. The almost vertical blue line is the strike of the June 21 fault plane, the second blue line is the average direction of the maximum horizontal stress. A) Data from north of 63.95 degree latitude. B) Data from south of 63.95 degree latitude.*

The stress variations are robust features of the data, we have tried various quadtree divisions of the seismicity and various applications of the tunable parameters of the stress inversion algorithm itself. We currently studying the J17 depth anomaly in detail, both in terms of different aspects of the stress tensor and the significance of the inversions. We are also actively testing hypothesis regarding the origin of the anomaly. Possible candidates for the heterogeneous stress state in the lower part of the seismogenic crust includes fluid intrusion, magmatic intrusion, structural heterogeneity or combinations thereof. The modelling work of Bonafede et al, WP 6.2 of this report, is of special interest for the interpretation of the J17 anomaly.

### 3 Socio-economic relevance

This research is a contribution to a better understanding of the deformation processes in the SISZ and other seismic areas in general. This can be of importance for possible future earthquake predictions which would be of important value for the society.

### 4 Discussion and conclusion

In this report we have tried to give information on the ongoing research and the results that we have available. We feel that the results from the various methods reported here and in previous reports are promising and will contribute to a better understanding of the ongoing processes in the seismogenic crust in SISZ.

## References

Angelier, J., R. Slunga, F. Bergerat, R. Stefansson and C. Homberg, Perturbation of stress and oceanic rift extension across transform faults shown by earthquake focal mechanisms in Iceland, *Earth Planet. Sci. Lett.*, 219, 271-284, doi 10.1016/S0012-821X(03)00704-0, 2004.

Lund, B and R. Bödvarsson, Correlation of microearthquake body-wave spectral amplitudes, *Bull. Seis. Soc. Am.*, 92, 2410-2433, 2002.

Lund, B and R. Slunga, Stress tensor inversion using detailed microearthquake information and stability constraints: Application to Ölfus in southwest Iceland, *J. Geophys. Res.*, 104, 14947-14964, 1999.

Townend and Zoback, Implications of earthquake focal mechanisms for the frictional strength of the San Andreas fault system, in *The Nature and Significance of Fault Zone Weakening*, edited by R.E. Holdsworth et al., *Geol. Soc. London Spec. Publ.*, 186, 13-21, 2001.

## WP2.5 Using shear-wave splitting above small earthquakes to monitor stress in SISZ

Author: Stuart Crampin

### Objectives

Overall objectives are to develop the technology and understanding of shear-wave splitting to stress-forecast earthquakes.

### Methodology and scientific achievements

The thirty months of the PREPARED Project have seen what are believed to be very significant advances in understanding, monitoring, and interpreting seismic shear-wave splitting, which could well lead to the most significant advances in solid-earth geophysics for many decades.

(Note that citations and references to papers supported by the PREPARED Project are printed in **bold type-face**.)

### THE VARIOUS ADVANCES

#### The large June 2000 earthquakes could have been stress-forecast

1) The major advance with respect to the aims of the PREPARED Project is that the improved Iceland Earthquake Catalogue, with magnitudes down to  $M$  0.0 (prepared by IMO) provided sufficient shear-wave source earthquakes for both stress-accumulation (see Item 4, below) and crack coalescence (Item 2, below) to be recognised before the two  $M_s$  6.6 June 2000 earthquakes (**Wu *et al.* 2005**). Figure 1 shows the variations at Stations SAU and BJA. Consequently, the largest events in the last 30 years in Iceland could have been stress-forecast had the catalogue with smaller magnitudes been available at that time.

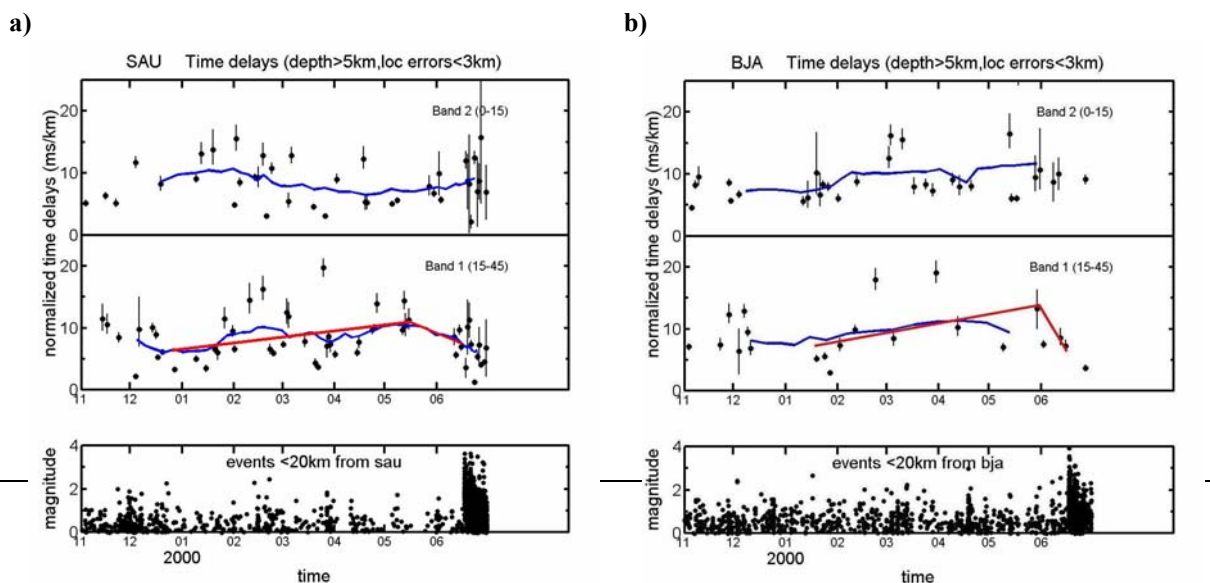
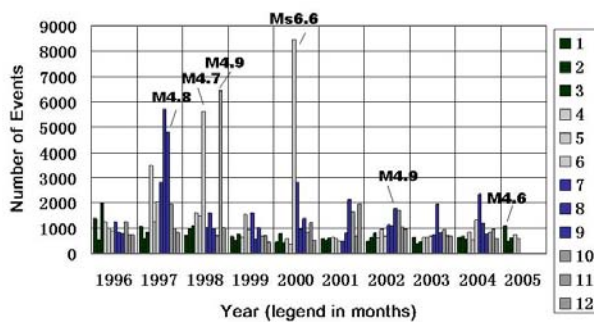


Figure 1. *Red lines are temporal increases and decreases in normalised time-delays before the  $M_s$  6.6 June, 2000, earthquakes at Stations a) SAU and b) BJA in SW Iceland (Wu *et al.* 2005).*

2) The reason why the June 2000 events were not stress-forecast in real time, was that the small earthquakes (that were missing in the previous catalogue) left a gap in the time-delay record which disguised the increase in time-delays. Monthly histograms of numbers of Icelandic earthquakes in the improved catalogue show that the reason for the gap in earthquakes was that the previous six-month total and immediate previous month (May) total show the smallest number of earthquakes in nine-years of records (Figure 2a). This suggests that both six-monthly and monthly quiescence indicate an imminent larger earthquake in Iceland.

The logarithm of precursory *decreases* in time-delays are self-similar to earthquake magnitude in Figure 2b. The logarithm of *increases* in time-delays are also self-similar to earthquake magnitude (not shown) for rather more earthquakes than in 2b (Wu *et al.* 2005). Both increases and decreases have the typical magnitude-duration relationships seen in Iceland and elsewhere.

a)



b)

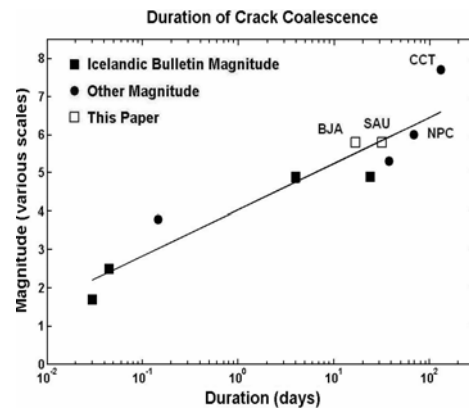


Figure 2. (a) Monthly histograms of number of earthquakes in the improved Iceland Earthquake Catalogue for the nine years 1996 to 2005. Note that before June 2000 Ms 6.6 events there is a minimum six months, and a minimum previous month (May), of the whole nine-years records. (b) Duration-magnitude relationship for precursory decreases of time-delays before earthquakes in Iceland (solid squares) and worldwide (solid circles) (Wu *et al.* 2005). The June. 2000, events are open squares for stations BJA and SAU. Points marked CCT and NPS refer to the 1988 North Palm Springs Earthquake, on the San Andreas Fault in California, and the 1999 Chi-Chi Earthquake in Taiwan (Wu *et al.* 2005).

### Other advances in understanding shear-wave splitting

3) Shear-wave splitting in critically-high pore fluid pressures results in the faster and slower split shear-waves exchanging polarisation. Known as 90°-flips (Crampin *et al.* 2002), such flips are recognised above major faults including the Húsavík-Flatey Fault (Figure 3a).

5) Such 90°-flips are now recognised as the cause of the pronounced  $\pm 80\%$  scatter in time delays above small earthquakes. This suggests that all fault planes are pervaded by high pore-fluid pressures close to the maximum horizontal compressional stress (Crampin *et al.* 2004).

6) In the past, increases in shear-wave time-delays before earthquakes have been established as monitoring the stress-accumulation before the earthquakes. This phenomenon has now been recognised (with hindsight) before some 15 earthquakes worldwide (Wu *et al.* 2005), with one successful stress-forecast of a  $M 5$  earthquake in the SISZ (Crampin *et al.* 1999). During PREPARED, it was recognised that there were also decreases in time-delays immediately before the

larger earthquakes (Figure 3b) which were initially assumed to be caused by stress relaxation (**Gao & Crampin 2004**). It is now recognised that the stress relaxation is almost certainly the result of microcracks coalescing into major fractures immediately before the larger earthquakes (**Wu *et al.* 2005**).

7) Since microcracked rock is very weak to shear stress, accumulation of stress necessarily takes place over very large volumes of rock. Consequently, the increases in time-delays indicating accumulation of stress are visible at substantial distances (up to 240km before the 1996 Vatnajokull eruption, Volti & Crampin 2003), represent stress changes and are not precursory to earthquakes in the usual sense. Whereas the decreases in time-delays have only been seen at shorter distances and in one case was not observed at larger distances (**Gao & Crampin 2005**), and may be considered as directly precursory.

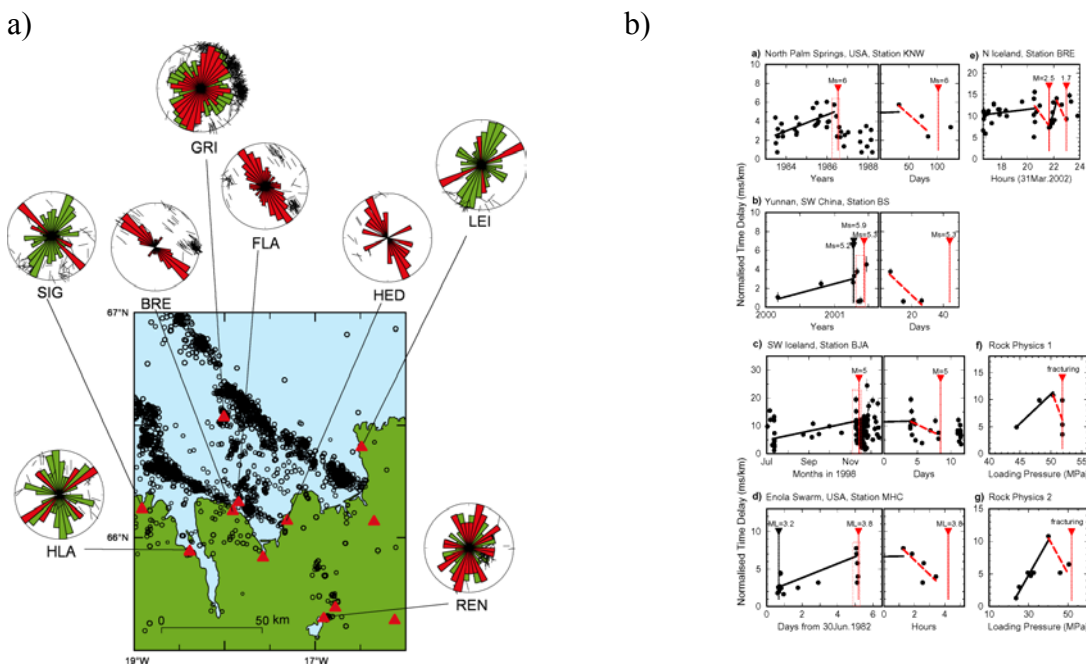


Figure 3. (a) Equal-area rose diagrams of shear-wave polarisations in north-central Iceland for 1996-2000 (green petals), and year 2001 (red petals) when BRE, FLA, and HED began operating, showing NE-SW orientations for all except BRE, FLA, and HED, which show 90°-flips caused by critically-high pore-fluid pressures on the Húsavík -Flatey Fault (Crampin *et al.* 2002). (b) Precursory decreases (in red) in shear-wave splitting time-delays now thought to be caused by crack coalescence immediately before earthquakes (Gao & Crampin 2004).

8) Whereas previously, evidence suggested that changes in shear-wave splitting were generally pervasive, it now appears that changes in shear-wave splitting can be shadowed by, for example, heavily fractured faults. The  $M_{4.9}$  16<sup>th</sup> September 2002 50km NW of Grímsey Island showed increases of time-delays at Station FLA, on the north side of the major Húsavík-Flatey Fault (HFF). In contrast, Station BRE, on the other side of the HFF, 4km south of FLA, did not show changes in shear-wave splitting. This is attributed to BRE being in the shadow of the heavily fractured HFF (**Gao & Crampin 2005a**).

9) As part of the general review of shear-wave splitting, **Crampin & Gao (2005a)** reviewed the first 25 years of the biennial International Workshops on Seismic Anisotropy (OIWSA – 12IWSA). These IWSAs have been crucial in the rapid advance of particularly shear-wave splitting in both

exploration and earthquake seismology. (IWSAs were initially founded by Stuart Crampin and Eugenie Chesnokov.)

### **Semi-Automatic reading and measurement of shear-wave splitting**

10) **Crampin & Gao (2005b)** review techniques for analysing and measuring shear-wave splitting. The original intention of WP2.5 was to develop Artificial Neural Network (ANN) analysis to analysis shear-wave splitting on three-component seismograms. Preliminary analysis indicated that ANN techniques were not likely to successful. Consequently, an Expert Analysis System (**Hao et al. 2005**) was developed, together with a user-friendly computer screen adjustment, leading to a Shear-Wave Analysis System (SWAS) (**Gao et al. 2005**), which is believed to be a major breakthrough in making analysis of shear-wave splitting more readily accessible to the general seismologist.

### **The Earth as a critical system of fluid-saturated stress-aligned microcracks**

11) The reason for these remarkable advances is that the fluid-saturated stress-aligned microcracks pervading most rocks are so closely spaced that they are critical systems verging on fracture-criticality and fracturing (**Crampin & Chastin 2003**). Critical systems have remarkable properties including: “butterfly wing’s” sensitivity to small changes; the statistics of the behaviour near criticality is more similar to that of other critical systems than it is the underlying sub-critical physics; consequently the deformation of fluid-saturated cracks near fracture-criticality can be modelled by Anisotropic Poro-Elastic (APE) (Zatsepin & Crampin 1997; Crampin & Zatsepin 1997). APE-modelling matches a large range of different phenomena concerning shear-waves, cracks, and stress (**Crampin & Chastin 2003**).

### **References**

(NOTE THAT AUTHORS OF PAPERS SUPPORTED BY PREPARED ARE IN bold-face type.)

**Crampin, S. & Chastin, S.**, 2003. A review of shear-wave splitting in the crack-critical crust, *Geophys. J. Int.*, **155**, 221-240.

**Crampin, S. & Gao, Y.**, 2005a. A quarter century of International Workshops on Seismic Anisotropy (0IWSA – 12IWSA): a historical review of anisotropy in the crust *The Leading Edge*, submitted.

**Crampin, S. & Gao, Y.**, 2005b. A review of techniques for measuring shear-wave splitting above small earthquakes, *Geophys. J. Int.*, submitted (GJI-05-0284).

Crampin, S. & Zatsepin, S. V., 1997. Modelling the compliance of crustal rock: II - response to temporal changes before earthquakes, *Geophys. J. Int.*, **129**, 495-506.

Crampin, S., Volti, T. & Stefánsson, R., 1999. A successfully stress-forecast earthquake, *Geophys. J. Int.*, **138**, F1-F5.

Crampin, S., Volti, T., Chastin, S., Gudmundsson, A. & Stefánsson, R., 2002. Indication of high pore-fluid pressures in a seismically-active fault zone, *Geophys. J. Int.*, **151**, F1-F5.

**Crampin, S., Peacock, S., Gao, Y. & Chastin, S.**, 2004. The scatter of time-delays in shear-wave splitting above small earthquakes, *Geophys. J. Int.*, **156**, 39-44.

**Gao, Y. & Crampin, S.,** 2004. Observations of stress relaxation before earthquakes, *Geophys. J. Int.*, **157**, 578-582.

**Gao, Y. & Crampin, S.,** 2005. A further stress-forecast earthquake (with hindsight), where migration of source earthquakes causes anomalies in shear-wave polarisations, *Geophys. J. Int.*, **Fast Track**, submitted (GJI-05-0141).

**Gao, Y., Hao, P. & Crampin, S.,** 2005. SWAS: a Shear-Wave Analysis System for semi-automatic measurement of shear-wave splitting above small earthquakes, *Geophys. J. Int.*, submitted (GJI-05-0283).

**Hao, P., Gao, Y. & Crampin, S.,** 2005. An Expert System for measuring shear-wave splitting above small earthquakes, *Pure. Appl. Geophys.*, submitted.

Volti, T. & Crampin, S., 2003. A four-year study of shear-wave splitting in Iceland: 2. Temporal changes before earthquakes and volcanic eruptions, in *New insights into structural interpretation and modelling*, ed. Nieuwland, D. A., *Geol. Soc. Lond., Spec. Publ.*, **212**, 135-149.

**Wu, J., Gao, Y., Crampin, S., Volti, T. & Chen, Y.-T.,** 2005. Smaller source earthquakes and improved measuring techniques allow the largest earthquakes in Iceland to be stress-forecast (with hindsight), *Geophys. J. Int.*, **Fast Track**, submitted (GJI-05-0289).

Zatsepin, S. V. & Crampin, S., 1997. Modelling the compliance of crustal rock: I - response of shear-wave splitting to differential stress, *Geophys. J. Int.*, **129**, 477-494.

## **Socio-economic relevance and policy implications**

The socio-economic relevance of progress towards predicting (stress-forecasting) earthquakes is fundamental to the security of life, culture, and livelihood in extensive parts of the world. The work reported in this section is believed to represent a significant advance in designing techniques for stress-forecasting the times and magnitudes of large earthquakes.

## **Discussion and conclusions**

The research supported by WP2.5 stimulated several significant advances in understanding and interpreting shear-wave splitting (see the eleven advances listed in Item b, above). Many of these are of fundamental important, but the three major advances relevant to the aims of the PREPARED Project are:

- 1) The improved earthquakes catalogue listing earthquakes down to  $M 0.0$ , would have allowed the large June 2000 events to have been stress-forecast;
- 2) The improved catalogue shows distinctive six-month and one month quiescence before the June 2000 events.
- 3) A Shear-Wave Analysis System (SWAS) has been developed for the semi-automatic analysis and measurement of records of shear-wave splitting. This is believed to be a significant advance which will open shear-wave splitting to the general seismologist.

However, a major result for geophysics is that the WP2.5 research has confirmed that the fluid-saturated stress-aligned microcracks in almost all rocks are so closely spaced they are critical-systems (with “butterfly wing’s” sensitivity). This has the major implications that low-level pre-fracturing deformation can be monitored with shear-wave splitting, future behaviour calculated by

APE, future behaviour stress-forecast/predicted, and at least in some circumstances future behaviour controlled by feedback.

## **WP 3 Short-term changes/precursors**

### **Objectives**

Analysis of observed short-term changes in various measurements, especially before the large earthquakes. Test and develop multidisciplinary short-term warning algorithms.

### **Methodology and scientific achievements related to workpackages including contribution from partners**

The input here is basically analysis and deliverables of WP3.1 and WP3.2. Also related deliverables from several other workpackages of the project which provide results applicable for developing new warning algorithms, such as WP2.1, WP2.2, WP2.3, WP2.5, WP4.1, WP5.5 and WP6.2.

The work here during the last 6 months of the project has been writing up results and discussions about how to interpret the observations and how to make them useful for alerting purposes.

The special PREPARED section at the EGU General Assembly in Vienna April 24-29, 2005 and a special PREPARED meeting after the EGU conference as well as a special fusion meeting in Reykjavik on July 12, were significant forums for discussion and comparison of results.

### **Socio-economic relevance and policy implication and future plans**

The prospects that it may be possible to warn ahead of earthquakes has become more evident during this last part of the project and by comparing results. Short-term alert tools have been demonstrated and methods for visualizing crustal processes leading to earthquakes.

Much work is ahead in preparing these tools for implementation in active warning procedures and statistically testing their significance. Much work is also ahead in further evaluation of the results and further modelling work. Advices for research policy and monitoring methods are also a significant continuation of the work.

### **Discussion and conclusions**

The main work in this workpackage was to create and edit tools on short-term hazard assessments or warnings based on results from various other WP's. Much progress has been made in this as described in the Final Report.

Progress in the various involved WP's provides various examples of observable processes approaching the 2000 earthquakes. Modelling work emphasizes that understanding of fluid migration and of high porous fluid pressures is of fundamental significance in providing the observed forerunning signals.

### **Deliverable**

Stefánsson R. & G.B. Guðmundsson 2005b. Ahead of the earthquake: Assessment of where, how and when. *Icelandic Meteorological Office – Report*. In press.

## **WP 3.1 Foreshocks and development of warning algorithms**

**Author: Ragnar Slunga**

This work package is dedicated to analyse the processes leading to earthquake nucleation by use of the microearthquake observations. This will then be used in short term earthquake warning algorithms.

The work has been concentrated to improve the previous EQWA (earthquake warning algorithm) given by Slunga (2003). The main new invention is the inclusion of stress estimates based on single event fault plane solutions. The FPS are estimated by use of impulse method (low frequency spectral amplitude method) given by Slunga (1981, 1982) and described by Roegvaldsson and Slunga (1993). The quality of the FPS is of major importance to reduce the scatter caused by bad FPS. Note that only microearthquakes for which at least one first motion direction is given can be included.

The inclusion of FPS in the EQWA is based on the view that asperity breaking is related to the late foreshock activity. A distorted stress field is expected around the locked part including volumes of highly increased stresses. The probability to observe FPS indicating high stress levels will thus increase around the asperity and hopefully especially when the breakdown starts.

The EQWPs (earthquake warning parameters) tested before the coming implementation of the EQWA into the Icelandic system are defined as  $-\log(P)$  where  $P$  is the probability to have the observed sequence of parameter values within a small space and time window (say 5 km and 24 hours).

As depth is a very important parameter, especially for the use of the observed stress tensors, the EQWP is estimated for different depth ranges. From the present study it looks like the major part of the precursory value of the microearthquakes comes from events at the depth of the nucleation and deeper. The nucleation depth varies between 3.5-7 km for the few larger EQ so far observed within SISZ.

In the following illustrations the stress level parameter, "1/b"-values, and some EQWPs based on a combination of a few parameters are shown.

Large part of the work has been spent on preparing the implementation of completely automatic on line algorithms into the Icelandic system. These algorithms will produce parameter observations, estimate the probabilities to have the observations, and EQWP for different depths. These can be reviewed by seismologists and observations of alarming nature can be linked to ring bells for the seismologist.

In conclusion the results are promising and both the EQWPs and the stress level observations and other precursory parameters are expected to become of value for the earthquake warning procedures in Iceland.

The progress of the work has continuously been reported in seminars and conferences, Slunga (2003b,c, 2004a,b,c, 2005). Details of the algorithms will be found in two papers under preparation (Slunga (1 and 2)).

## Illustrations of the stress level parameter

As discussed above we expect to observe events with FPS indicating high stress levels close to asperities and being an indicator that the asperity is starting to break. The stress level parameter I use is the mean of the three principal stresses divided by the vertical stress which is assumed to equal the lithostatic stress. The value of this parameter is checked by looking on the observations before the major earthquakes we have had within the network in Iceland.

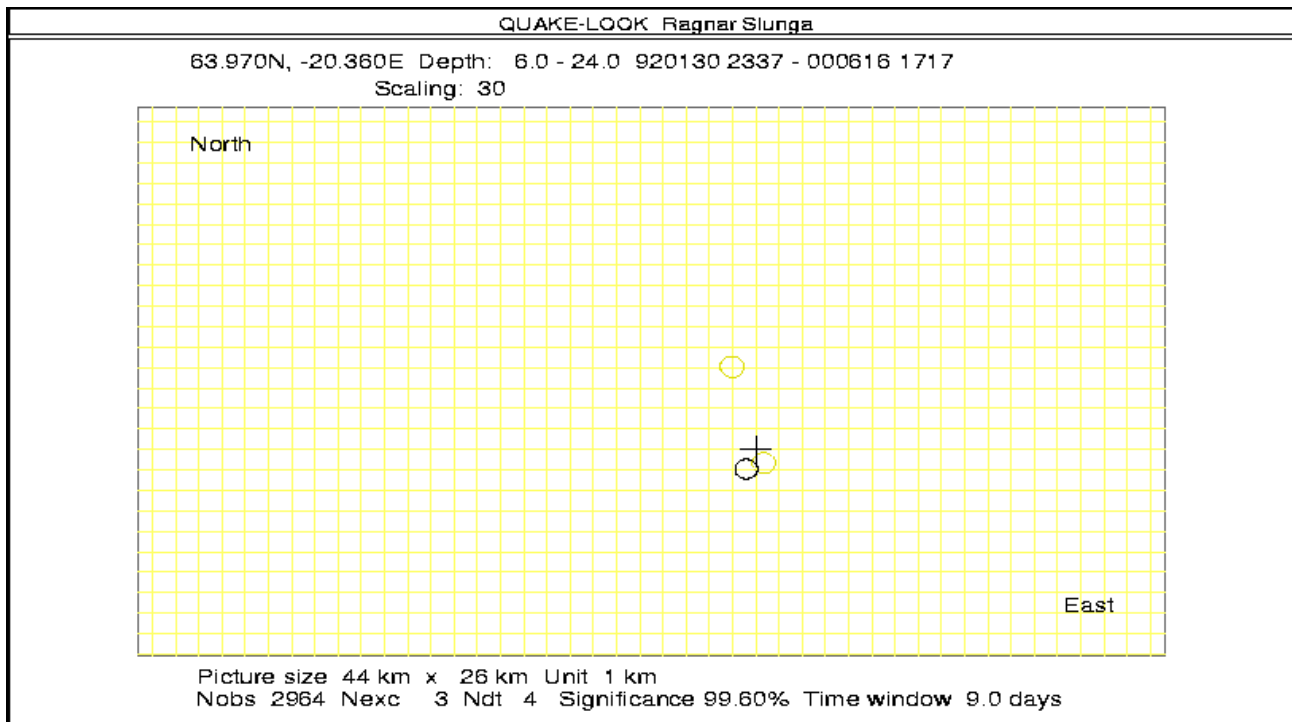


Figure 1. A map over the SIL area, 44 km times 26 km. The circles mark stress level observations (the mean of the principal stresses divided by the lithostatic stress) as given by single event FPS. The depth range is 6-24 km. The time period is 19920101-20000817 1540. The black circle marks the highest stress level observed during the last 9 days of the time period. Only those of the 2964 observations within the map, depth range and time period having equal or larger stress levels than the black one are marked. It is only two. The circles are scaled according to the stress level, denoted 30 in the figures. The coordinates given in the figure are for the black cross. See further the text.

Figure 1 is a map, 44 times 26 sqkm covering the SIL area around the two large earthquakes 2000, June 17 and June 21. The epicenter of the June 17 EQ is marked by a cross. The time period included is Jan 1 1992 to GMT 1530 June 17 2000, about 8.5 years. The number of stress level observations within the map and within the time period and in the depth range 6-24 km is 2964. Note that all events are not giving stress estimates as at least one first motion direction is required. The largest observation within a time window of 9 days before the end of the time period is marked by the black circle and occurred 3.3 days before the EQ and less than 1.5 km from the epicenter. The value of the stress level of that event is used as a threshold for including the observations in the figure. Only two additional such high stress values in this depth range was found. The positions of those events are marked by not black circles. The size of the circles are scaled according to the stress level sizes. The number Ndt in the figure gives the number of events (observations) as close or closer to the epicenter as the black circle and at later times. If the stress value estimate for each event is random the probability that a single event equals or exceeds the black event value can be estimated to be  $3/2964=0.0010$  or 0.1%. Now we have 4 events as close in time and space as the

black one which means that the probability that none of them would have such a high value by randomness is 99.6%.  
 Only in 4 cases of 1000 would such a good agreement between theoretical expectations and random observations be expected.

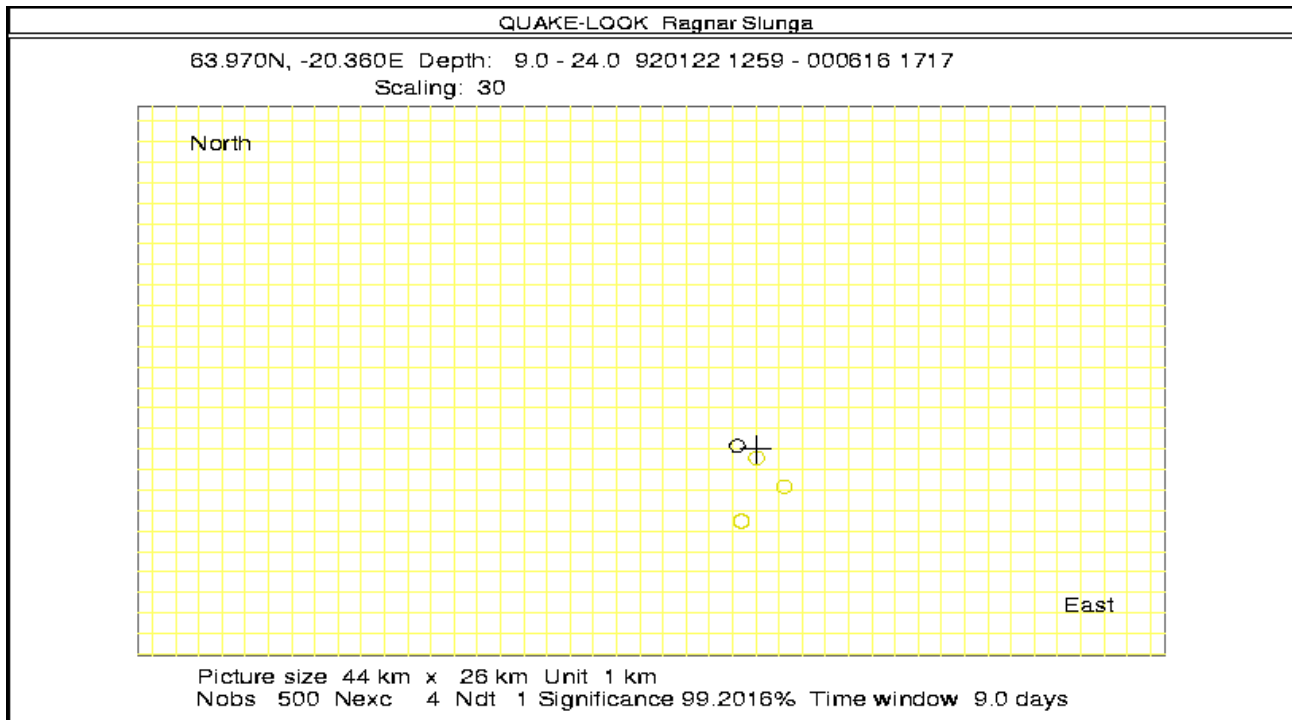


Figure 2. The same as figure 3.1.01 but for the depth range 9-24 km. See the text.

The figure 2 further increases the total significance. The difference from figure 1 is the depth range which is changed to 9-24 km. Notice that a high stress value is associated with another event marked by black and again a high significance, 99.2%, is observed. The lower significance in this case is due to the fact that only 500 observations were available at this greater depths.

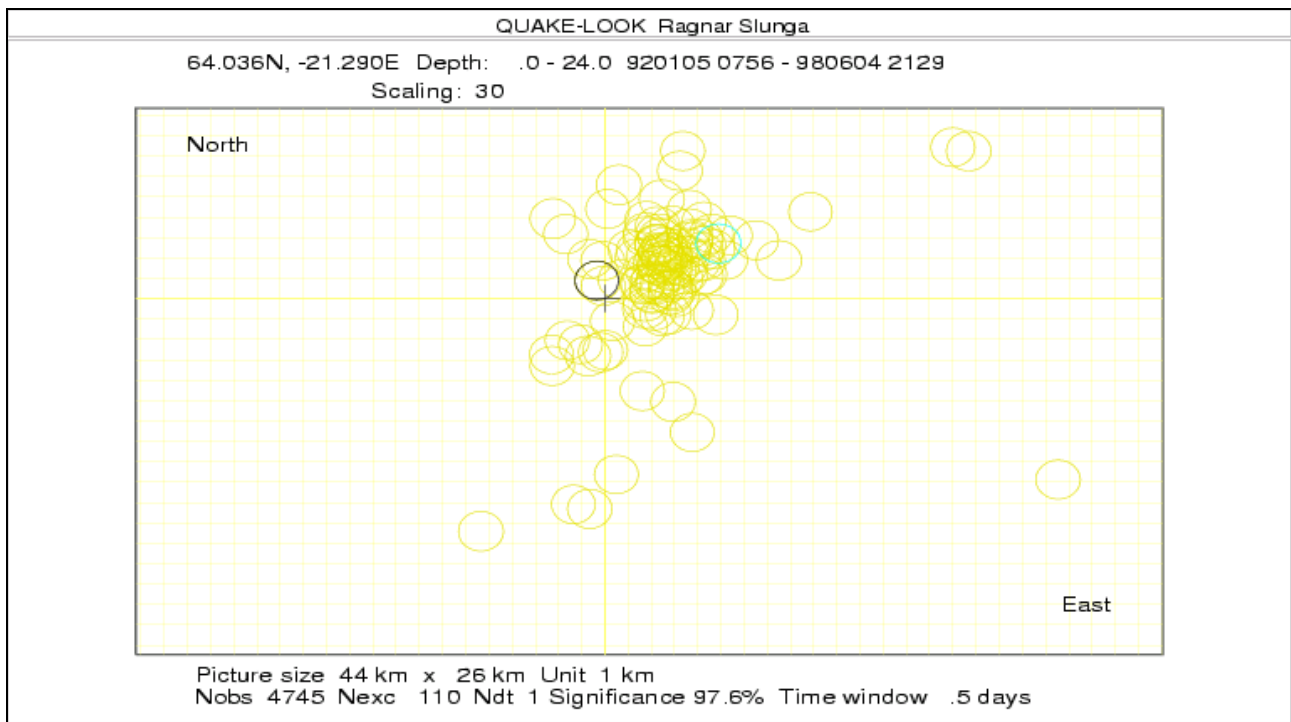


Figure 3. *Similar to the previous but now showing the Hengill area and the time period before the June 4 1998 EQ. Again the scaling 30 means that the stress level is shown.*

Another case is shown in figure 3 which is a map of the Hengill area. During the time period Jan 1 1992 to GMT 2130 June 4 1998 44463 events gave stress estimates. The cross in the figure shows the epicenter of the GMT 2136 June 4 1998 Hengill EQ. The black circle marks the largest stress level observation within the map and within 12 hours before the EQ. In this case only the largest stress observations for each time period of 12 hours were plotted, 4745 such observations. 110 such observations gave then a significance of the size of the stress observation during the last 12 hours of 97.6%. In addition the observation is very close to the epicenter which can be used to further increase the significance.

Further to the west from Hengill an EQ occurred GMT 0200 Aug 23 2003. Although it was not as large as the Hengill EQ it is interesting because of the relative lack of foreshocks. Figure 4 shows a map of the area with the cross marking again the EQ epicenter. The black circles mark the events during the last week before the EQ and they are scaled according to stress level. The other circles mark previous activity also scaled with stress level. Even if all three events closest to the epicenter all show fairly large stress levels this case is not significant (76.3%). However the stress level observation seems to be the best one of all so far tested precursor parameters for this minor EQ.

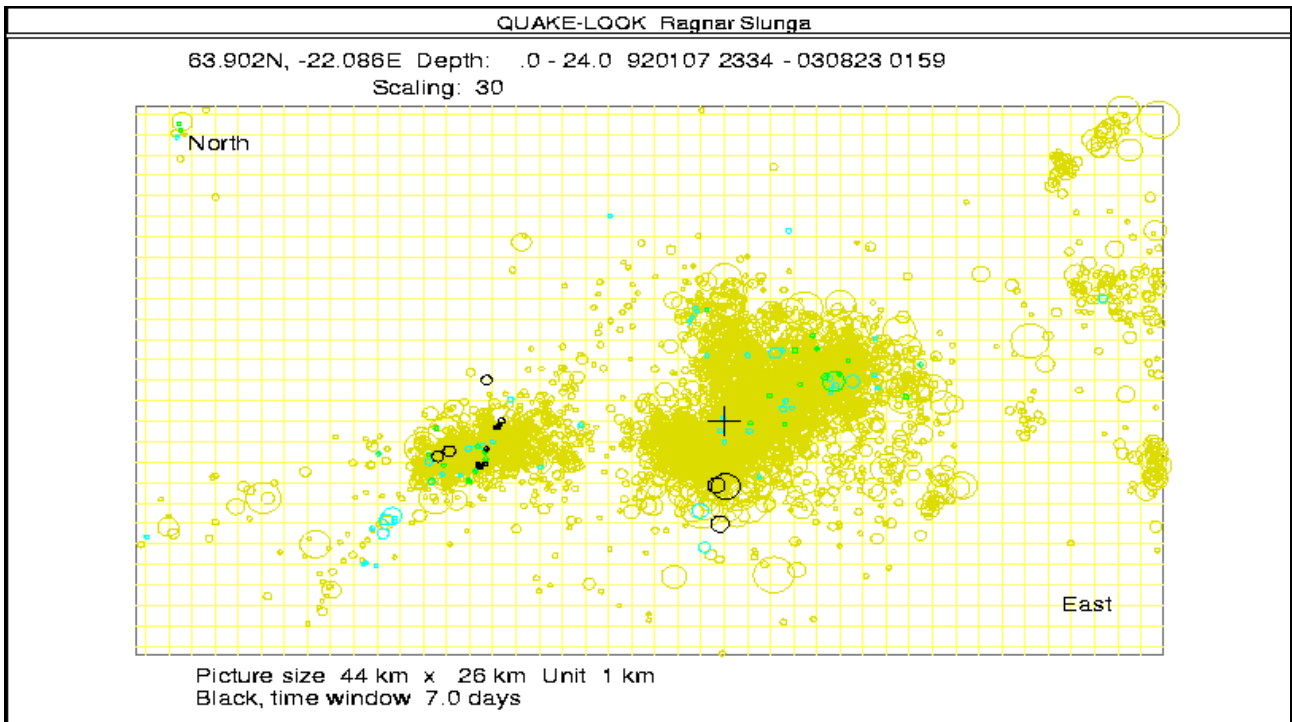


Figure 4. This figure show all observations of the stress level (single event values) within an area west of Hengill. The cross is the epicenter of the Aug 23 2003 EQ. The black circles were observed during the last 7 days of the period. Note that the three black circles closest to the cross also are the largest ones of the black which is a little positive. See the text.

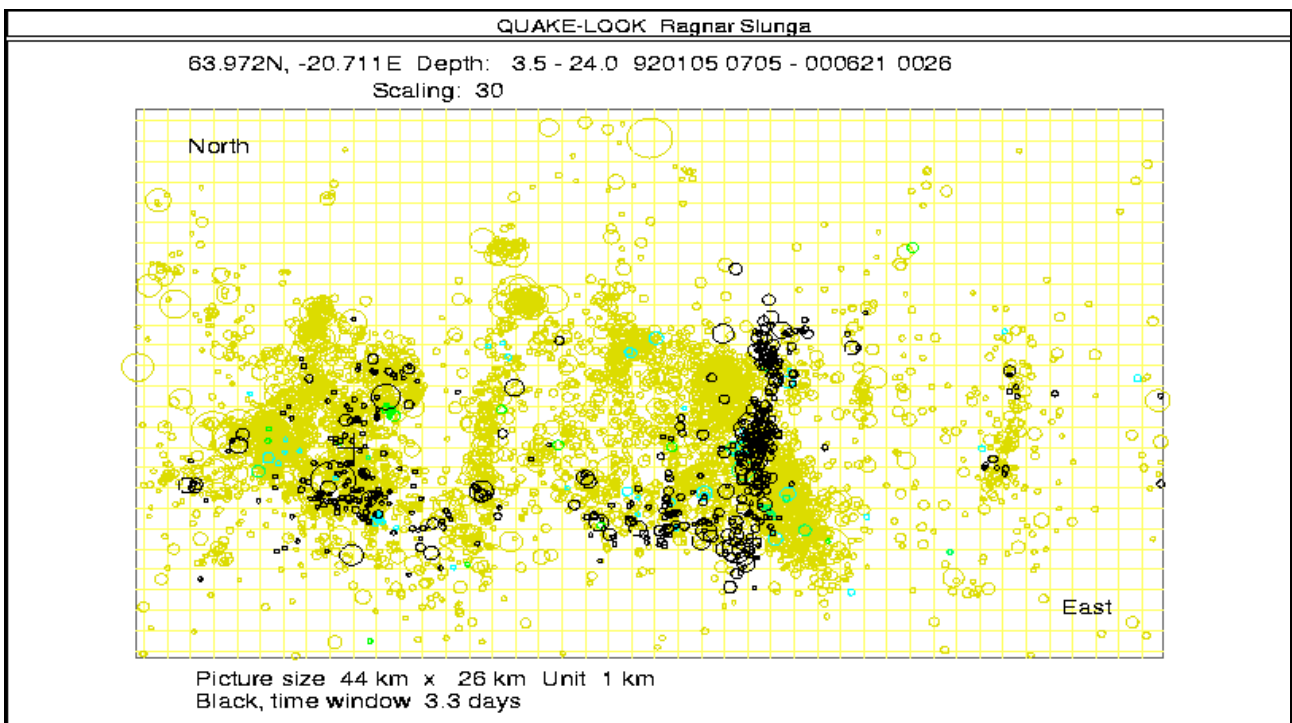


Figure 5. Similar to figure 3.1.04 but showing the SIL area and the cross marks the epicenter of the June 21 2000 EQ. The black time period is 3.3 days, almost the whole time between the June 17 and June 21 EQs. Again the stress level is given by the scaling. See text.

Finally figure 5 shows again the SIL area for the time period Jan 1 1992 to GMT 0030 June 21 2000. The cross marks the epicenter of the large earthquake GMT 0030 3.35 days after the large June 17 EQ. The black circles marks all stress observations for 3.3 days before the June 21 EQ. Again scaled according to estimated stress level. The aftershocks along the fault of the June 17 EQ forms the lineament 18 km east of the epicentrum. The not black circles mark previous observations, each observation given by one microearthquake. Note the three fairly large stress estimates close to the cross. In figure 6 only stress estimates exceeding the largest "black" stress are shown. Of 5950 events (observations) only two additional exceeds the black circle which again gives a high significance to the stress level parameter, 99.3%.

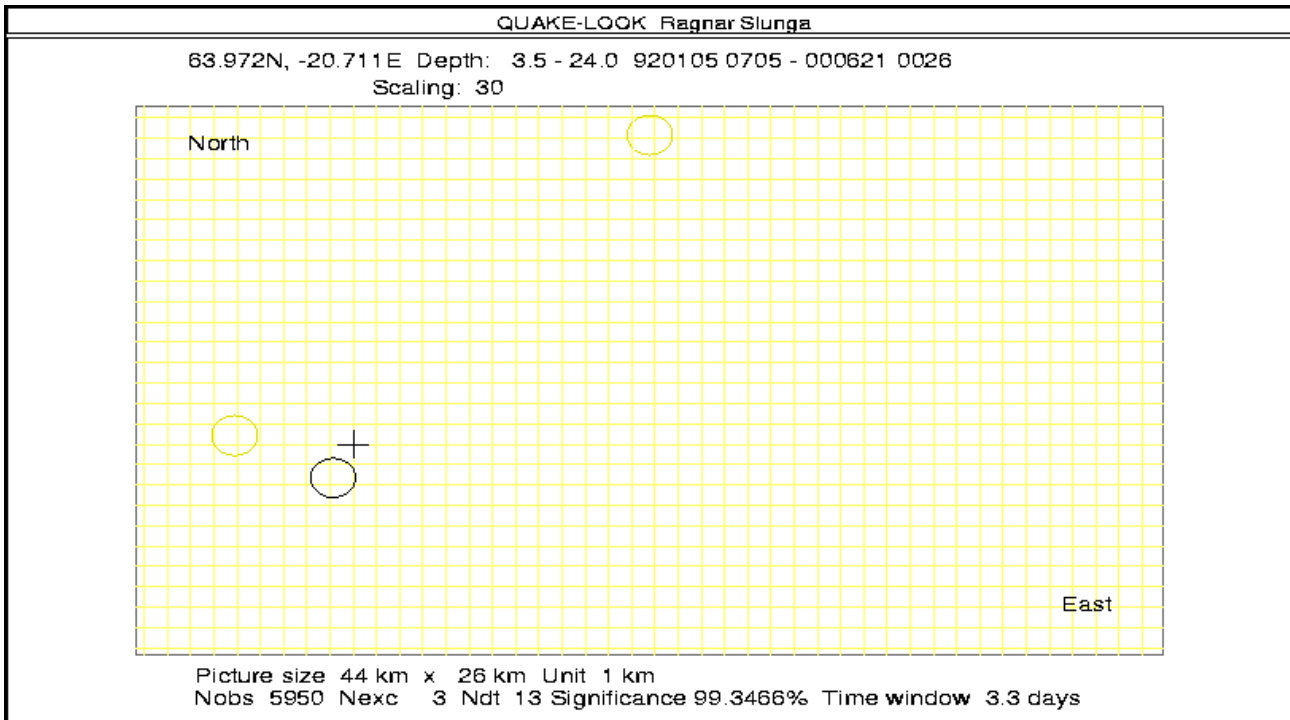


Figure 6. The same as figure 5 but now only the stress level observations exceeding the largest black observation are shown. Only twice in the period 1992 - June 21 2000 has that observation been equaled or exceeded. See text.

In conclusion the stress level estimate based on single event fault plane solutions (FPS) is of enough quality to be of precursory value. The start of the breaking of strong asperities is expected to detected prior to the EQ if microearthquake information (including FPS) is available.

### "1/b"-values

Small b-values have been interpreted as indications of high stresses. This is strongly supported also by the work within WP3.1. However, as WP3.1 is concerned with short term warning and one typically wants groups of 50 events or more for good estimates of the b-value we use the denotation "b" or "1/b" for the parameter discussed here. The inverted value is used just for having a parameter expected to be large before the EQ. The parameter "1/b" is formally an estimate of 1/b but is based on groups of only 9-15 events.

Figure 7 shows "1/b" for the SIL area and the period Jan 1 1992 to GMT 1540 June 17 2000. The cross marks the epicenter of the major June 17 EQ at the end of the period. The black circle shows the largest "1/b"-value observations within the map and during the last 7 days and only observations larger than or equal to the black circle are shown. In addition only the largest observation for each

7-day period is shown giving a total of 442 observations. The significance in time is 97.5% but the closeness of the black circle to the epicenter increases the significance further. Figure 8 shows the same as figure 7 but now the depths are shown. The black circle is at 6-7 km depth, close to the point where the EQ rupture started. For this "1/b" value groups of 15 events were used.

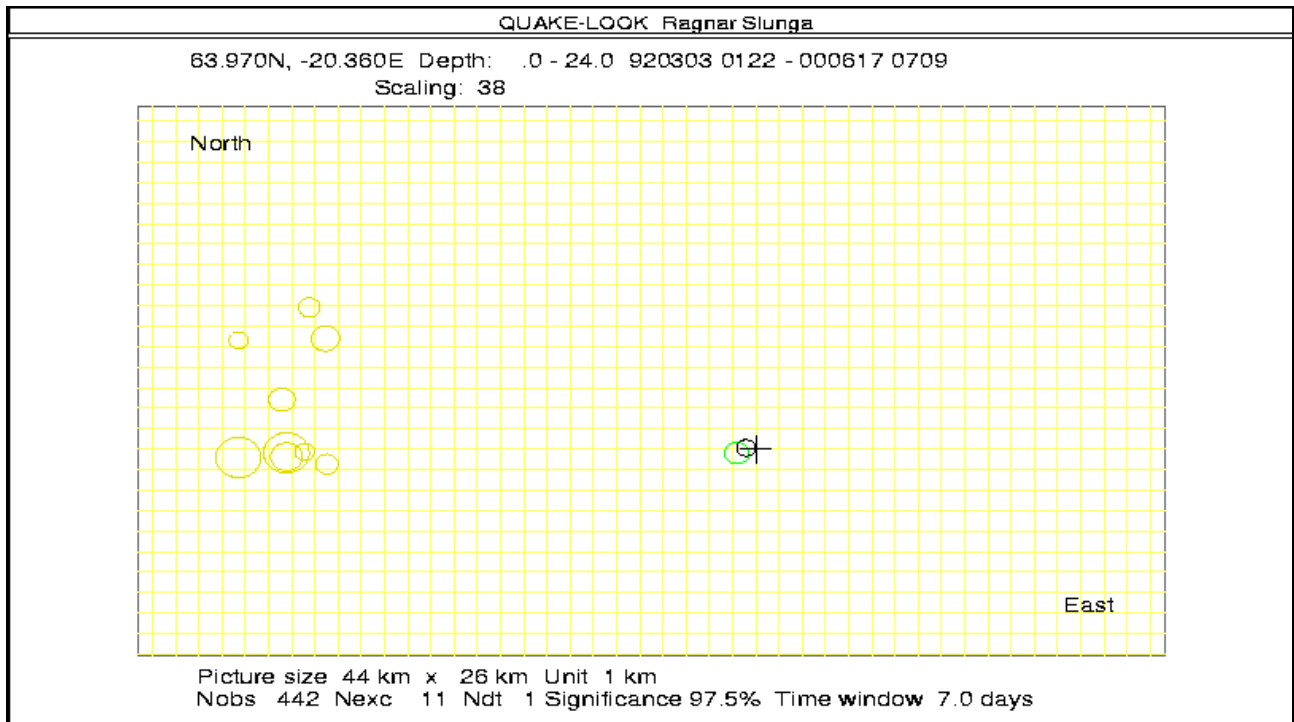


Figure 7. Similar to figure 3.1.01 but now scaled according to "1/b"-values instead of stress level. Only observations exceeding the black circle are shown. See text.

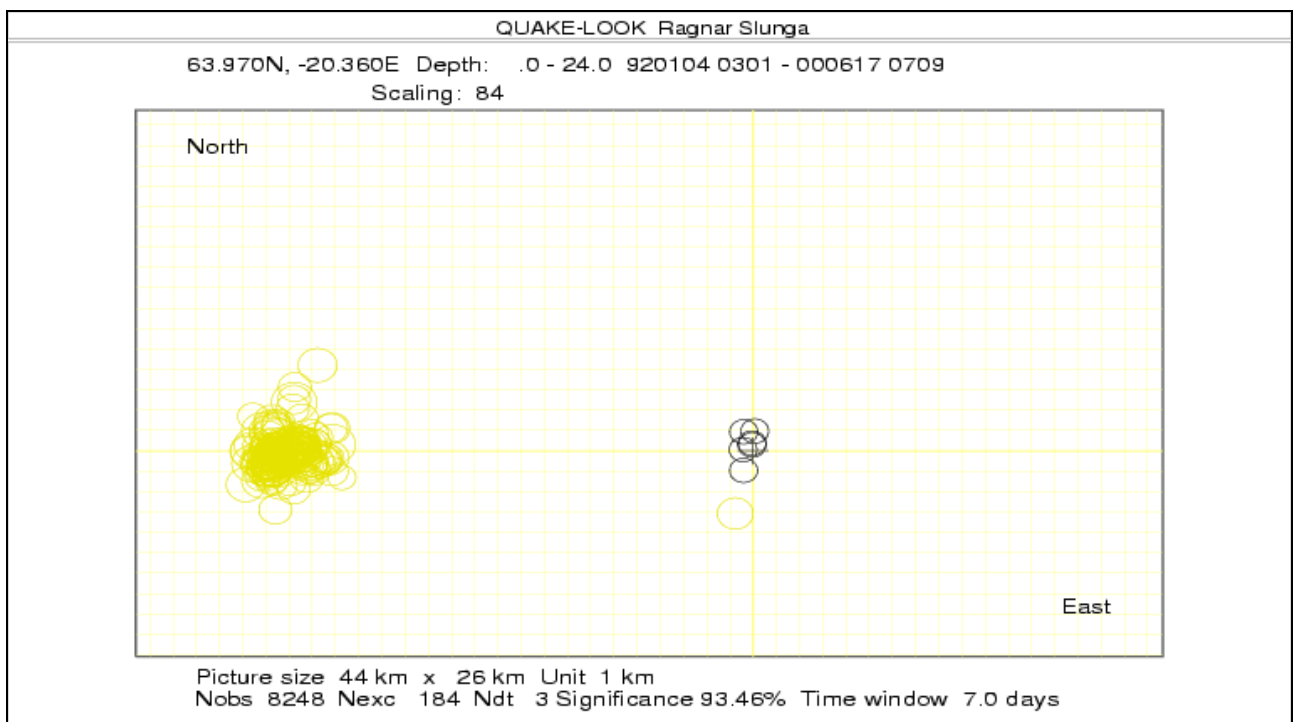


Figure 8. The same as figure 3.1.07 but now showing the depth section. The black observation is at the depth of the nucleation point of the June 17 2000 EQ.

## The EQWP (earthquake warning parameters)

The EQWP used in this presentation are based on stress level estimates, "1/b"-values, fault radius estimates, and activity rates. The parameters are labeled 80-86 associated with different upper depth ranges, 0, 3, 4, 5, 6, 7, 8km. Figures 9-11 show EQWP before the June 17 2000 large EQ. We see in figure 3.1.09 that all observations in the SIL area of EQWP 84 are close to the epicenter of June 17 EQ (marked with a cross) or to the epicenter of the June 21 EQ to the left. All black circles (within the last week) are around the cross. In figure 3.1.10 the same parameter is shown but now only one circle is given for each 7 day period (except for the black period) and the significance in time is 98.0%, three false alarm weeks during the 8.5 years. The significance is enhanced by the closeness to the epicenter of the black circles. Figure 11 shows the same area and period but for the EQWP 80, the figure is similar to 10 . When all shallow activity is included the significance drops due to the "noise" within the shallow activity.

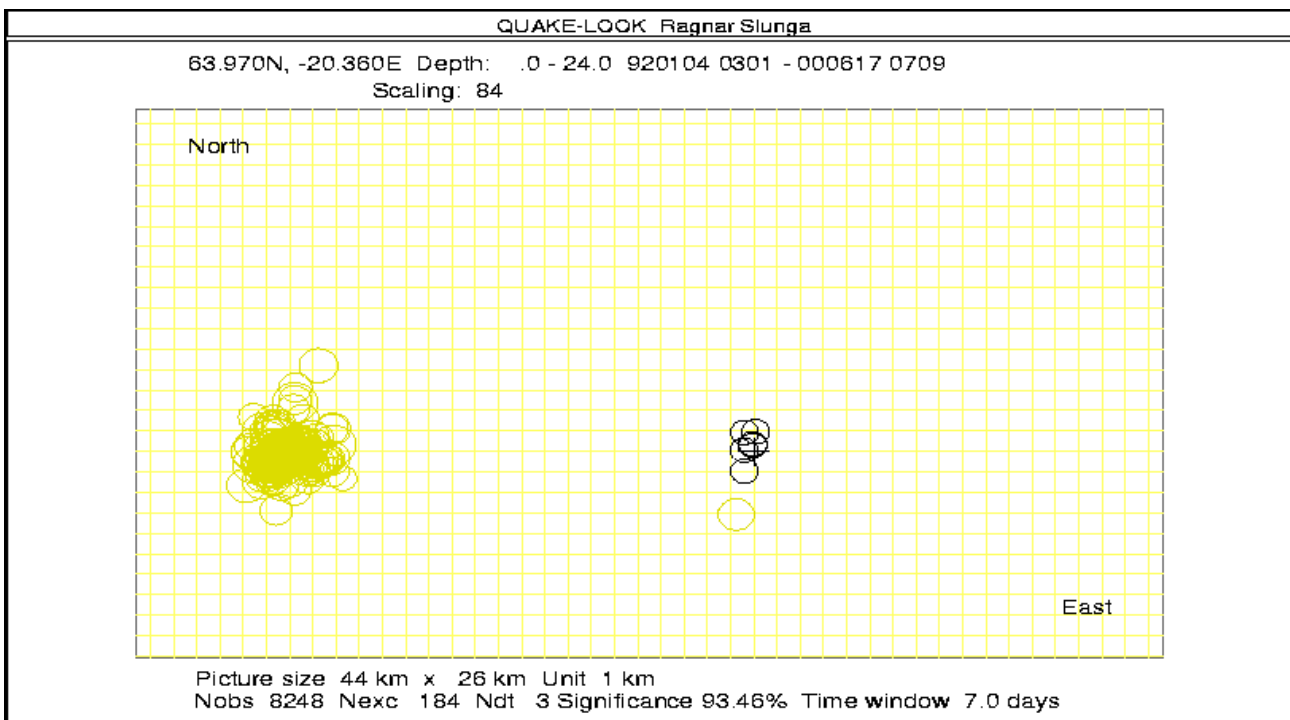


Figure 9. A map of the SIL area showing the EQWP 84 (see text) before the June 17 2000 EQ. The black are observations within 7 days before the EQ, only previous observations equal to or larger than the largest black circle are shown. Of the 184 exceedences most are within short time periods, see next figure. The cross mark the epicenter of the EQ.

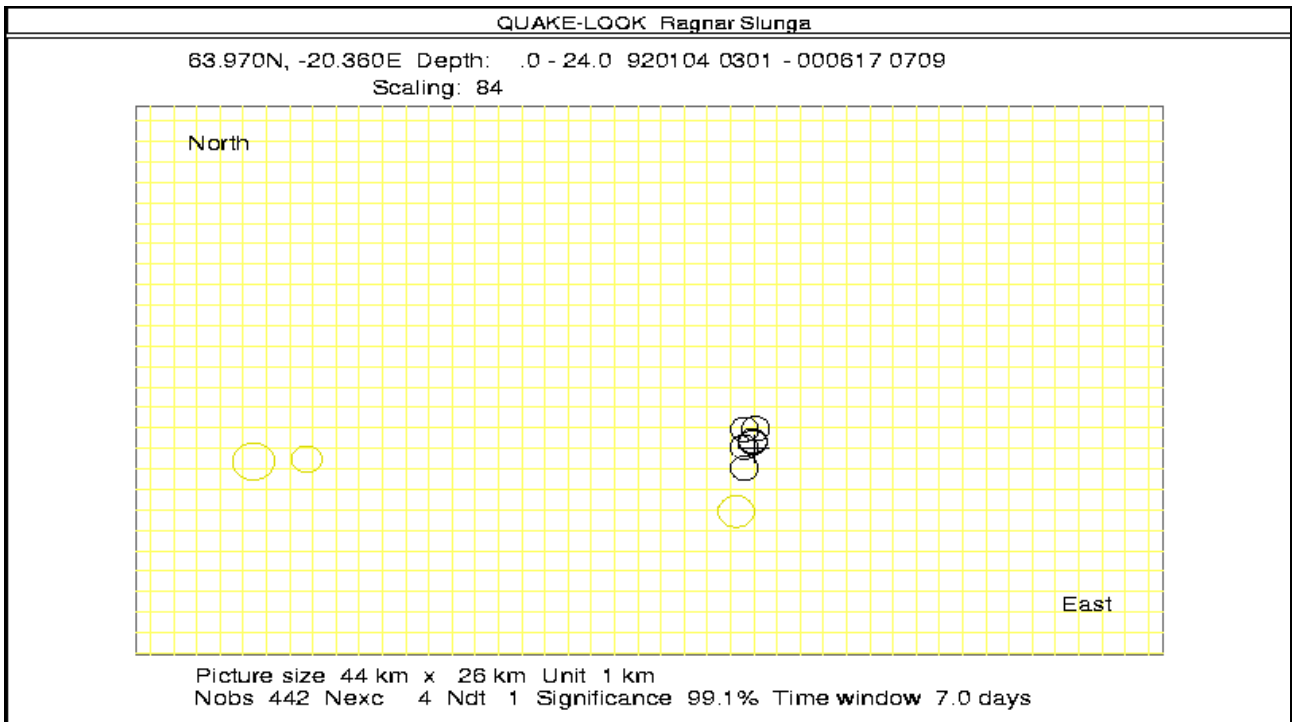


Figure 10. *The same as figure 3.1.09 but now only the first exceedence within a 7 day period are shown. Thus each not black circle marks an alarm period of one week. There are three false alarms, one at the epicenter of June 17 EQ and two close to the epicenter of the later June 21 2000 EQ. See text.*

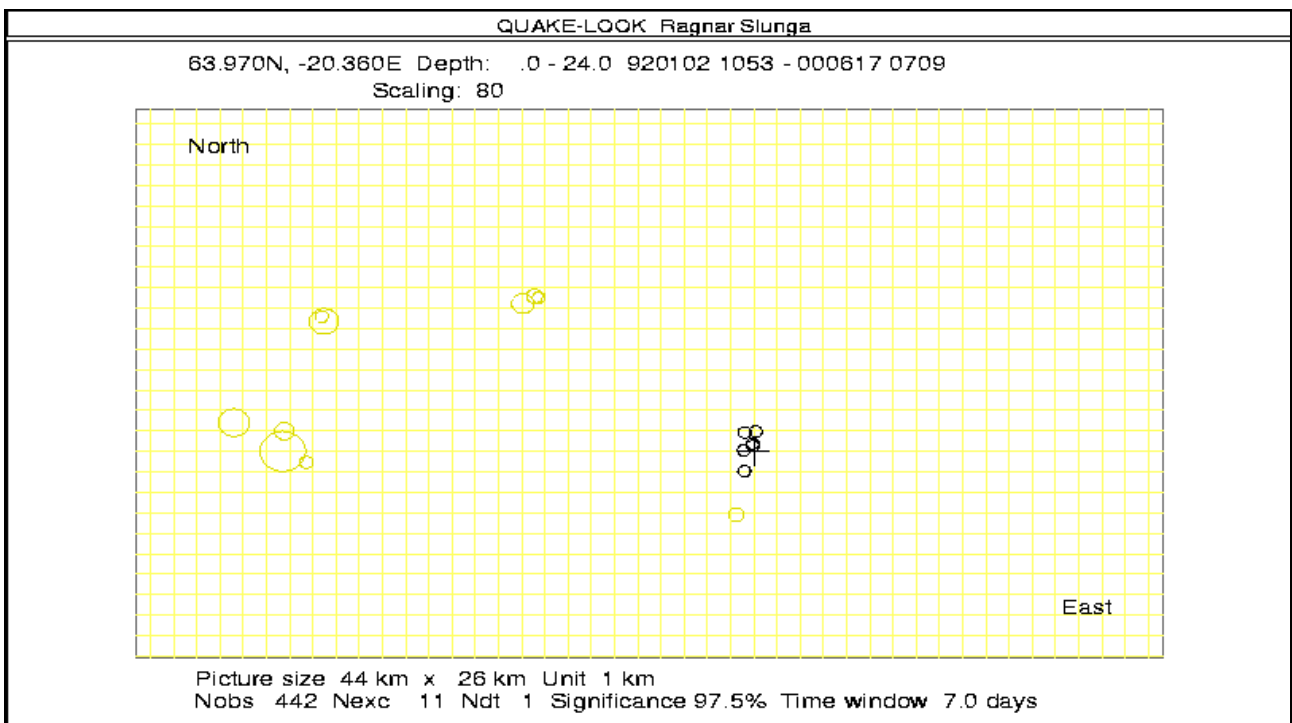


Figure 11. *The same as figure 3.1.10 but for the EQWP 80, see text.*

Figures 12-13 show the weekly picture of EQWP 80 and EQWP 81 for the Hengill EQ June 4 1998. This is a moderate size earthquake and the Hengill area showed an extreme activity from 1994-1998

causing several false alarms and this reduces the weekly significance to about 95%. However most of the alarms are rather close to the epicenter and often before and/or after ML=4 events.

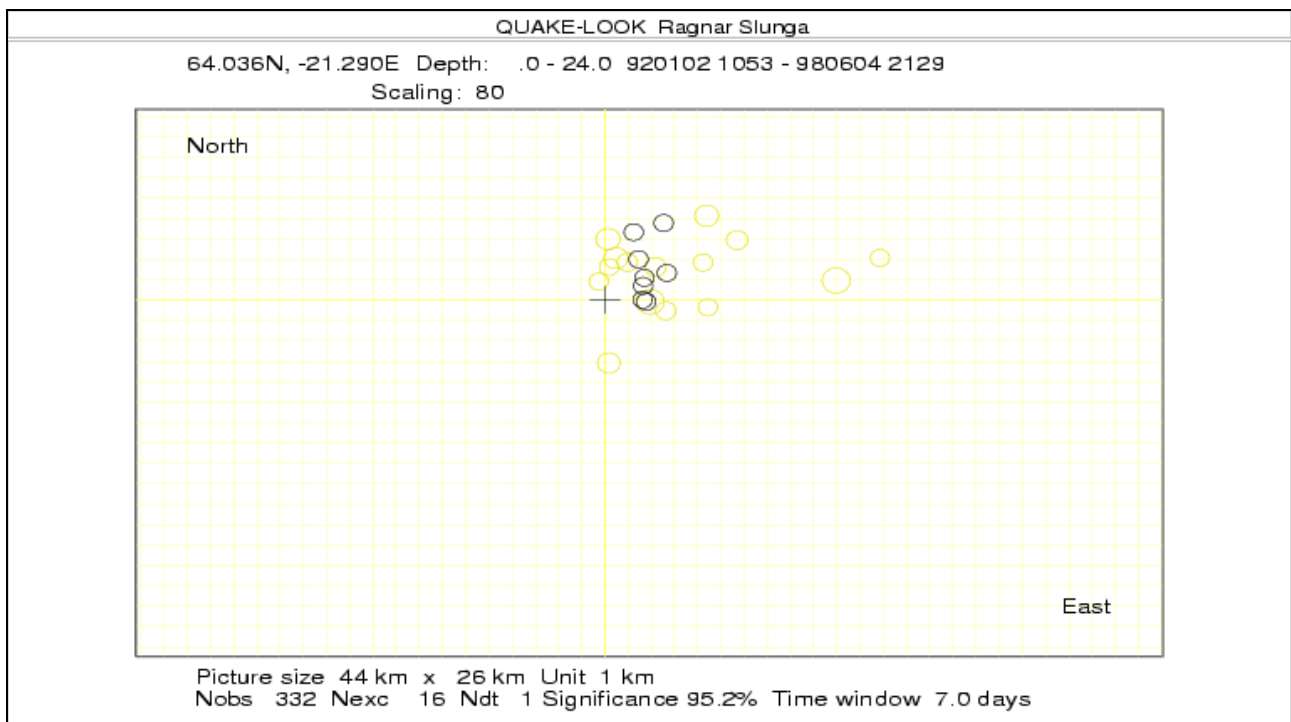


Figure 12. Similar to figure 3.1.10 but now the map covers the Hengill area and the time period is Jan 1 1992 to GMT 2130 June 4 1998. The cross marks the epicenter of the GMT 2136 June 4 1998 EQ. The EQWP 80 is shown. See text.

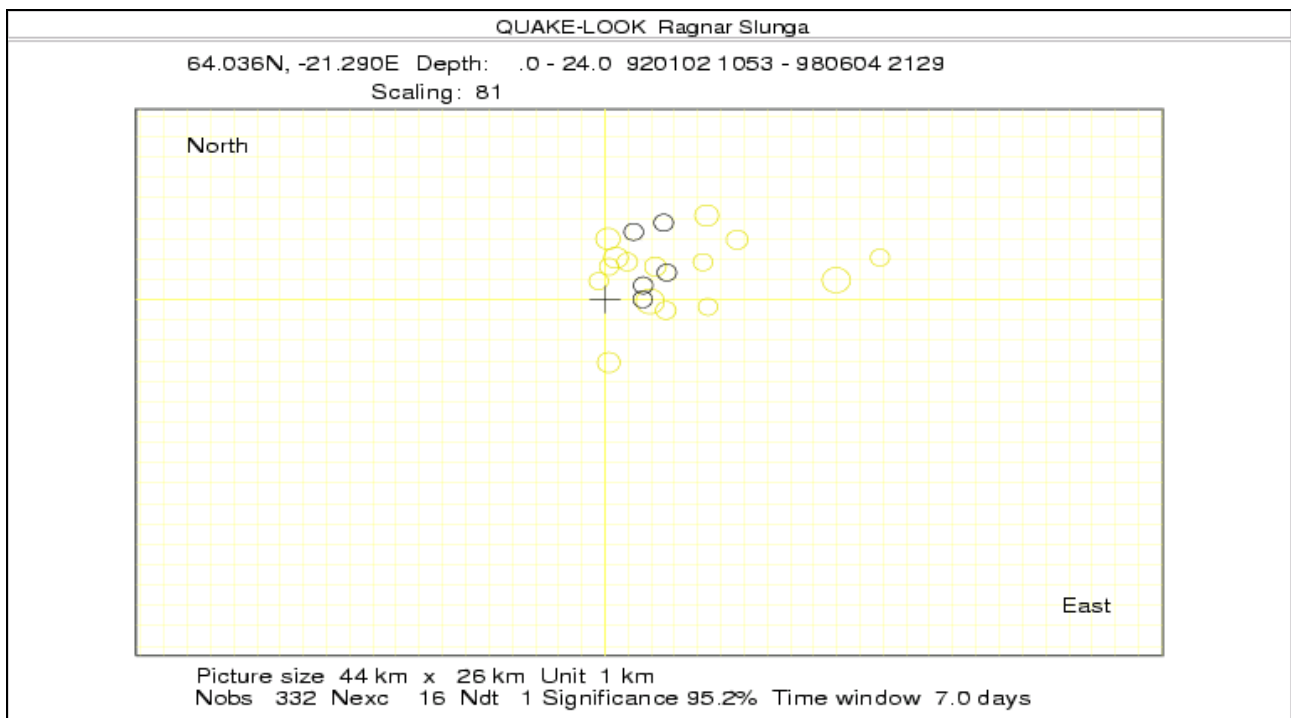


Figure 13. The same as figure 3.1.12 but showing the EQWP 81. See text.

Figure 14 shows the SIL area for the period Jan 1 1992 to GMT 0030 June 21 2000. The EQWP 86 (deep activity) is shown and the black circles are observations within 3.3 days of the large June 21 EQ. The cross marks now this EQ. We can see increased values of EQWP 86 just south of the cross. The EQWP 80 (including all activity) is shown in figure 15. The cross is within the central northern part of left cloud. The epicenter of the June 21 EQ is clearly marked and the aftershock activity causes false alarms along the fault of June 17 EQ.

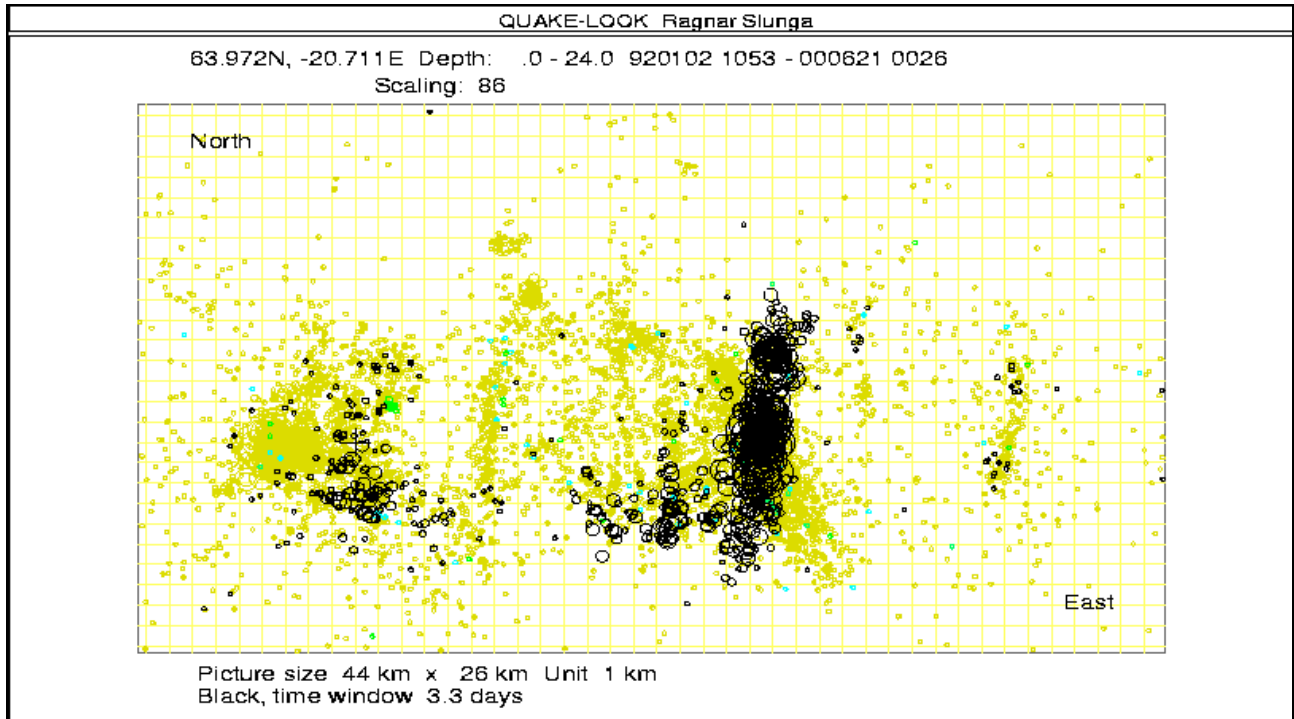


Figure 14. *The SIL area and the time period Jan 1 1992 to GMT 0030 June 21 2000. The cross marks the epicenter of the June 21 EQ. The deep EQWP 86 is shown and one can see slightly increased EQWP 86 south of the epicentre. The black circles mark observations during the last 3.3 days before the EQ. All observations are shown.*

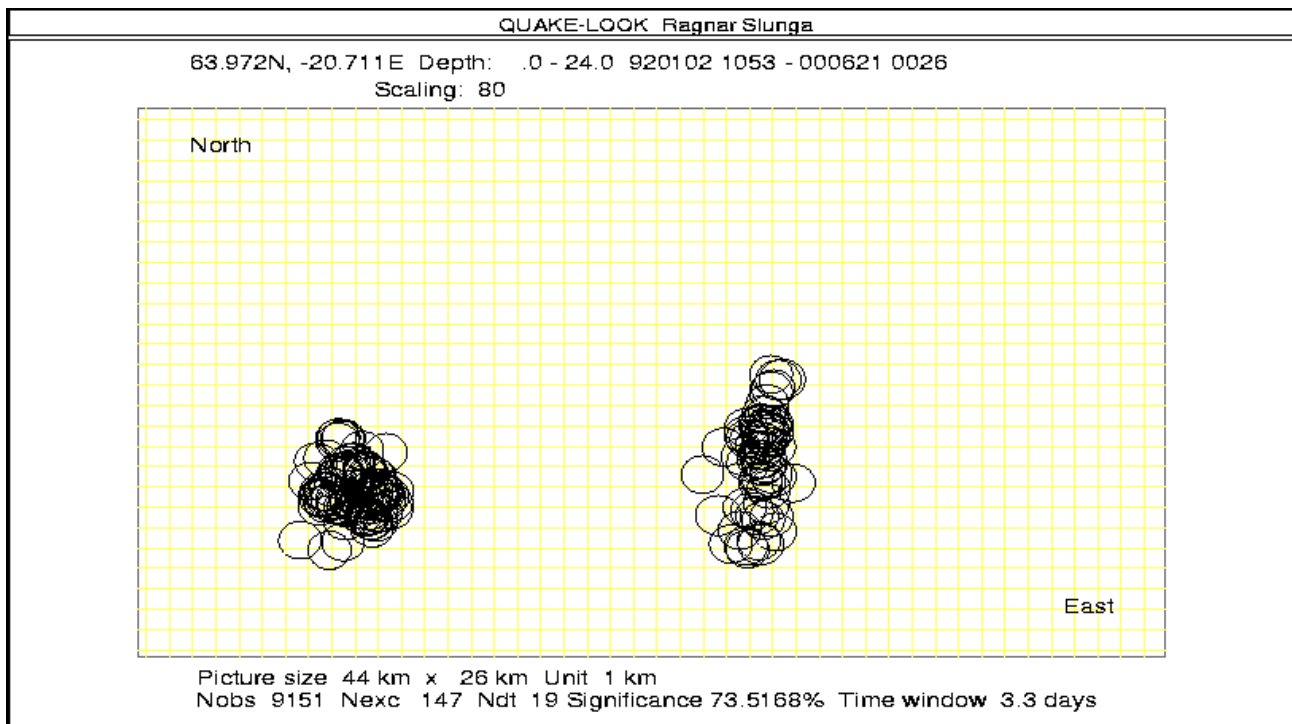


Figure 15. The same area and time period as in figure 3.1.14 but for EQWP 80. Now only observations of the largest sizes are shown. The cross is in the central part of the northern edge of the left cloud. It is quite clear where a second EQ can come, false warnings are produced along the fault of the previous EQ and are caused by the aftershocks in that highly disturbed area.

The August 23 2003 EQ of moderate size on the Reykjavik Peninsula did not cause any kind of prior alarm. Very few foreshocks occurred and the stress level seems to be the best precursory observation for this EQ, figure 4.

### The EQWP for the period up to June 30 2005

Figure 16-17 shows the EQWP 80 and 85 in the SIL area for the period Jan 1 1992 to June 30 2005. The black circles mark the largest observations during the two last years. The non black are previous observations. We see no indication of an earthquake coming soon in this area but, of course, there is so far no guarantee. Anyway this indicates a rather low false alarm rate.

Figure 18 shows the same for the western part of SIL and the Hengil area. The black cross marks the position 63.95N 21.00W. The black show the activity for the last year before June 30 2005. There are slightly increased observations of EQWP 82 7-8 km west of the cross. Note the rather high values early in this period at about the cross at 21W.

The EQWP 86 for TFZ north of Iceland is shown in figure 19 for the period Jan 1 1994 to June 30 2005. The cross marks the position 66N 18W. The black observations are within the last 5 months and is in the Husavik area. The levels are not alarming but rather high. Of the two largest EQ (less than ML=5) in this area only one (Sep 20 1997) was preceded by high EQWP 86 values. Most of the large values observed in this area are related to aftershock activity to ML=4 events. The station coverage is less good in this area than within SISZ which means more uncertain FPS.

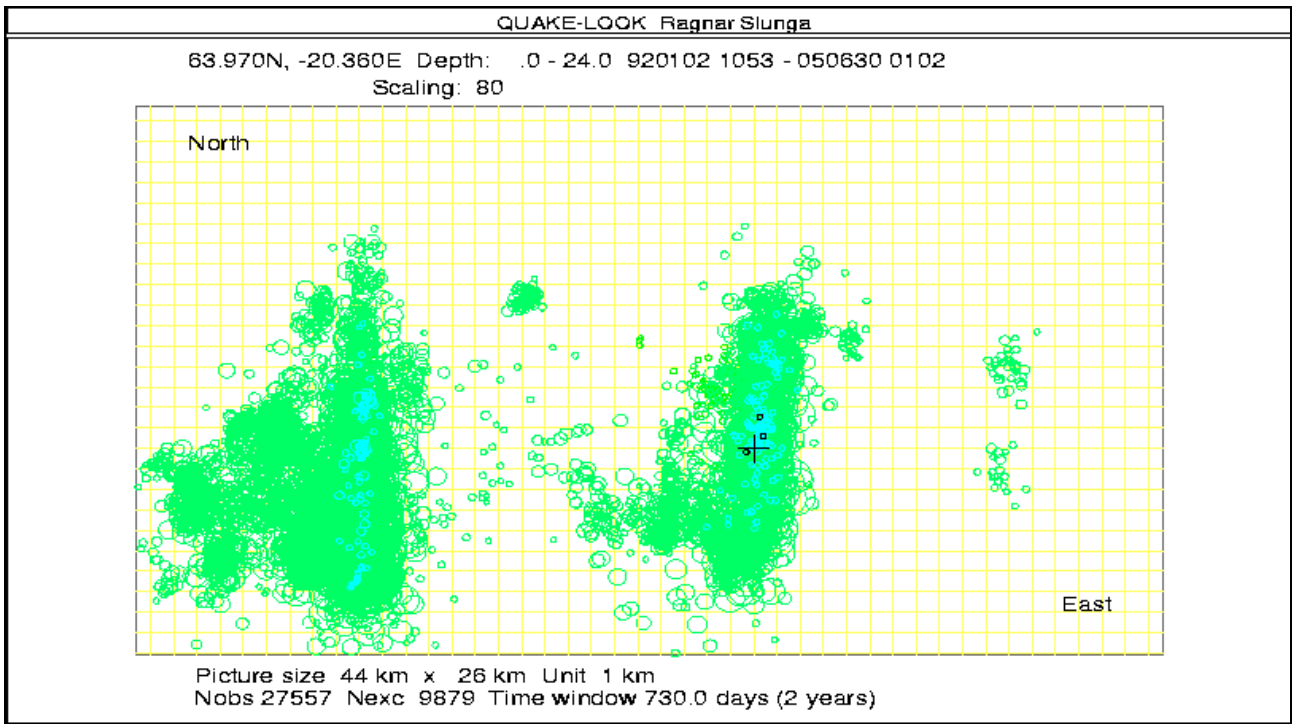


Figure 16. The EQWP 80 for the SIL area for the period Jan 1 1992 to July 1 2005. The black circles show the last two years of the period and only observations exceeding the black observations are shown. No false alarm for these two years and no indication for another EQ in this central area of SIL.

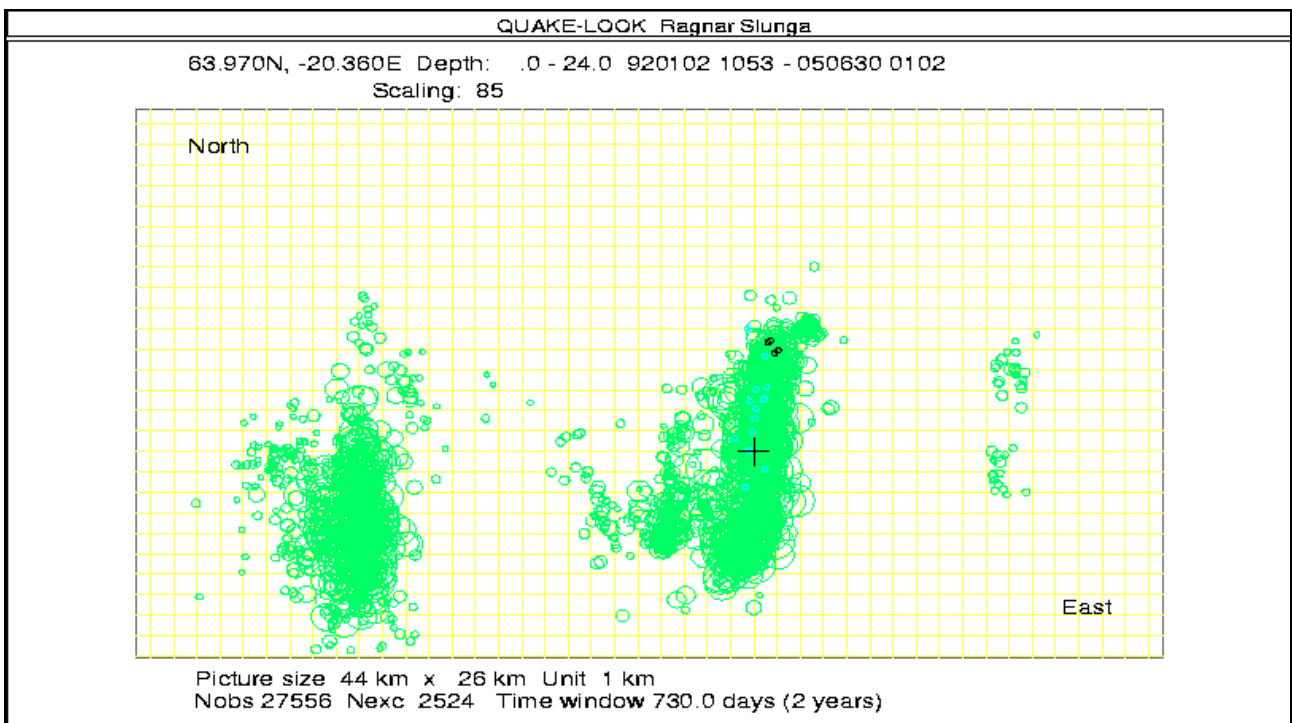


Figure 17. The same as figure 3.1.16 but for EQWP 85. See text.

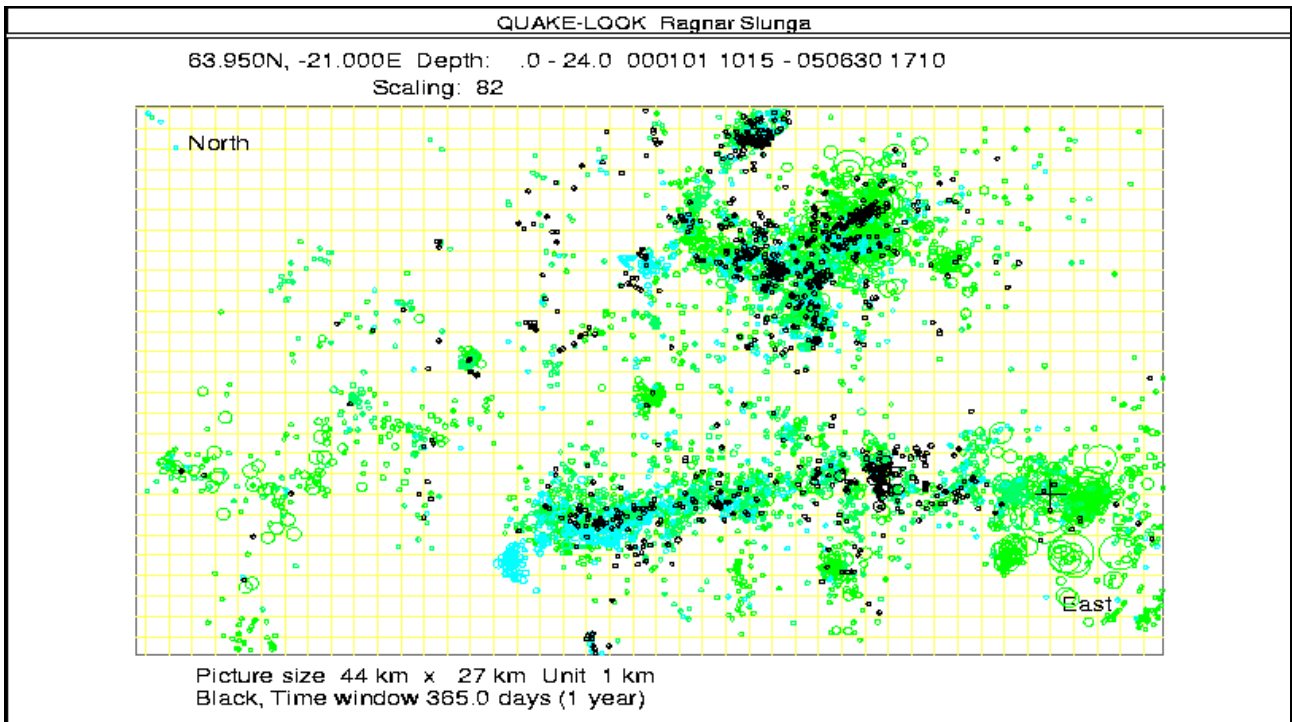


Figure 18. *The Hengill area and the time period Jan 1 2000 to July 1 2005. The EQWP 82 is shown. We see large observations close to the cross (62.95N 21W) a 3-4 years ago plus black slightly increased values 8 km west of the cross. It can be wise to keep an eye around the activity at longitude 21W in the time to come.*

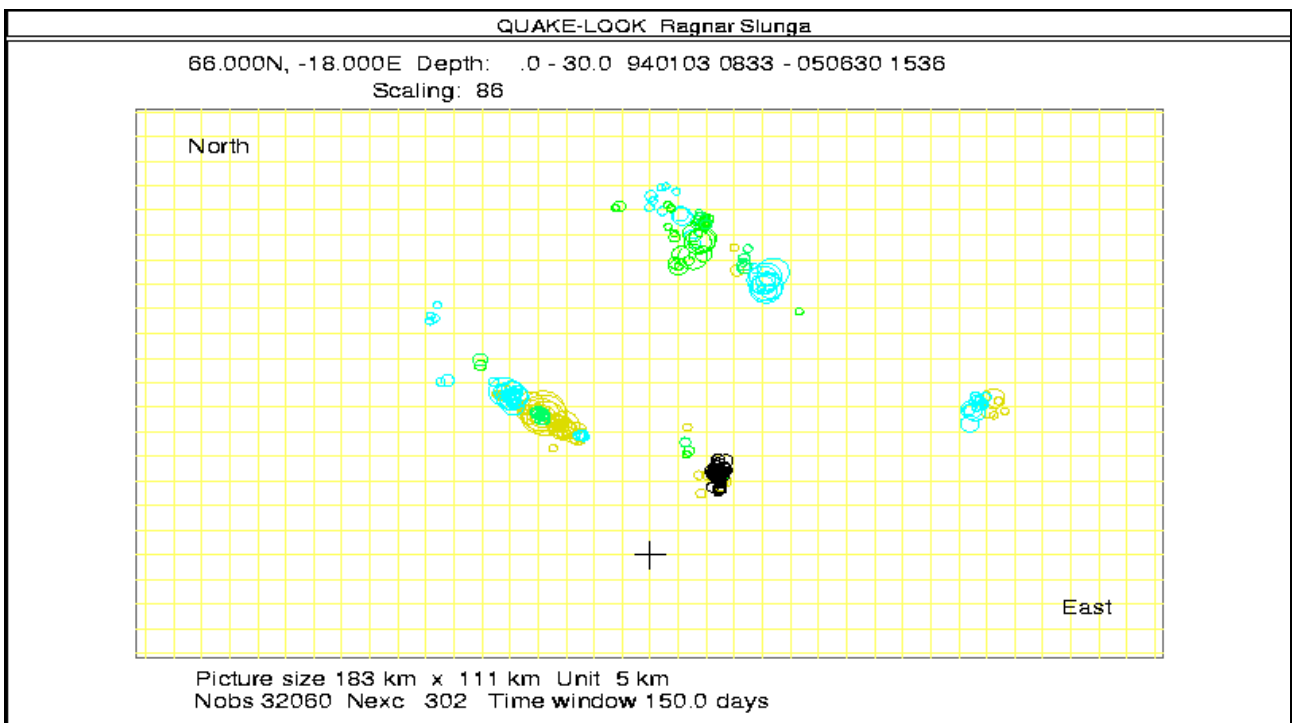


Figure 19. *Now this is a map over the EQWP 86 observations in a 183 km times 111 km area north of Iceland. The cross is at 66N 18W. The black period is the last 5 months prior to Jul 1 2005. There is a slight increase in the Husavik area. See text.*

## References

- Slunga (1981), Earthquake source mechanism determination by use of body-wave amplitudes - an application to Swedish earthquakes. *Bull. Seism. Soc. Am.*, 71, pp 25-35.
- Slunga (1982), Research on Swedish Earthquakes 1980-1981. FOA Report C 20477-T1, Nov 1982, Stockholm, Sweden.
- Roegvaldsson and Slunga (1993), Routine fault plane solutions for local and regional networks: a test with synthetic data. *Bull. Seism. Soc. Am.*, 83, pp 1232-1247.
- Slunga (2003), Microearthquakes Analysis at Local Seismic Networks in Iceland and Sweden and Earthquake Precursors, in *Lecture Notes in Earth Sciences*, 98, Methods and Applications of Signal Processing in Seismic Network Operations, Springer Verlag, Germany.
- Slunga (2003b), Use of microearthquakes in the networks in Iceland and Sweden, (invited lecture), Summer School on Tectonic-Magmatic Interaction, Aug 31 - Sept 8, Geysir, Island.
- Slunga (2003c), Multi-event micro-earthquake analysis based on high accuracy locations and fault plane solutions in Iceland and Sweden, Nordic Seminar on Detection Seismology, June 4-6, Falum, Norway, 2003.
- Slunga (2004a), Rock-water interaction in the crust. Abstract in *GFF*, volume 126, part 1, p 61, January 2004.
- Slunga (2004b), Stress monitoring based on microearthquake analysis, Abstract, European Seismological Commission XXIX General Assembly, Sept 12-17, Potsdam, Germany, 2005.
- Slunga (2004c), Rock Stress Tensor Estimation and Rock-Water Interaction, The 35th Nordic Seminar on Detection Seismology, Sept 29 - Oct 1, Sweden, 2004.
- Slunga (2005), Stress monitoring by single event stress tensor estimates based on microearthquake fault plane solutions, EGU General assembly, Apr 24-29, Vienna, Austria, Geophysical Res., abstract, 2005.
- Slunga (in preparation), Complete stress tensor estimates from single event fault plane solutions.
- Slunga (in preparation), A short term earthquake warning algorithm based on microearthquake analysis.

## WP 3.2 Radon anomalies

**Contributors:** Páll Einarsson, Ásta Rut Hjartardóttir, Gísli Jónsson and Páll Theodórsson

### Objectives

To establish the significance of the radon anomalies that occurred prior to the June 2000 earthquakes by comparing them to earlier results of the radon monitoring program in South Iceland and other results world-wide. Characteristics of the anomalies were to be determined with the aim of developing a warning algorithm.

#### *Deliverables:*

1. *Time series of radon at all measuring stations in South Iceland since 1977 were to be compiled and distributed.* All time series are now available on a CD (Hjartardóttir et al., 2005).
2. *Paper in a refereed journal on the radon anomalies identified.* A manuscript is under revision (Einarsson et al., 2005a). Another manuscript on radon anomalies of 1977-1983 is in the final stages of preparation (Einarsson et al., 2005b).
3. *Presentation of the radon results at 2 international meetings.* The radon findings have been presented at several meetings and in lectures, notably at the EGU-meeting in Vienna 2005, at a science conference in Reykjavík in 2004, and in a lecture at Lamont-Doherty Earth Observatory in New York in 2004.
4. *Warning algorithm.* The radon anomalies observed in the time series have been quantified, both in the 1977-1993 series and in the 2000 time series. They are ready to be incorporated into any warning algorithm developed on basis of the different precursory phenomena.

### Methodology and scientific achievements

The relationship between radon and earthquakes in this area has been studied since 1977 when Egill Hauksson of the Lamont-Doherty Earth Observatory installed the first equipment for this purpose (Hauksson, 1981, Hauksson and Goddard, 1981). The instruments were operated until 1993. A summary of the results until then was given by Jónsson and Einarsson (1996). A very clear relationship could be established and a number of premonitory radon anomalies were identified.

The positive results spurred further work and a new instrument was designed and tested for the purpose of radon monitoring. The instrument is based on a novel liquid scintillation technique where counting only Bi-218/Po-218 pulse pairs gives high sensitivity with a simple construction. The system represents a significant progress in the radon measuring technique (Theodórsson, 1996, Theodórsson and Guðjónsson, 2004).

A new program of sampling from geothermal wells in the South Iceland Seismic Zone was initiated in 1999, a year before the destructive earthquakes of June 2000 occurred. The two M6.5 earthquakes originated in the middle of the sampling network. These events were preceded by clear anomalies at six out of seven stations (Theodórsson et al. 2000, Kerr, 2001, Einarsson et al., 2005a, Hjartardóttir, 2003). Four types of change could be identified in the radon time series in association with the earthquake sequence of June 2000:

1. Pre-seismic decrease of radon. Anomalously low values were measured in the period 101-167 days before the earthquakes.
2. Pre-seismic increase. Spikes appear in the time series 40-144 days prior to the earthquakes.
3. Co-seismic step. The radon values decrease at the time of the first earthquake. This is most likely related to the co-seismic change in ground water pressure observed over the whole area (Björnsson et al., 2001).
4. Post-seismic return to pre-seismic levels about 3 months after the earthquakes, probably also linked with the pressure change in the geothermal systems reported by Jónsson et al. (2003).

A paper on these results was submitted for publication in a refereed journal (Einarsson et al., 2005a). A revised manuscript is in the final stages of preparation.

In view of the positive results of the project we are developing and testing a new, automatic radon instrument, Auto-Radon, based on the same design, that continuously monitors the radon concentration in the geothermal ground water (Theodórsson and Guðjónsson, 2004). The instruments are situated at the drill hole stations, taking 4 radon readings each day. Four stations have been installed so far.

### **Socio-economic relevance and policy implication**

So far the radon program is a purely scientific endeavour. Its socio-economic relevance and policy implications are impossible to judge at this time.

### **Discussion and conclusion**

The most significant finding of this study is the high correlation between the radon time series over the entire area in the time period 1999-2001. Stations that are tens of kilometres apart show very similar fluctuations in the concentration of radon (Einarsson et al., 2005a). Considering the short half-life of radon these fluctuations can hardly be ascribed to material transport between the stations. A common origin of the fluctuations must be assumed. Two significant events occurred in the crust of South Iceland during this time, the Hekla eruption of February 26 – March 8 and the earthquake sequence of June. It must be considered very likely that these events were the causal agents for the radon fluctuations. This conclusion is further strengthened by the temporal correlation of the post-earthquake radon recovery with the pore-pressure recovery and its poro-elastic response observed by Jónsson et al. (2003). We believe these observations are of crucial importance for the understanding of the physical mechanism of premonitory radon anomalies.

### **Plan and objectives for the next period**

The radon data collected in the South Iceland Seismic Zone to date are extensive. The research that they allow is without doubt far reaching and difficult to foresee at this time. The data have now been compiled on a CD that can be distributed to everyone interested (Hjartardóttir et al., 2005). This was one of the main deliverables of this WP. Future research projects, which are obviously of considerable interest, include:

1. Find a statistics test for significance of correlation between the radon and the earthquake time series.

2. Work on an algorithm that detects radon anomalies in a time series and assesses the probability that they constitute an earthquake precursor.

## References

Björnsson, G., Ó. Flóvenz, K. Sæmundsson, E. M. Einarsson. Pressure changes in Icelandic geothermal reservoirs associated with two earthquakes in June 2000, in: Proceedings of the Twenty-Sixth Workshop on Geothermal Reservoir Engineering, Stanford University, Stanford, CA, 2001.

Einarsson, P., P. Theodórsson, G. I. Guðjónsson. Radon anomalies prior to the earthquake sequence in June 2000 in the South Iceland Seismic Zone. Manuscript under revision 2005a.

Einarsson, P., S. Jónsson, S. Björnsson, and Á. R. Hjartardóttir. Radon anomalies and earthquakes in the South Iceland Seismic Zone 1977-1993. Manuscript in prep., 2005b.

Hauksson, E., Radon content of groundwater as an earthquake precursor: Evaluation of worldwide data and physical basis. *J. Geophys. Res.*, 86, 9397-9410, 1981.

Hauksson, E., and J. Goddard, Radon earthquake precursor studies in Iceland. *J. Geophys. Res.*, 86, 7037-7054, 1981.

Hjartardóttir, Á. R. Radonfrávik sem fyrirboðar Suðurlandsskjálftanna 2000. (Radon anomalies occurring before the earthquakes of 2000 in South Iceland, in Icelandic). BS-thesis, Department of Natural Sciences, University of Iceland, 35 pp and Tables, 2003.

Hjartardóttir, Á. R., P. Einarsson, P. Theodórsson and G. Jónsson. Radon Data from the South Iceland Seismic Zone, 1977-1993 and 1999-2003. Report and CD, Science Institute, University of Iceland, 2005.

Jónsson, S., and P. Einarsson. Radon anomalies and earthquakes in the South Iceland Seismic Zone 1977-1993. In: *Seismology in Europe* (Ed. B. Thorkelsson et al.), European Seismological Commission, Reykjavík, p. 247-252, 1996.

Jónsson, S., P. Segall, R. Pedersen, G. Björnsson. Post-earthquake ground movements correlated to pore-pressure transients. *Nature*, 424, 179-183, 2003.

Kerr, R. A. Predicting Icelandic fire and shakes. *Science*, Jan. 26, 2001.

Theodórsson, P., Improved automatic radon monitoring in ground water. In: *Seismology in Europe* (Ed. B. Thorkelsson et al.), European Seismological Commission, Reykjavík, p. 253-257, 1996.

Theodórsson, Páll, Páll Einarsson, Guðjón I. Guðjónsson. Radon anomalies prior to the earthquake sequence in South Iceland in June 2000. *Am. Geophys. Union, Fall Meeting, Abstract in Eos*, 81, p. 891, 2000.

Theodórsson, P. and Guðjónsson, G. I. A simple and sensitive liquid scintillation counting system for continuous monitoring of radon in water. *Advances in Liquid Scintillation Spectrometry*, 249-252, 2003.

## **WP 4 A model of the release of the two June 2000 earthquakes based on all available observations**

### **Objectives**

To model the source process in time and space of the two large earthquakes based on multidisciplinary information.

### **Methodology and scientific achievements related to workpackages including contribution from partners**

The main input here are results and deliverables of WP4.1, WP4.2, WP4.3 and WP4.4., and results from other WP's like the modelling packages WP6.1 and WP6.2 as well as WP5.5.

The earthquake process is complex even if it is short lived process and we must use various methods to understand it as we have done in PREPARED. But it is also significant to add to the complexities the pre- and the post-earthquake process.

A significant part of the modelling is of the immediate fault movement during the earthquake slip, as well as resulting changes expressing the pre- and post-earthquake slip and deformation. Also is significant to observe and to model the size and form of the fault plane as well as the surface effects.

The work in WP4 for the last 6 months has mainly been used for writing up and comparing results.

Significant forums for this work were at the special session organized at EGU General Assembly in Vienna, April 24-29, 2005, about the project "The latest results of the PREPARED project", within the Natural Hazards program of the assembly. After the EGU meeting a special PREPARED meeting was held in Vienna for discussing and fusing results of individual partners of the project. Other significant forums for fusing the earthquake modelling results were the July 12 and the July 21 meetings in Reykjavík, attended by Icelanders as well as some participants coming from other countries.

### **Socio-economic relevance and policy implication and plans for the future**

Such a modelling is a significant basis for predictions of earthquake effects or hazard estimations, as well as for short-term warning methods. It is a basis for various methods in mitigating earthquake risk in the area.

Much work awaits the coordinator as well as others in applying the results of this work to such purposes.

### **Discussion and conclusions**

It was possible to constrain an earth-realistic model for the two earthquakes, based on different kinds of observations, mainly local Icelandic seismic observations, geological observations, teleseismic observations from around the world, deformation observations from GPS and InSAR, and inversion of strong motion observations.

The main conclusions are that the multidisciplinary observations and evaluation in many WP's of PREPARED provides an internally consistent information that will help in predicting future processes in the SISZ as well as at other locations.

## **Deliverables**

Hjaltadóttir, S., K.S. Vogfjörð, Þ. Árnadóttir, P. Einarsson & P. Suhadolc 2005. A model of the release of the two June 2000 earthquakes based on all available observations. *Icelandic Meteorological Office – Report 05020*.

Hjaltadóttir, S. & K.S. Vogfjörð 2005. Subsurface fault mapping in Southwest Iceland by relative location of aftershocks of the June 2000 earthquakes. *Icelandic Meteorological Office – Research Report 21*, 18 pp.

## **WP 4.1 Source mechanism and fault dimensions of the June 17 and June 21 earthquakes determined from mapping of aftershocks**

**Authors: Kristín S. Vogfjörð and Sigurlaug Hjaltadóttir**

### **Objectives**

To determine the source mechanisms and fault dimensions of the two large earthquakes on June 17 and June 21, using local events. That is:

- Define the locations, dimensions and possible sub-fault details in the fault planes of the J17 and J21 earthquakes, by relatively locating the thousands of aftershocks on each of the two faults.
- Map the post-seismic slip as a function of location and time on the two large faults in order to understand the evolution of the post-seismic stress.

In addition:

- Determine the fault planes and dimensions of the two  $M \sim 5$ , dynamically triggered events on Reykjanes Peninsula on June 17.

### **Methodology and scientific achievements**

Interactively analyzed events are fed into the multievent relative location algorithm described in the M12 report, in order to map the fault dimensions and finer details of J17 and J21.

Joint interpretation of the improved hypocenter distribution and the possible fault-plane solutions of individual microearthquakes is performed, in order to study the finer details of post-seismic slip on the two large faults as a function of time and space.

The faults have already been mapped in details, as well as conjugate faults:

#### **June 17**

Aftershocks are mainly at the edges on the fault and in the center, below the hypocenter. During the first 24 hours, however, aftershocks are distributed over the entire fault, after that, activity concentrates along the fault margins, mostly below  $\sim 3$  km.

The overall strike of the fault is  $\sim 7$  degrees and near vertical, but, as shown in figure 1, it is composed of many smaller patches, with differing strikes.

Above 8 km depth the aftershocks display a rather discontinuous pattern composed of three main patches, see figure 1a). The activity delineates a very planar central patch, which is active throughout the year. Its strike ( $\sim 11$  degrees) is slightly east of the overall strike of the fault. Overall dip of the fault is near vertical. Activity on the northern patch is confined to its northern edge, where it is composed of a few short patches mostly with a northerly strike. The southern patch is more continuous and bends westwards with decreasing latitude. At the southern tip the fault jumps half a kilometer to the west and continues on a  $\sim 2$  km long segment. West of the southern edge, a few small faults were also activated. Their strikes are generally west of north.

Below 8 km depth the aftershocks define a continuous fault, but with kinks at the intersection of the main patches above. North of the center patch the bottom appears to be composed of a few smaller en-echelon faults and then breaks up into separate parallel branches farther north. Activity on the southern part, on the other hand, appears to be continuous and more linear, bending slightly westward towards the southern end.

The distribution of rake angles in the fault plane solutions of the bottom events describe predominantly right-lateral, normal motion, whilst rake angle distribution for the center patch also shows a dominant right-lateral movement but with an accompanying smaller thrust component.

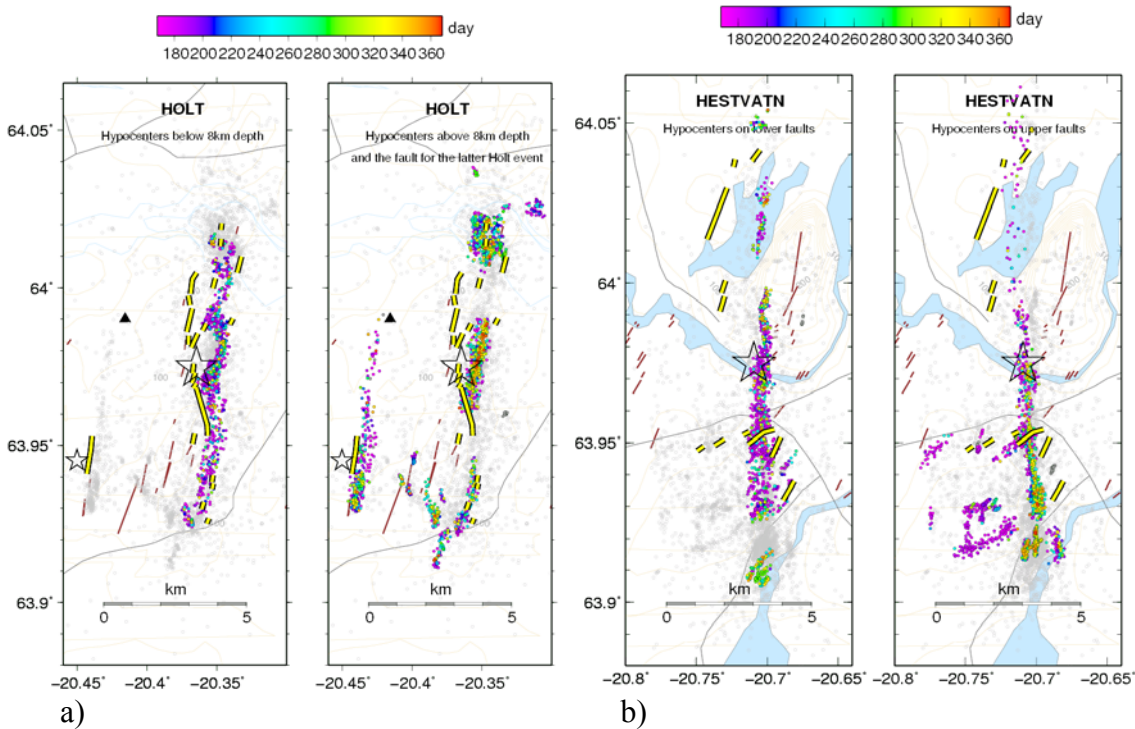


Figure 1. The aftershocks on the Holt fault (a) and the Hestvatn fault (b). The hypocentre of the two  $M=6.5$  events are denoted with stars. The hypocenter for the second Holt event, occurring roughly 2 minutes later, is also marked on the left map by a smaller star. All events are shown in the background in grey. Events on identified faults are displayed in colour, according to timescale (from June 17<sup>th</sup> to December 31<sup>st</sup>, and June 21<sup>st</sup> to December 31<sup>st</sup>, respectively) and for different depth ranges. Yellow lines display surface rupture from 2000 (Clifton and Einarsson, 2005). a) Aftershocks on the second Holt fault (to the west) are all shown on the right map, though extending down to a 9.2 km depth. The bending of the southern tip is clearly seen, as well as the widening of the fault to the north, and the overall en-echelon structure of the fault with its three main patches. b) Hypocenters along the bottom and below 6-7 km are shown on the left map but faults mostly extending between 2 and 6 km are shown on the right. The largest conjugate E-W fault is shown as an upper fault, although extending from 2 km down to roughly 9 km depth. The branching into two faults with different dips occurs just north of the hypocenter, where the shallower activity bends westwards.

## June 21

South of the hypocenter, aftershocks are evenly distributed over the fault. North of the hypocenter the activity is more sparse and mostly concentrated near the bottom. The overall fault strike is 179 degrees and dip is near vertical. The depth range of the seismicity defines a fault with depth increasing southward, from ~6 km on the northern part to ~10 km at the southern margin.

During the first 24 hours following the June 21 event, aftershocks were distributed over the entire fault up to about 1 km depth. After that, activity concentrated along the bottom and through the whole depth range at the southern end, where it is continuous throughout the year.

South of the hypocenter, the fault is vertical, but at the hypocenter, the northern half of the fault branches into two faults with differing dips, see figure 1b). The one that continues as a vertical fault extends north to latitude 64 degrees and ends at the southern shore of lake Hestvatn. The other, dips 77 degrees east and extends to the northern margin of the fault (64.05 degrees N). Both branches continue with a similar northerly strike and follow approximately the same trace at the bottom, creating an approximately 3 km long wedge. The intersection of the dipping segment with the surface, approximately matches the mapped surface ruptures west of lake Hestvatn (Clifton and Einarsson, 2005).

At the location of the mapped conjugate surface-rupture, the earthquake distribution is denser and extends westward, mostly on short easterly striking segments. Farther south, a second set of conjugate faults, extending over a wide depth range is also defined by the seismicity. At the southern margin of the fault, it breaks up into many small fault segments of 1-2 km dimension and varying strike.

Rake angles for the southern end show a dominant right-lateral movement with a slightly smaller normal component. The distribution of rake angles for the bottom layer is not as homogeneous and shows both thrust and normal components accompanying the dominant right-lateral motion, similar to the bottom layer of the Holt fault.

### **Socio-economic relevance and policy implication**

Large historic earthquakes in the South Iceland Seismic Zone (SISZ), like the June 2000 earthquakes, have caused devastation on farms and small towns in southern Iceland. As was borne out by the J17 event, they can also remotely trigger other large events in the SISZ and on Reykjanes Peninsula (RP); either dynamically, like the two M~5 events on RP, or statically, like the J21 earthquake. Increased knowledge about the location of major faults, the character of faulting in the SISZ, and the possibility of remote triggering of earthquakes, can lead to clearer regulations on building standards and building sites in southwest Iceland. This knowledge may also increase awareness in local communities and help inhabitants to prepare for and cope with the effects of future destructive earthquakes.

### **Discussion and conclusion**

The accurate relative locations, used to map the finer details of the structure of the two main faults, show an interesting difference in structure between the two. The Holt fault, of the J17 event, is nearly vertical, has an overall strike of 7°A and is broken up in three main patches, with each striking a few degrees more east than than the overall fault. The Hestvatn fault, on the other hand, is more linear, has an overall strike of 179°A and a dip of ~88° to the west, but dip changes to 77° east, just north of the epicenter. Furthermore, large conjugate faults, which became active west of the southern (vertical) part of the J21 fault, have been mapped. They extend as far as 2-3 km westward. Both faults tend to bend westwards at the southern tip. The induced activity following the two M=6.5 events illuminated many of the large historical faults in the SISZ. In most cases only separate patches on each one were active, but these can in many cases be linked by use of surface fault maps provided by WP 4.3. En echelon structure, as seen on the Holt fault, has been observed on some of these older faults. Although surface faults in the SISZ have been mapped quite accurately, large faults in Iceland have not been mapped at depth in such detail before.

### **Plan and objectives for the final period**

A report on fault mapping for workpackages 4.1 and 5.1 is in print. An article about fault mapping and the correlation between sub-surface faults and mapped surface faults is in preparation, as well

as an article on the source mechanism of the dynamically triggered earthquakes on June 17.

## **Abstracts**

Hjaltadóttir, S. and K. S. Vogfjörð, 2004. Relative event locations and mapping of faults in southwest Iceland (in Icelandic). Geoscience Society of Iceland, Spring meeting 2004. p. 54-55.

Hjaltadóttir, S., K. S. Vogfjörð, R. Slunga, 2005. Mapping subsurface faults in southwest Iceland using relatively located microearthquakes. *Geophysical Research Abstracts*, Vol. 7, 06664, EGU General assembly, Vienna, Austria, 24-29 April, 2005.

Hjaltadóttir, S., K. S. Vogfjörð, R. Slunga, 2005. Fault Patterns in the South Iceland Seismic Zone Revealed by Double-Difference Mapping of Microearthquakes. Abstract submitted to AGU for the Fall Meeting in San Francisco, December 2005.

Vogfjörð, K. S., 2003. Triggered seismicity in SW Iceland after the June 17, Mw=6.5 earthquake in the South Iceland Seismic Zone: The first five minutes. *Geophysical Research Abstracts*, Vol, 5 11251, EGS-AGU-EGU Joint Assembly, Nice, France, 6-11 April, 2003.

Vogfjörð, K. S., S. Hjaltadóttir and R. Slunga, 2005. The M~5 triggered events in the South Iceland Seismic Zone on June 17, 2000: Determination of fault plane magnitude and mechanism. *Geophysical Research Abstracts*, Vol 7, 10274, EGU General Assembly, Vienna, Austria, 24-29 April, 2005.

## **References**

Clifton, Amy and Páll Einarsson, 2005. Styles of surface rupture accompanying the June 17 and 21, 2000 earthquakes in the South Iceland Seismic Zone. *Tectonophysics*, 396, 141-159.

Vogfjörð, K. S., 2003. Seismicity following the June 17, 2000 earthquake. The first five minutes (in Icelandic). Geoscience Society of Iceland, Spring meeting 2003, p. 43

## WP 4.2 Fault slip distribution of two June 2000 Mw 6.5 earthquake in South Iceland estimated by strong motion inversion

Author: Peter Suhadolc

### Method

In the past, several attempts were undertaken to solve the inverse problem for the source of a particular earthquake. The formulation of the problem, that is to determine the spatial and temporal distribution of slip or slip rate over the fault area using teleseismic as well as near field waves, is well known. Using the representation theorem the displacement record at a station on the earth surface can be expressed in terms of the slip distribution over a fault surface  $\Sigma$  as an integral equation (Das and Kostrov, 1990):

$$u_k(x_1, t_1) = \int_0^{t_1} dt \int_{\Sigma} K_{ik}(x_1, x, t_1, t) a_i(x, t) dS \quad (1)$$

where  $i, k=1,2,3$ ,  $u_k(x_1, t_1)$  are the components of the displacement vector,  $a_i(x, t)$  are the components of the slip and  $K_{ik}(x_1, x, t_1, t)$  are the components of the impulse response of the medium at  $(x_1, t_1)$ , due to a dislocation point source at  $(x, t)$ . By moving the time derivative that exists in the kernel  $K$  to the slip term in (1), we obtain an equivalent representation in terms of the slip rate distribution over the fault, with the corresponding kernel  $G$ . In short,

$$u = K * a = G * \dot{a} \quad \text{Where } K = \dot{G} \quad (2)$$

In Eq. (2)  $u$  is the displacement vector,  $a$  and  $\dot{a}$  are the slip and the slip rate vectors, respectively, the asterisk denotes convolution over the fault area and source duration, and the dot denotes the time derivative.

We shall assume that the fault is planar and that the slip direction is constant over the fault. Discretizing the problem, by dividing the fault into square cells and the source time function into steps, reduces (2) to the system of linear equations:

$$Ax \approx b \quad (3)$$

Where  $A$  is the matrix obtained by integrating  $G$  or  $K$  over fault cells and time steps, each column of  $A$  being the appropriate discretized set of kernel for all stations corresponding to different cells and time instants, ordered in the same way as the observations  $b$ , and  $x$  are the unknown slips or slip rates.

In this work, we use the formulation in terms of the slip rates and the kernel  $G$ . The Green functions (GF) are determined using the multimodal summation method for layered, anelastic medium (Panza, 1985; Panza and Suhadolc, 1987; Florsch et al., 1991). We use the crustal model proposed by Vogfjord (2002) with plane parallel layers considering lateral discontinuities. The seismic source is included in the computation using the formulation due to Harkrider (1964), Ben-Menahem and Harkrider (1964). The extended fault is modeled as a grid of point sources, and the synthetic seismogram at each station due to the moment release on the fault is computed by summing the contribution from each point source with appropriate delays and weights. The GF are computed for a maximum frequency of 1Hz. The size of the time step used in constructing the GF is taken as about 0.1s.

Since the integral equation (1) is unstable, we need to stabilize it by the use of additional constraints. The physically based constraints we shall use in this work are as follows (Das and Suhadolc, 1996): no back slip constraint (we assume the slip direction to be constant over the fault during the process and coincide with the stress drop direction, and the only component of slip rate vector to be non negative); causality constraint (the rupture is constrained to move at or more slowly than some preassigned speed) and seismic moment constraint (the final moment must equal some preassigned value).

To solve the constrained linear system we shall use the method of linear programming (Press et al., 1986), in which the vector of the residuals is minimized following the formulation developed and applied to the earthquake faulting problem by Das and Kostrov (1990,1994).

## Pre-processing of the data

We used only strong motion data from a set of rock stations distributed around the fault, obtained from the ISESD database (Ambraseys et al., 2004). We chose only stations on sites as much as possible on rock and within an epicentral distance of 50 km. Unfortunately, there are no such stations in the North and in the South of the two epicenters (Fig.1).

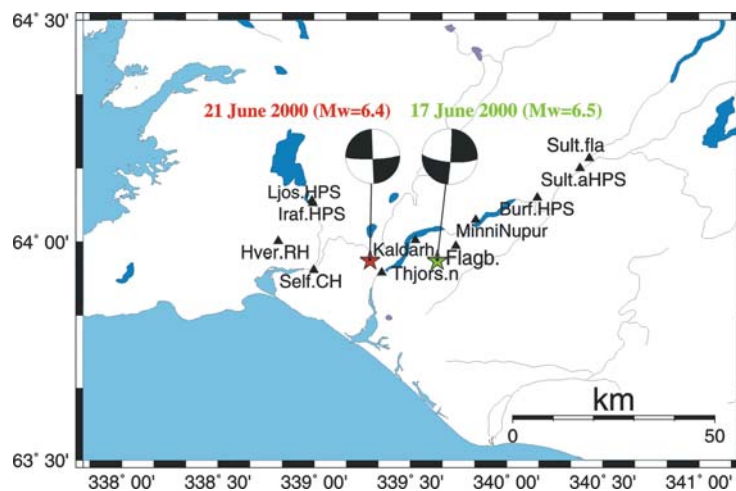


Figure 1 Location map of the stations used in this study and their position relative to the epicenter of the two events.

The accelerograms are filtered at 1Hz and we model about the first 10-15 seconds of the accelerograms. However, we had a problem with the time. The absolute time is unknown for most of stations. For the synthetic seismograms the beginning time is the origin time of the event, whereas for real data the beginning of registration is given by the trigger time minus the pre-trigger time. Knowing the crustal velocity model and the distance hypocenter receiver, we have calculated the arrival time of the P-waves at each station. Picking the first arrival in the raw data, we had thus a time reference and from this, it was possible to estimate the initial time of the registration (Minigutti, 2002).

At first, we decided to use only the vertical component of the accelerograms, then to better constraint the moment slip distribution, we decided to use also the horizontal components.

## 21 June Event

In the table are reported all the models tested using the moment constraint. The best result is obtained for MODEL1\_R.

Event	Model	nx	nh	x-step	dip	strike	rake	NP	idt	nu( eq.)	nv (unk.)	l1-err	l2-err	fit	Comments
J21	M1_IDT3	10	6	2	90	358	172	5,3	3	1008	827	0.6	0.77	ok 1.48	
	M1_IDT5	10	6	2	90	358	172	5,3	5	1008	553	0.64	0.84	ok 1.6	
	M2_IDT5	14	8	1.5	90	358	172	7,4	5	1255	1024	0.6	0.81	ok 1.32	
	M2_IDT3	14	8	1.5	90	358	172	7,4	3	1255	1515	0.59	0.78	ok 1.29	
	M1_IDT3_3c	10	6	2	90	358	172	5,3	3	2898	827	0.76	0.78	ok 2.53	3-components
	M1_R	10	6	2	90	358	172	5,3	3	2898	827	0.74	0.76	ok 2.48	fault relocation

Table 1.  $nx$  is the number of cells along strike,  $nh$  is the number of cells along dip,  $x$ -step is the

cell's dimension and  $NP$  the nucleation point,  $l1-error = \frac{1}{n_u} \sum \frac{|s_i - r_i|}{|r_i|}$ ,  $l2-error = \sqrt{\frac{\sum (s_i - r_i)^2}{\sum (r_i)^2}}$ ,

where  $s_i$  are the values of the calculated synthetic seismograms and  $r_i$  those of the real ones,  $fit = \sum |x_i \cdot col_j - col_i|$ , where  $x_i$ =inverted slip rates,  $col_i$ = data,  $col_j$ = synthetics from contributing grids.

MODEL1 correspond to a rupture that spreads over a 20 km-long and 12 km wide fault in 22 time steps with an assumed rupture velocity of  $v_r=0.7v_s$ . The number of cells ( $nx$ ) along strike is 10 and the number ( $nh$ ) along dip is 6, the dimension of the square cells ( $x$ -step) is 2 km. At the beginning, we used only the vertical component of the accelerograms. Several inversions were performed, changing the value of IDT (IDT is the source time function time step and it is an integer number of  $\Delta t$ , the sampling interval of the seismograms), and the dimension of the cell ( $x$ -step equal to 1.5km for MODEL2). The waveform fit was not perfect and the moment slip distribution obtained was concentrated at the bottom in the Southern part of the fault, which was found not to be satisfactory.

To better constrain the moment slip distribution we decided to use also the horizontal components of the records (MODEL1\_IDT3\_3c) and the adjustment of the fault's position and the nucleation point after a re-analysis of the aftershocks distribution (MODEL1\_R).

The result for MODEL1\_R shows that the maximum release is located at a depth of about 6km, about 2 km south of the hypocenter and just north of the intersection of the main fault and the westward extending conjugate fault (where surface rupture was observed). An increase in moment release follows approximately the distribution of aftershocks along the bottom of the fault, increasing in depth from 6 km at the northern end of the fault to 10 km just south of the hypocenter. Two additional maxima are located at the surface. The smaller one is 4km south of the fault center, close to the above-mentioned intersection. The other is 2 km north of the fault center, just south of Lake Hestvatn, approximately in the same location as the westward step in the aftershock distribution.

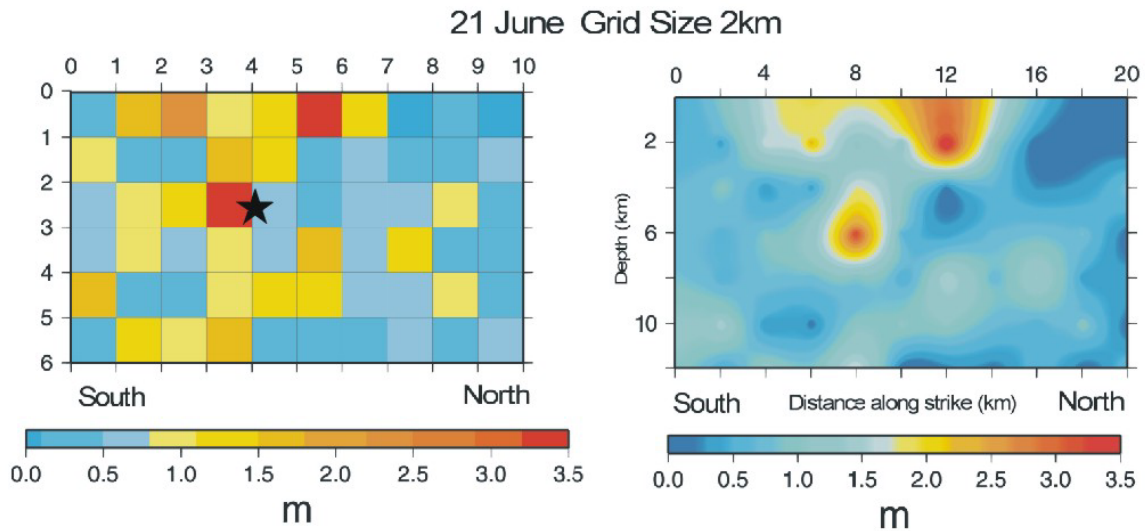
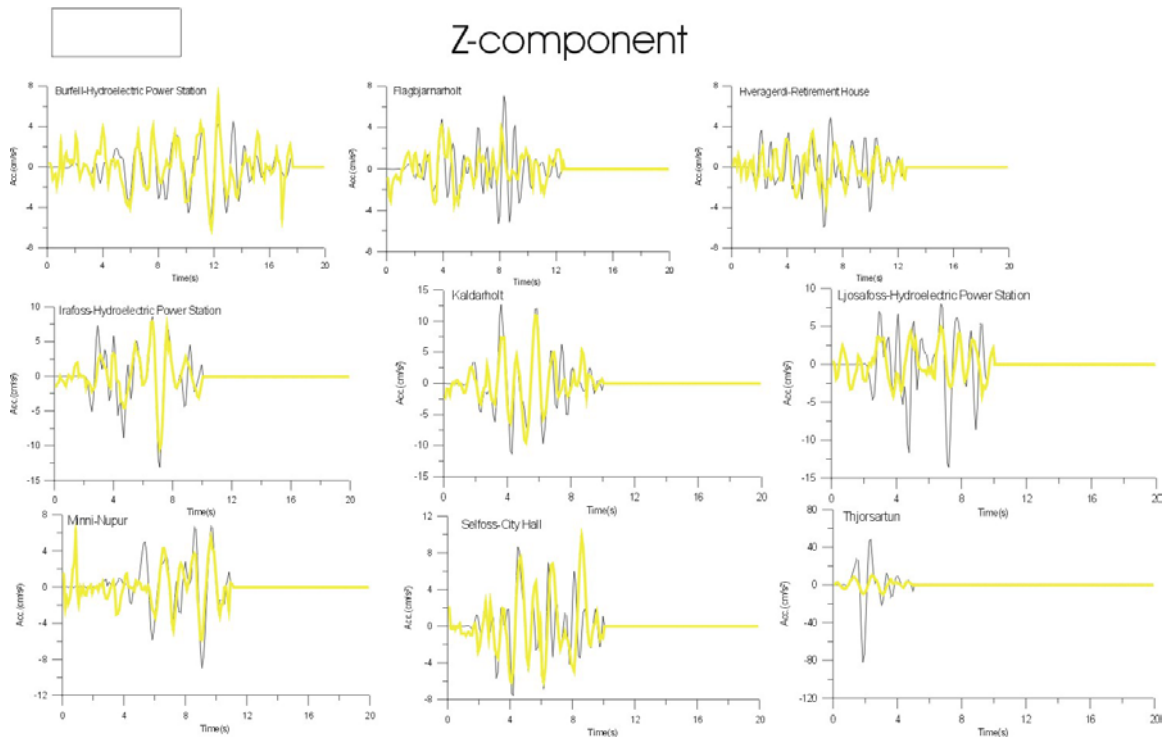


Figure 2. Moment slip distribution obtained for MODEL1\_R. On the left: the value of slip for each grid cell plotted in a discrete coloured scale of intensities. On the right: contour map of the same slip distribution in a continuous scale of intensities. The orientation of the fault is South-North from left to right.

The waveform fit is shown in Fig.3. For the Z-component, the fit is particularly appreciable for Burfell-Hydroelectric Power Station, Irafoss-Hydroelectric Power Station, Kaldarholt, Minni-Nupur. As regards the NS-components, the comparison is quite good for Burfell-Hydroelectric Power Station, Irafoss-Hydroelectric Power Station, Ljosafoss-Hydroelectric Power Station whereas in general the amplitude of the calculated signals is less than the real ones. The EW-components are better reproduced in the station located in the East of the epicenter like Burfell-Hydroelectric Power Station, Kaldarholt, Minni-Nupur.



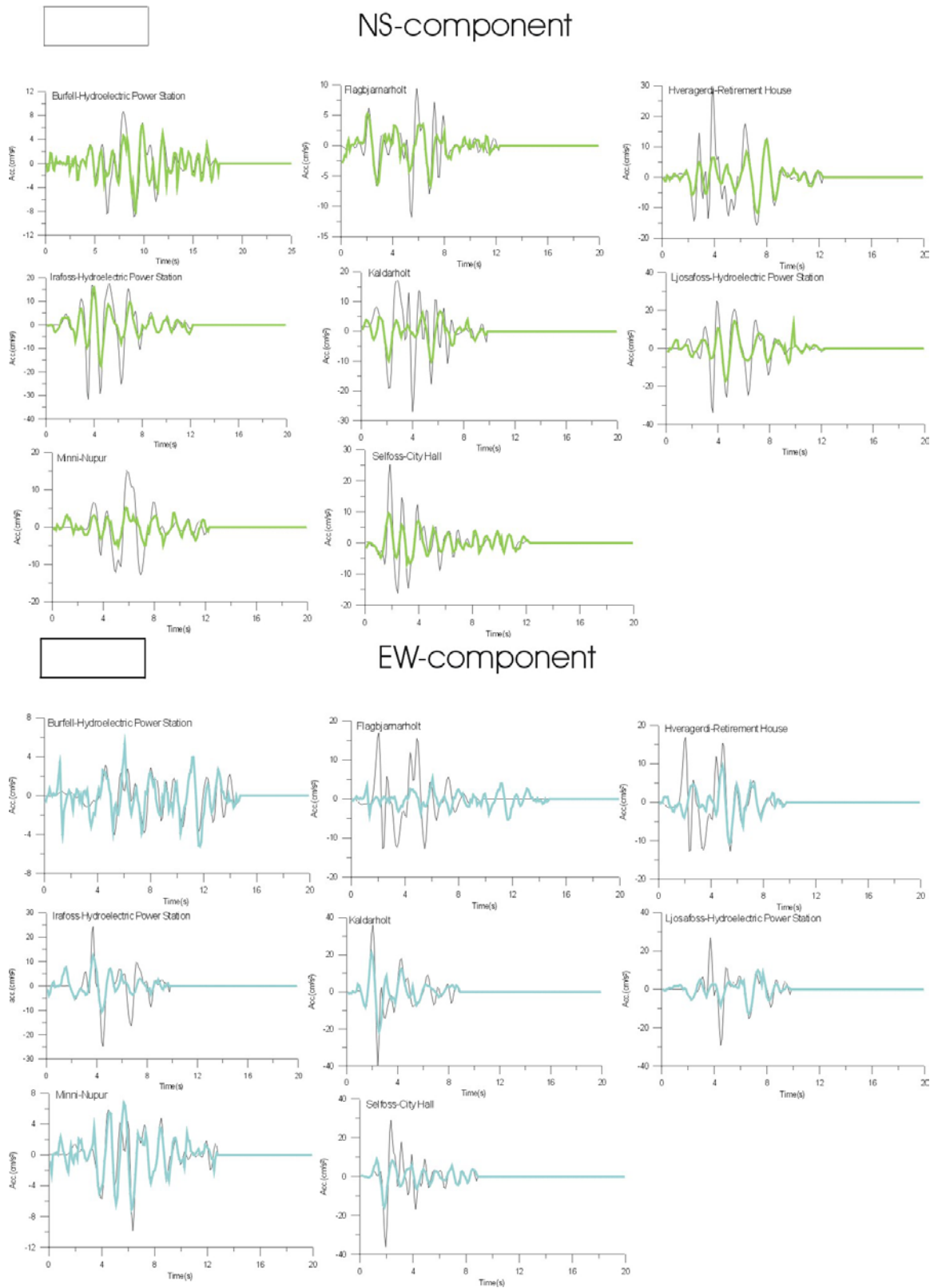


Figure 3. Comparison for each station between the real (thin black solid line) and the synthetic (thick coloured solid line) accelerograms related to the June 21 event.

## 17 June Event

In the table are reported all the models tested using the moment constraint. The best result is obtained for MODEL1\_R.

J17	M1_IDT3	10	6	2	87	4	196	6,3	3	2021	27	1.4	1.3	no	1.85	
	M2_IDT3	14	8	1.5	87	4	196	8,4	3	2021	1513	1.1	0.97	no	1.5	
	M2_IDT5	14	8	1.5	87	4	196	8,4	5	2021	1022	5.4	6.4	no	7.12	
	M2_IDT5_7s	14	8	2	87	4	196	8,4	5	1050	1022	0.51	0.5	ok	0.95	7 stations, 10s
	M1_IDT3_7s	10	6	2	87	4	196	6,3	3	850	827	0.75	0.7	no	1.51	
	M1_5s_3C	10	6	2	87	4	196	6,3	3	1635	827	0.78	0.87	ok	3.58	5 nearest sta, 3-components
	M1_R	10	6	2	87	4	196	6,3	3	1635	827	0.72	0.84	ok	3.32	fault relocation

Table 2.  $n_x$  is the number of cells along strike,  $n_h$  is the number of cells along dip,  $x$ -step is the

cell's dimension and  $NP$  the nucleation point,  $l1-error = \frac{1}{n_u} \sum \frac{|s_i - r_i|}{|r_i|}$ ,  $l2-error = \sqrt{\frac{\sum (s_i - r_i)^2}{\sum (r_i)^2}}$ ,

where  $s_i$  are the values of the synthetic calculated seismograms and  $r_i$  those of the real ones,  $fit = \sum |x_i \cdot col_j - col_i|$ , where  $x_i$ =inverted slip rates,  $col_i$ = data,  $col_j$ = synthetics from contributing grids.

The sequence of the tests made for this event is the same as for the 21 June event. We first selected 15 sec. of the duration of the accelerograms to invert without realizing that part of the signals were contaminated by the trigger event in Reikjanes peninsula. We did not reach the minimum of the linear programming problem (MODEL1\_IDT3, MODEL2\_IDT3, MODEL2\_IDT5) and we obtained a not reasonable maximum of moment release at the top of the fault. We realized that this situation was due to a second event very close to the main one, happened near the Hveragerdi-Retirement House station.

To avoid the influence of this second event we did not use data from Hveragerdi-Retirement House station and from the farthest stations, and we reduced the part of the signals to invert to the first 10s (MODEL1\_IDT3\_7s).

Also for the 17 June event, we made an inversion using the three components of the accelerograms for the MODEL1 fault model inverting the first 10s of the signals of the 5 nearest stations (MODEL1\_5s\_3c).

The result for MODEL1\_R shows that most of the moment is released on the central patch, below and north of the hypocenter, extending about 8km long the fault and down to about 8km depth in the center. A second maximum is located at shallow depth at the Southern edge of the fault.

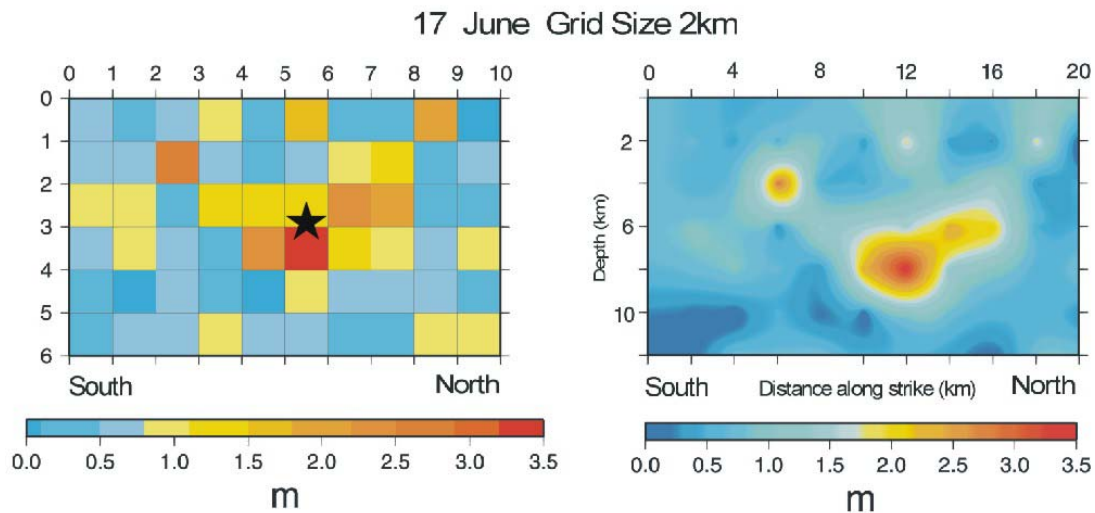


Figure 4. *Moment slip distribution obtained for MODEL1\_R. On the left: the value of slip for each grid cell plotted in a discrete coloured scale of intensities. On the right: contour map of the same slip distribution in a continuous scale of intensities. The orientation of the fault is South-North from left to right.*

## Conclusion

Strong motion data of two Icelandic June 2000 events have been inverted for the slip on the fault. The lack of absolute timing has been successfully overcome by estimating the propagation of P waves in a detailed structural model. The inversion was only possible by imposing physical constraints such as causality, positivity and total moment. The best results are obtained using all three components of motion.

Given the source details, one can “estimate” the ground motion that would have been recorded in the surroundings of the earthquake (Fig. 6 for the June 17 one) and appreciate the differences relative to a uniform slip on the fault (Fig. 7).

This is important for possible future shaking scenarios to be used by earthquake engineers.

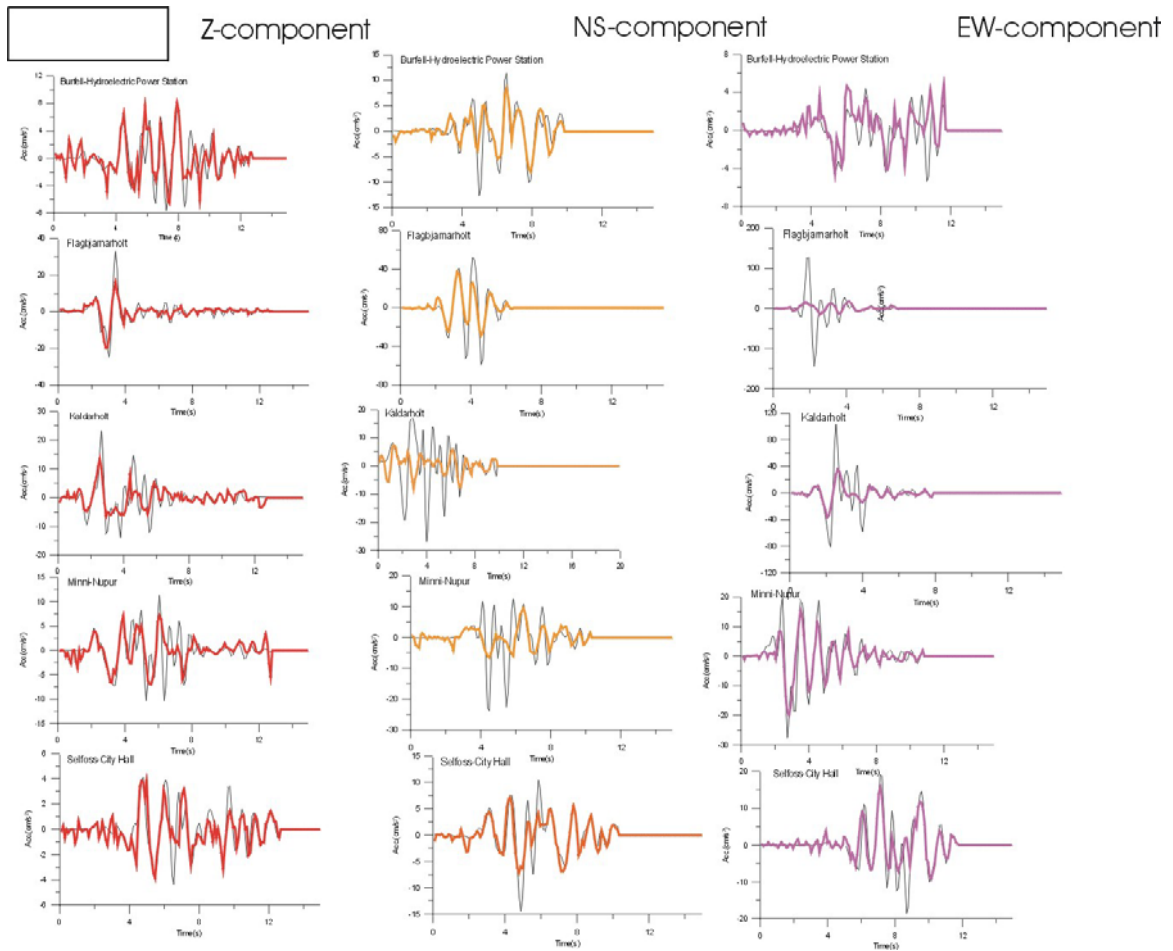


Figure 5. Comparison for each station between the real (thin black solid line) and the synthetics (thick coloured solid line) accelerograms related to the June 17 event.

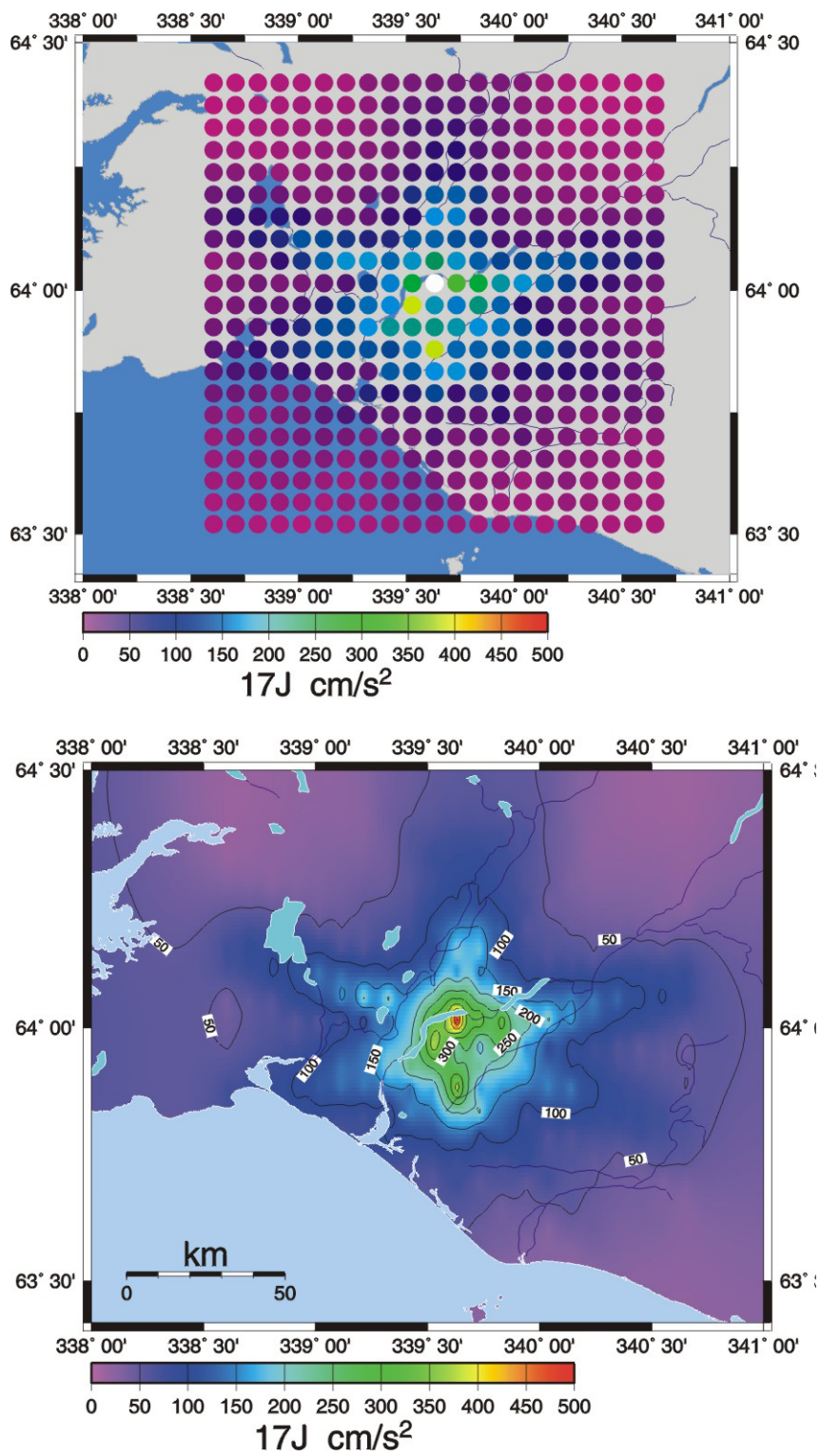


Figure 6. *Groundshaking scenario for the June 17, 2000 event: slip distribution on the fault plane derived from the inversion of observed strong motion waveforms.*

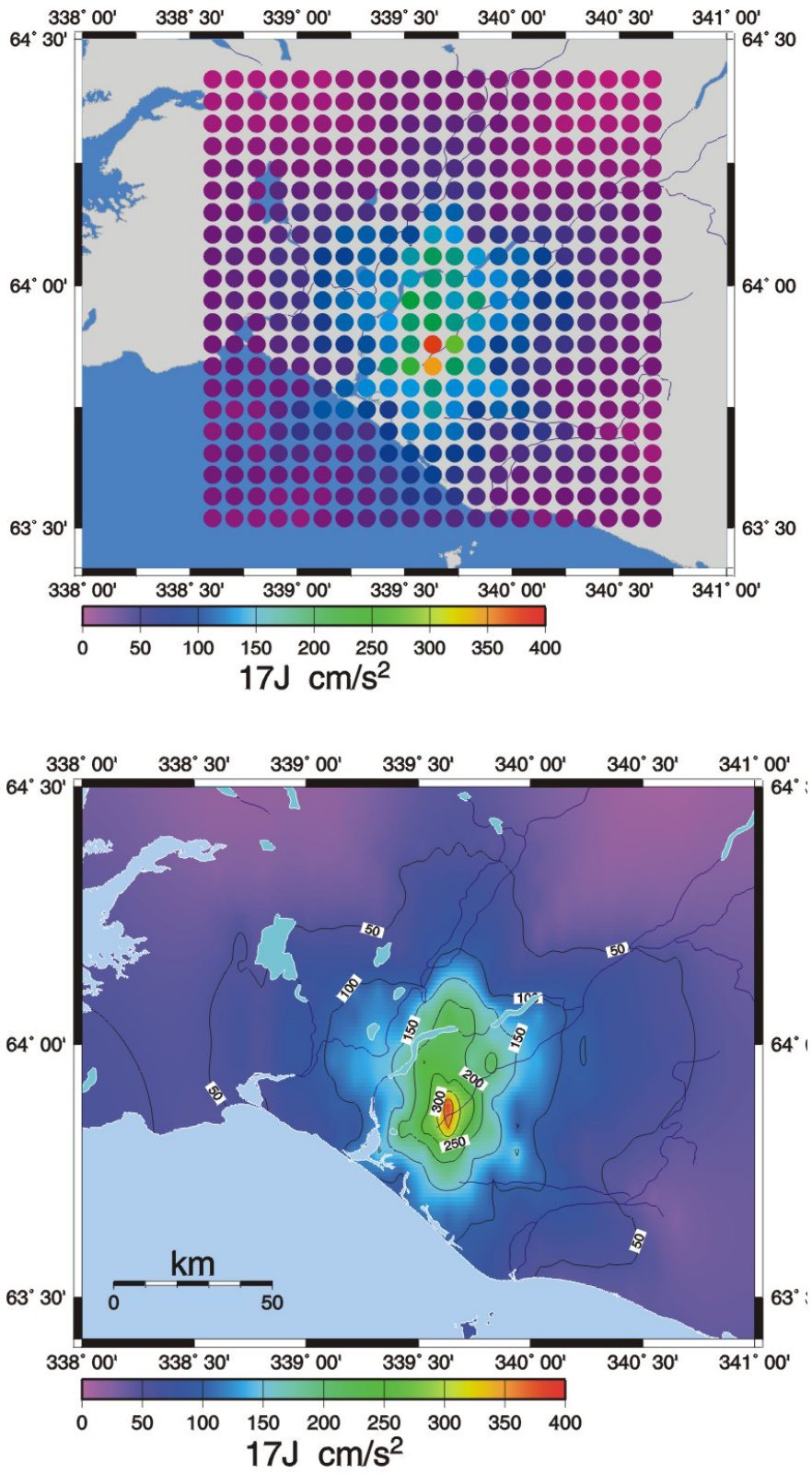


Figure 7. *Groundshaking scenario for the June 17, 2000 event: uniform slip distribution on the fault plane.*

## References

- Ambraseys, N.N., Smit, P., Douglas, J., Margaris, B., Sigbjornsson, R., Olafsson, S., Suhadolc, P. and Costa, G., 2004. Internet Site for European Strong-Motion Data. *Boll. Geof. Teor. Appl.*, 45, n. 3, 113-129.
- Ben-Menahem A. and D.G. Harkrider, Radiation patterns of seismic surface waves from buried dipolar point sources in a flat stratified Earth. *J.Geophys. Res.*, 69,2605-2620,1964.
- Das, S. and Kostrov, B.V., 1990. Inversion for seismic slip rate and distribution with stabilizing constraints: Application to the 1986 Andreanof Islands earthquake. *J. Geophys. Res.*, 95, 6899-6913.
- Das, S. and Kostrov, B.V., 1994. Diversity of solutions of the problem of earthquake faulting inversion. Application to SH waves for the great 1989 Macquarie Ridge earthquake. *Phys. Earth Planet. Int.*, 85, 293-318.
- Das, S. and Suhadolc, P., 1996. On the inverse problem for earthquake rupture. The Haskell-type source model. *J. Geophys. Res.*, 101, 5725-5738.
- Florsh, N., Fäh, D., Suhadolc, P. and Panza, G. F., 1991. Complete synthetic seismograms for high-frequency multimode SH waves. In: A. Udias and E. Buforn (eds.), *El Escorial workshop proceedings*, Pageoph **136**, 529-560.
- Harkrider, D.G., Surface waves in multilayered elastic media, 1, Rayleigh and Love waves from buried sources in a multilayered elastic half-space, *Bull. Seismol. Soc. Am.*, 54,627-679,1964.
- Minigutti, F. 2003. Modellazione di forme d'onda accelerometriche dei due forti terremoti islandesi del giugno 2000. PhD thesis in Physics at the University of Trieste.
- Panza, G.F., 1985. Synthetic seismograms: the Rayleigh waves modal summation. *J. Geophys.*, 58, 125-145.
- Panza, G. F., Suhadolc, P., 1987. Complete strong motion synthetics. In: B. A. Bolt (ed.) *Seismic Strong Motion Synthetics, Computational Techniques* **4**, Academic Press, Orlando, 153-204.
- Press, W.H., B.P. Flannery, S.A. Teukolsky and W.T. Vetterling, 1986. *Numerical recipes. The Art of Scientific Computing*, Cambridge Univ. Press, N.Y., 818 pp.
- Vogfjord, K., 2002, Crustal structure beneath western and eastern Iceland from surface waves and receiver functions: *Geophysical Journal International*, v. 149, p. 349-363.

## **WP 4.3 Surface fractures in the source region of the June 2000 events**

**Contributors: Páll Einarsson, Benedikt Ófeigsson, Ásta Rut Hjartardóttir and Maryam Khodayar**

### **Objectives**

1. Cast light on the relationship between surface faulting and faulting at depth during the June 2000 events.
2. Map the surface fractures in the area surrounding the two main faults active in the earthquakes.

#### *Deliverables:*

1. *A map of surface fractures in the central part of the South Iceland Seismic Zone.* An overview map of the whole zone has been prepared, and detailed maps in scale 1:50 000 are available as well.
2. *Map of surface faulting during the June 2000 events.* This map is available and published.
3. *Presentations at two international meetings.* The results of fracture mapping have been presented at several meetings, including the EGU-meeting in Vienna 2005, Spring meetings of the Icelandic Geosciences Society in 2004 and 2005, in a lecture at Lamont-Doherty Earth Observatory in New York in 2004, etc.
4. *Paper in a refereed journal.* A paper on surface fracturing during the June 2000 events was published in 2005 (Clifton and Einarsson, 2005). At least three more papers are in different stages of preparation.
5. *Input into the general modelling of the June 2000 events.*

### **Methodology and scientific achievements**

The epicentral zone of the SISZ shows widespread evidence of recent faulting (Einarsson et al., 1981). Historical documents mention surface faulting during some of the earthquakes, and in the case of the events of 1630, 1784, 1896 and 1912 the fractures have been located and mapped in detail (e.g. Einarsson and Eiríksson, 1982, Bjarnason et al., 1993). The fractures of 2000 have been mapped as well (Clifton and Einarsson, 2005). Structures resembling those of the 1912, 1896 and 1630 ruptures are found throughout the seismic zone. They can be grouped into systems interpreted to represent faults, more than 25 of which have been identified so far. The faults are transverse to the seismic zone and are arranged side-by-side with spacing of about 1 km between them.

In WP 4.3 we use differential GPS instruments to map in detail the remaining fractures of 2000 as well as all older fractures in the surrounding areas.

This work package consisted mainly of fieldwork in the source areas of the South Iceland Seismic Zone. During this reporting period emphasis was put on the Grímsnes district, both on extending known fracture systems and on fractures thought to be associated with the Grímsnes volcanic system near the northern border of the zone. A field assistant, Benedikt Ófeigsson, was hired for the summer months of 2005 to assist PE in the field and analyse the data. Student groups from the University of Iceland contributed significantly to the mapping effort on field trips in October 2004. Teaching assistants were Dr. Maryam Khodayar, Benedikt Ófeigsson, and Ásta Rut Hjartardóttir.

The work was mainly mapping previously known fractures, tracing them in the field with the GPS-mapping tools. With the experience and confidence gained during the 2000 earthquakes it was possible to identify considerably more fault structures than before. The fracture systems thus turned out to be more continuous than previously thought. Several fault segments were found that had not been identified before. Two fracture systems of the Flói district were traced farther to the north, into the Grímsnes district. A site of historical faulting was identified. In addition, the whole fissure swarm of the Grímsnes volcanic system was mapped. This enigmatic volcanic system is exposed within the Hreppar microplate, right next to the South Iceland Seismic Zone, and is hard to separate from the plate boundary structures. It appears to be in *statu nascendi*. This volcanic system is located at or slightly outside the margin of the Western Volcanic Zone and appears to be drifting off the plate boundary. In addition, the Western Volcanic Zone is being replaced by the Eastern Volcanic Zone as the main branch of the mid-Atlantic plate boundary in this region (Geirsson et al., 2005). The Grímsnes volcanic system may therefore never reach a mature state.

*Work delivered so far:*

1. All major, known surface fault segments of the South Iceland Seismic Zone have been field checked and mapped by differential GPS instruments.
2. Surface faulting of the 2000 earthquakes was more extensive than previously thought. Additional faults have been mapped and a paper published in *Tectonophysics* (Clifton and Einarsson, 2005).
3. A simplified map of all known surface faults of the SISZ has been prepared for general use. This map is already in use on the earthquakes information website of the Iceland Meteorological Office ([vedur.is](http://vedur.is)) as a background to the real-time earthquakes locations of the South Iceland Seismic Zone. The map is also to be seen on a public information sign of the Icelandic Road Department at the epicentre of the June 21 earthquake of 2000.
4. The general map base of the Icelandic Geodetic Survey in scale 1:50 000 has been incorporated into the mapping software. Detailed maps of faults can now be produced on that base for any sub-area.
5. Results of work under this work package have been presented at several meetings, including the Spring Meetings of the Icelandic Geoscience Society 2004 and 2005 (Einarsson et al., 2004, 2005a) and at the EGU meeting in Vienna in 2005 (Einarsson et al., 2005b).

### **Socio-economic relevance and policy implication**

The earthquakes of June 2000 had many socio-economic implications. One of them was that structures in a seismically active region can be built to withstand earthquakes as long as reasonable building practices are used and the structures are not built directly across faults. A reliable and detailed fault map, one of our deliverables, is clearly of high importance here. An effort has been made to provide easy access to the fault data so that a fault map can be produced on the conventional map base for any area of the seismic zone. Recent examples show, however, that the construction community is still not ready to make use of this new knowledge. It should be one of the priority issues to publicise the new fault map and educate the construction sector about its use. It should also be mentioned that the National Energy Company (Landsvirkjun), who is planning two hydropower projects within the seismic zone, is making every effort to circumvent fractured bedrock as foundation for their structures. Furthermore, the Road Department is using the fault map in their planning work for a new bridge on the river Ölfusá.

## Discussion and conclusions

The mapping effort under this work package has filled in the previously known picture of the South Iceland Seismic Zone. A more complete picture has been gained of the previously known faults and new fault segments have been discovered. With the new fault map in hand it is interesting to compare it to the distribution of hypocenters in the zone. This comparison has led to new insights into the connection between faults at depth and surface fractures.

## Plan and objectives for the next period

We have made a general map of all known Holocene fault structures in the South Iceland Seismic Zone and thus laid the groundwork for future studies of these structures and the mechanics of this most active source area of large earthquakes in Iceland. There is no doubt, however, that this work can be improved and there are several lines of work that will be pursued:

1. *Mapping.* We recognise that not all faults have been found so far in spite of considerable effort. Further fieldwork is recommended, particularly in the western part of the Grímsnes district and northern part of the Land district.
2. *Faults at depth.* We will work with other researchers of the PREPARED-project to correlate faults on the surface with faults at depth as shown by hypocenters.
3. *Reconstruction of historic earthquakes.* Assuming that the present background activity is a combination of late aftershocks of previous earthquakes and events due to stress accumulation in the interseismic period, one can make inferences about the source faults of the latest historic earthquakes. We have started work on the 1912 earthquake along these lines (Einarsson et al., 2004) and plan to continue with the 1896 and 1784 sequences.
4. *Presentation of results to users.* An effort should be made to make the planning and construction communities aware of the hazards associated with bedrock fractures and show how to utilise fracture maps to avoid them.

## References

- Bjarnason, I. P., P. Cowie, M. H. Anders, L. Seeber and C. H. Scholz. The 1912 Iceland earthquake rupture: Growth and development of a nascent transform system. *Bull. Seism. Soc. Am.*, 83, 416 - 435, 1993.
- Clifton, A., P. Einarsson. Styles of surface rupture accompanying the June 17 and 21, 2000 earthquakes in the South Iceland Seismic Zone. *Tectonophysics*, 396, 141-159, 2005.
- Einarsson, P., and Jón Eiríksson. Earthquake fractures in the districts Land and Rangárvellir in the South Iceland Seismic Zone. *Jökull*, 32, 113-120, 1982.
- Einarsson, P., S. Björnsson, G. Foulger, R. Stefánsson and Þ. Skaftadóttir. Seismicity pattern in the South Iceland seismic zone. Í: *Earthquake Prediction - An International Review* (Ed. D. Simpson and P. Richards). American Geophys. Union, Maurice Ewing Series 4, 141-151, 1981.
- Einarsson, Páll, Maryam Khodayar, and Steingrímur Þorbjarnarson, and students of the courses Tectonics and Current Crustal Movements in the Faculty of Science of University of Iceland in 2003.. Surface ruptures in the South Iceland earthquake of 1912. *Icelandic Geoscience Soc. Spring Meeting 2004. Abstracts of papers and posters*, p. 47.

Einarsson, P., M. Khodayar, Á. R. Hjartardóttir, B. Ófeigsson, and students in Tectonics and Current Crustal Movements, UI fall semester 2004. Mapping of Holocene fractures in the Grímsnes fissure swarm, South Iceland. Icelandic Geoscience Soc. Spring Meeting 2005. Abstracts of papers and posters, p. 52.

Einarsson, P.; Khodayar, M.; Clifton, A. ; Ofeigsson, B.; Thorbjarnarson, S.; Einarsson, B.; Hjartardóttir, A. R. A map of Holocene fault structures in the South Iceland Seismic Zone. Paper at the General Assembly of the European Geosciences Union, Vienna, April, 2005. Abstract EGU05-A-08858, 2005.

Geirsson, H., Th. Árnadóttir, C. Völksen, W. Jiang, E. Sturkell, T. Villemin, P. Einarsson, F. Sigmundsson, R. Stefánsson. Current plate movements across the Mid-Atlantic Ridge determined from 5 years of continuous GPS measurements in Iceland. J. Geophys. Res., accepted 2005.

## **WP 4.4 Deformation model for the June 2000 earthquakes from joint interpretation of GPS, InSAR and borehole strain data**

**Author: Thóra Árnadóttir**

### **Background**

The June 2000 earthquake sequence caused significant co-seismic surface deformation that was observed by GPS and InSAR (*Árnadóttir et al.*, 2001,2004; *Pedersen et al.*, 2001; *Pedersen et al.*, 2003; *Pagli et al.*, 2003). In addition to co-seismic deformation, InSAR measurements document deformation signals due to post-seismic ground water movements, for the first two months following the earthquakes (*Jónsson et al.*, 2003). The June 2000 earthquake sequence provides the first opportunity to study co-seismic deformation in the SISZ and on Reykjanes Peninsula.

### **Scientific/technological and socio-economic objectives**

The objectives of the work package are to evaluate the 3D co-seismic deformation associated with the June 2000 earthquakes and derive a deformation model for the earthquakes based on joint interpretation of all the available geodetic data. The deliverables of this workpackage are the first detailed estimates of co-seismic slip distribution on faults in the South Iceland seismic zone and a detailed study of three triggered events on the Reykjanes Peninsula. They provide important information that can be used in estimation of seismic hazard in the area. The algorithm we have developed can be adapted for use for similar scenarios of events, in other hazardous areas in Europe.

### **Applied methodology, scientific achievements and main deliverables**

We have analysed InSAR and GPS data to estimate the co-seismic displacement field for the June 17 and June 21, 2000, main shocks and three triggered earthquakes on the Reykjanes Peninsula. The data for the June 2000 main shocks have been modelled in a joint inversion of the InSAR and GPS data for fault geometry and slip distribution (*Pedersen et al.*, 2003), assuming rectangular dislocations in an elastic half-space. The same method of analysis and inversion has been used to obtain best fit source parameters and locations for the three M~5 triggered earthquakes on Reykjanes Peninsula (*Árnadóttir et al.*, 2004). Figure 1 shows the dataset used in the joint inversion for the events in the SISZ.

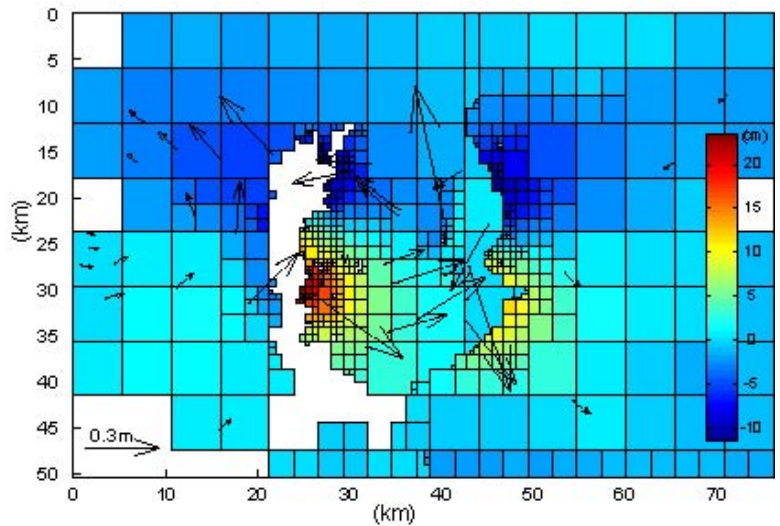


Figure 1. Three-dimensional co-seismic displacement field for June 17, and June 21, 2000 main shocks (D71). The color map shows the quadtree partitioned, unwrapped InSAR data from Track 52 and Track 95 covering the June 2000 earthquakes. Co-seismic GPS displacements are shown with black arrows.

The preferred model for the June 2000 main shocks indicates two simple 15 km long, near vertical faults extending from the surface to approximately 10 km depth (Figure 2).

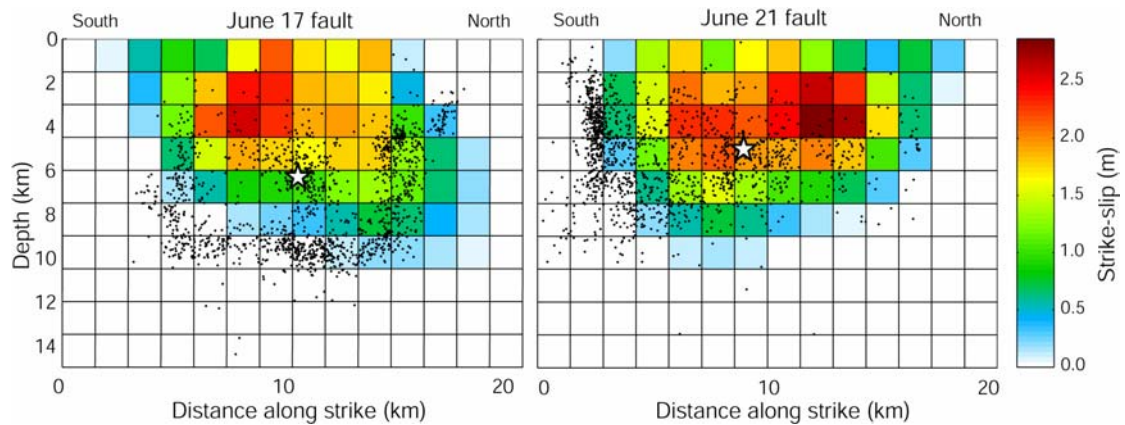


Figure 2. Right-lateral strike slip distribution estimated for the June 17 and June 21 earthquakes (D72). Hypocenters are shown with white stars, and aftershocks from June 17 to November 31, 2000, located near the modelled faults, as black dots.

Table 1. *Fault parameters for the June 2000 events estimated from different datasets. Latitude and Longitude is for the center of the fault plane at the upper edge. From Pedersen et al. (2003).*

June 17	Length (km)	Width (km)	Depth (km)	Dip (°E)	Strike (N°E)	Lon (°)	Lat (°)	Strike slip (m)	Dip slip (m)	Rake (°)	M <sub>0</sub> (Nm)×10 <sup>18</sup>	M <sub>w</sub>
Uniform slip	10.6	7.9	0.0*	87*	1	-20.347	63.973	1.7	0	180	4.4	6.4
Distributed slip	~15	~10	0.0	87*	2*	-20.347	63.973	0.0-2.6	0*	180	4.5	6.4
Árnadóttir et al. [17]	9.5	9.8	0.1	90*	3	-20.351	63.970	2.0	0.2	174	5.6	6.5
Pedersen et al. [18]	16.0	10.0*	0.0*	86*	5*	-20.342	63.979	0.3-2.4	0.0-0.2	175	5.4	6.5
NEIC [9]	-	-	-	75	-1	-20.487	63.966	-	-	173	4.3	6.4
Harvard CMT [33]	-	-	-	87	4	-20.47	63.99	-	-	-164	7.1	6.5
June 21	Length (km)	Width (km)	Depth (km)	Dip (°E)	Strike (N°E)	Lon (°)	Lat (°)	Strike slip (m)	Dip slip (m)	Rake (°)	M <sub>0</sub> (Nm)×10 <sup>18</sup>	M <sub>w</sub>
Uniform slip	11.9	8.2	0.0*	90*	0	-20.705	63.987	1.8	0	180	5.3	6.4
Distributed slip	~15	~10	0.0	90*	0*	-20.705	63.987	0.0-2.9	0*	180	5.0	6.5
Árnadóttir et al. [17]	12.3	8.0	0.0*	90*	0.5	-20.691	63.984	1.5	0	180	4.5	6.4
Pedersen et al. [18]	15.0	9.0*	0.0*	90*	0*	-20.703	63.982	0.5-2.2	0	180	5.1	6.4
NEIC [9]	-	-	-	79	-4	-20.758	63.980	-	-	-173	5.0	6.4
Harvard CMT [33]	-	-	-	85	2	-20.85	63.98	-	-	-167	5.4	6.5

Many studies have shown that static stress changes as small as 0.01 MPa(0.1 bar) caused by large earthquakes affect aftershock locations and may trigger subsequent events in a crust near to the critical state of failure (e.g. *Harris*, 1998 and references therein). This has been demonstrated using the Coulomb failure criterion, where failure will occur on a plane when the applied stress increment, defined as the change in Coulomb failure stress

$$\Delta\text{CFS} = \Delta\tau_s + \mu(\Delta\sigma_n - \Delta p),$$

where  $\Delta\tau_s$  is the change in shear stress resolved in the slip direction of a fault that may fail in a subsequent earthquake,  $\Delta\sigma_n$  is the change in normal stress due to the first earthquake, perpendicular to the subsequent earthquake fault plane,  $\Delta p$  is the change in pore pressure, and  $\mu$  is the coefficient of friction.

The slip model shown in Figure 2 has been used to calculate the static Coulomb stress change due to the June 17 and June 21, 2000, earthquakes in South Iceland (*Árnadóttir et al., 2003*). Figure 3 shows that the June 17 earthquake increased the static Coulomb stress by about 1 bar in the area of the June 21 hypocenter, promoting failure on the second fault. The static coseismic Coulomb failure stress change is very small at the locations of the three M~5 events triggered on the Reykjanes Peninsula stress calculations. The timing of these events and dynamic stress calculations indicate that these events were dynamically triggered by the surface wave from the June 17 main shock (see WP 6.2).

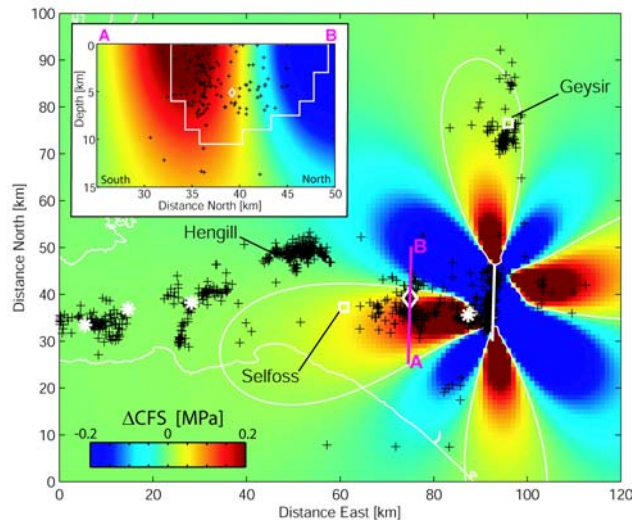


Figure 3. *Static coseismic Coulomb failure stress changes ( $\Delta CFS$ , in MPa) due to the June 17 fault slip (Figure 2), calculated at 5 km depth for vertical N-S faults with right-lateral strike slip motion. The contours surround areas where the CFS increased by more than 0.01 MPa (0.1 bar). The white diamond shows the location of the June 21 earthquake and white stars mark the largest aftershocks on June 17; note the three earthquakes triggered on Reykjanes Peninsula. Smaller aftershocks (location errors < 2.5 km horizontally and < 5 km vertically) with  $M > 1.0$ , from June 17 to June 21, are shown with black crosses. The coastline and the location of the June 17 fault model are shown with white lines. The white squares mark the Geysir geothermal area and the town of Selfoss. The inset shows the  $\Delta CFS$  in a N-S cross section along profile A-B. The extent of the June 21 fault is shown by the white box. Aftershocks from June 17 to June 21, located within 2.5 km east and west of the profile are shown with black crosses.*

The aftershock locations also correlate well with areas of increased Coulomb failure stress after the June 21 earthquake, particularly in the area between the two faults (Figure 4). The activity north of the two mainshocks appears to have extended westward in response to the increase in CFS following the June 21 earthquake. Less activity appears to have been triggered in the Hengill area (see Figure 4 inset) and on Reykjanes Peninsula following the June 21 earthquake, although it occurred closer to these areas than the June 17 event.

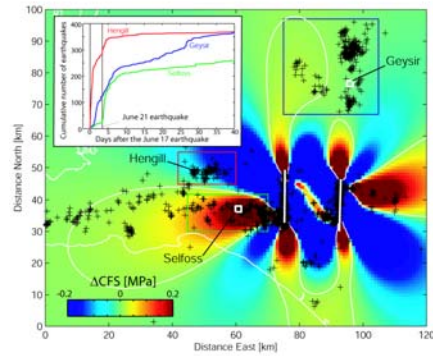


Figure 4. *Static coseismic Coulomb failure stress changes (in MPa) due to both the June 17 and 21 earthquakes, calculated at 5 km depth for vertical N-S faults with right-lateral strike slip motion. The contours surround areas where the CFS increased by more than 0.01 MPa (0.1 bar). Aftershocks ( $M > 1.0$ ) from June 21 to December 31, 2000, are shown with crosses. The inset shows the cumulative number of earthquakes ( $M > 1.0$ ) in three areas, as a function of days after the June 17 mainshock. The locations of the areas are outlined with color boxes and labelled.*

We use the same non-linear inversion algorithm to estimate the fault geometries and locations for the three triggered events on June 17, assuming uniform slip on three rectangular faults from GPS and InSAR data (Figure 3). The preferred model indicates three near vertical faults with primarily right-lateral strike slip (Figure 4). The largest observed coseismic deformation signal is near lake Kleifarvatn. Our study suggests that the event near Kleifarvatn (second triggered event) had significantly larger moment ( $M_w = 5.9$ ) than seismic estimates ( $M_w \sim 5-5.5$ ), indicating a component of aseismic slip or rapid afterslip on the fault.

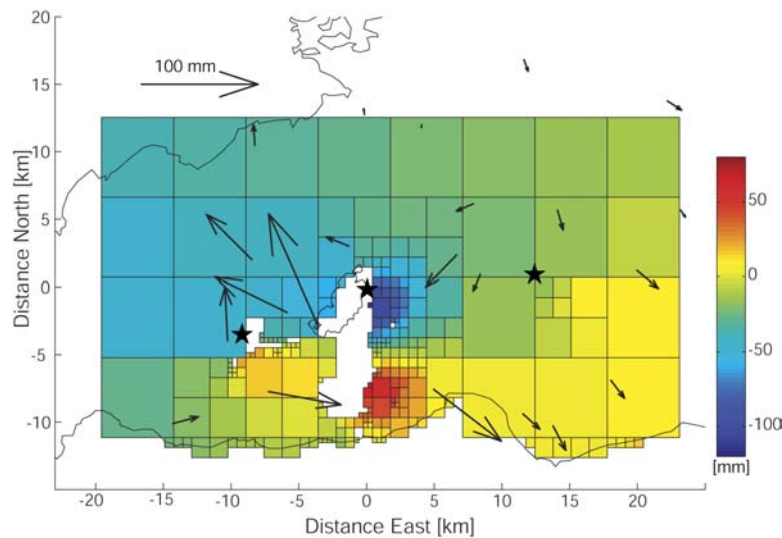


Figure 5. *Three-dimensional co-seismic displacement field for June 17, 2000 triggered earthquakes on Reykjanes Peninsula (D71). The color map shows the quadtree partitioned, unwrapped InSAR data from Track 367. The colour scale shows slant range displacements ( $\sim 23$  degrees from vertical), in the direction toward the satellite in mm. Blue is range increase, and red is range decrease, signifying subsidence and uplift respectively. The co-seismic GPS displacements are shown with black arrows. Black stars show epicentre locations determined from seismic data.*

## Conclusions including socio-economic relevance, strategic aspects and policy implications

We have modelled the co-seismic surface displacements due to the June 17 and June 21, 2000, main shocks and three triggered events on the Reykjanes Peninsula from GPS and InSAR data. We have used the fault models to calculate static Coulomb failure stress changes for the whole area. The models obtained from geodetic data can be compared with similar models obtained in other workpackages (e.g. WP4.2), and have been implemented in the dynamic stress calculations in WP6.2.

### Main literature produced (D73)

Árnadóttir, Th., S. Jónsson, F.F. Pollitz, W. Jiang and K.L. Feigl (2005b), Post-seismic deformation following the June 2000 earthquake sequence in the south Iceland seismic zone, submitted to *J. Geophys. Res.*, February 2005.

Árnadóttir, Th., H. Geirsson and P. Einarsson (2004), Coseismic stress changes and crustal deformation on the Reykjanes Peninsula due to triggered earthquakes on 17 June 2000, *J. Geophys. Res.* 109, B09307, doi:10.1029/2004JB003130.

Árnadóttir, Th., S. Jónsson, R. Pedersen and G. Gudmundsson (2003), Coulomb stress changes in the South Iceland Seismic Zone due to two large earthquakes in June 2000, *Geophys. Res. Lett.*, vol. 30, doi:10.1029/2002GL016495, no. 5.

Clifton, A.E., C. Pagli, J.F. Jónsdóttir, K. Eythórsdóttir, and K. Vogfjörð (2003), Surface effects of triggered fault slip on Reykjanes Peninsula, SW Iceland, *Tectonophysics* 369, 145-154.

Jónsson, S., P. Segall, R. Pedersen, G. Björnsson (2003), Post-earthquake ground movements correlated to pore-pressure transients, *Nature*, 424, 179-183.

Pagli et al., Triggered fault slip on June 17, 2000 on the Reykjanes Peninsula, SW Iceland captured by radar interferometry (2003), *Geophys. Res. Lett.*, 30(6), 1273, doi:10.1029/2002GL015310, 2003.

Pedersen, R., S. Jónsson, Th. Árnadóttir, F. Sigmundsson, and K.L. Feigl (2003), Fault slip distribution of two Mw=6.5 earthquakes in South Iceland estimated from joint inversion of InSAR and GPS measurements, *Earth and Planetary Science Letters*, 213, 487-502.

### References

Árnadóttir, Th., S. Hreinsdóttir, G. Guðmundsson, P. Einarsson, M. Heinert, and C. Völksen (2001), Crustal deformation measured by GPS in the South Iceland Seismic Zone due to two large earthquakes in June 2000, *Geophysical Research Letters*, 4031-4033, 2001.

Harris, R.A. (1998), Introduction to special section: Stress triggers, stress shadows, and implications for seismic hazard, *J. Geophys. Res.*, 103, 24,347--24,358.

Jónsson, S., P. Segall, R. Pedersen, G. Björnsson (2003), Post-earthquake ground movements correlated to pore-pressure transients, *Nature*, 424, 179-183.

Pagli et al., Triggered fault slip on June 17, 2000 on the Reykjanes Peninsula, SW Iceland captured by radar interferometry (2003), *Geophys. Res. Lett.*, 30(6), 1273, doi:10.1029/2002GL015310, 2003.

Pedersen, R., S. Jónsson, Th. Árnadóttir, F. Sigmundsson, and K.L. Feigl (2003), Fault slip distribution of two  $M_w=6.5$  earthquakes in South Iceland estimated from joint inversion of InSAR and GPS measurements, *Earth and Planetary Science Letters* 213, 487-502.

Pedersen, R., F. Sigmundsson, K.L. Feigl and Th. Árnadóttir (2001), Coseismic interferograms of two  $M_s = 6.6$  earthquakes in the South Iceland Seismic Zone, June 2000, *Geophysical Research Letters*, 28 , 3341-3344.

## **WP 5 New hazard assessment/New methods for improving assessment of probable earthquake effects**

### **Objectives**

On basis of the unique observations made in relation to the June 2000 earthquakes in the SISZ as well as on basis of results of modelling the earthquake sources in time and space we aim towards a more detailed hazard assessment both as concerns the the location and severity of probable earthquake hazard. This improvement is very significant basis for general risk assessment.

### **Methodology and scientific achievements related to workpackages including contribution from partners**

Probable faults of future large earthquakes have been mapped. Following the June 2000 earthquakes an area of 100 km length along the SISZ and the Reykjanes Peninsula, and to some extent towards north, was activated by triggered activity of small earthquakes, reflecting faults movements on numerous faults, which either were not known before or not accurately known. Accurate mapping of these faults at depth by microearthquakes information has been brought to an end and comparison has been made with geological mapping which has been carried out during the project.

New findings concerning the nature of the SISZ earthquake release and models of the two 2000 earthquakes obtained in various workpackages have been applied to the historical data to extract more information out of these.

The general time-independent hazard assessment as well as dynamic hazards assessment, which is significant during earthquake processes gains directly from results obtained in most workpackages and from the meetings during the last 6 months of the project period: The EGU special session in Vienna, the following PREPARED meeting, and the July 12 and July 21 meetings in Reykjavík.

### **Socio-economic relevance, policy implication and plans for the future**

Information of what ground motions can be expected at various places in populated areas is socially and economically significant. Where will the faults rupture the surface and when is of huge significance in any earthquake-prone country.

Social and economic impacts of a destructive earthquake or the knowledge that a destructive earthquake is to be expected is enormous and can be of such an effect to break up communities.

Knowledge of what can be expected leads to direct precautions in where and how man-made structures are built, or leads to strengthening or removal of existing vulnerable buildings.

The results here imply various technical and social precautions and preparedness that must be undertaken to mitigate the impact of earthquake hazards in various ways, on people and on society.

The work that awaits in the SISZ after the end of the project brings forward its objectives in many ways in cooperation with engineers, civil protection and other scientists to implement the results into the Icelandic Early Warning and Information System for routine use for mitigating earthquake risks in Iceland.

## **Discussion and conclusion**

The multidisciplinary fault mapping in SISZ and Reykjanes Peninsula, and mapping of surface effects together with progress in modelling the earthquake processes in the area has provided a basis for enhanced hazard assessment for the region. A special application real-time or dynamic hazard assessment, for nowcasting and short-term warnings, when the probable location is detected of a probably impending earthquake, or as soon as possible after its occurrence.

## **Deliverable**

Halldórsson P. and R. Stefánsson 2005. Reevaluation of historical earthquakes. *Icelandic Meteorological Office – Report*. In press.

Hjaltadóttir, S. & K.S. Vogfjörð 2005. Subsurface fault mapping in Southwest Iceland by relative location of aftershocks of the June 2000 earthquakes. *Icelandic Meteorological Office – Research Report 21*, 18pp.

## **WP 5.1 Mapping subsurface faults in southwestern Iceland with the microearthquakes induced by the June 17th and June 21st earthquakes**

**Authors: Sigurlaug Hjaltadóttir and Kristín Vogfjörð**

### **Objectives**

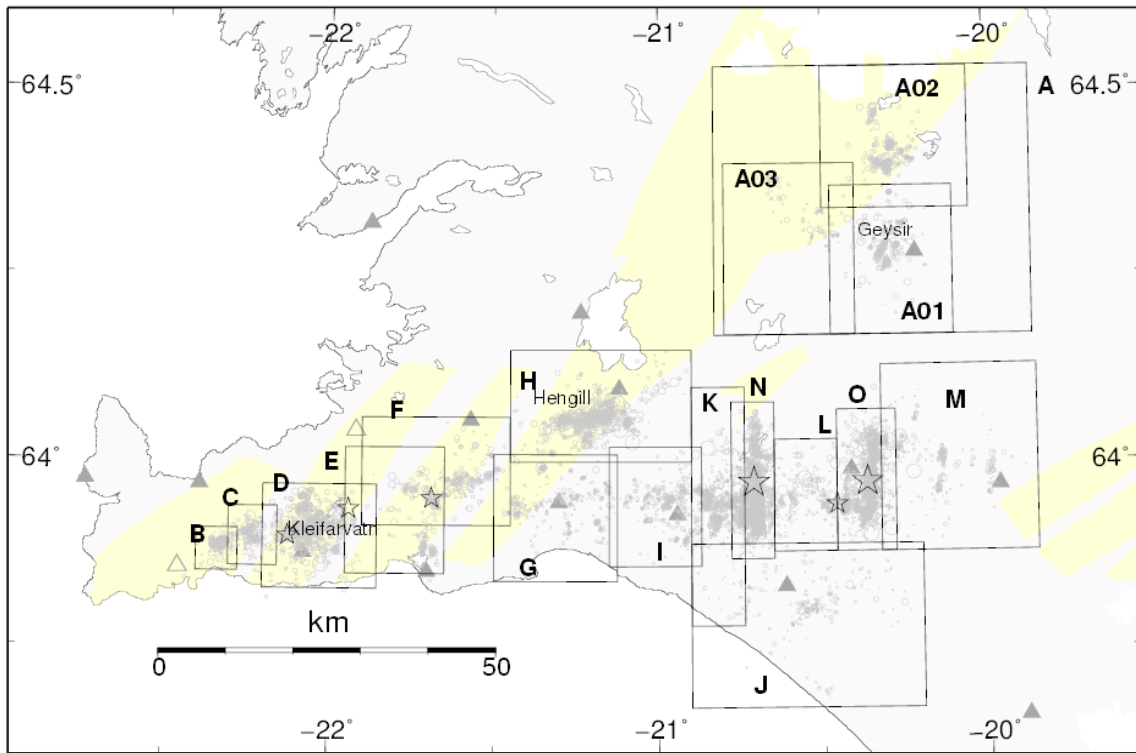
To map sub-surface fault planes and slip directions on faults in south-west Iceland that were illuminated by the microseismicity induced by the June 17<sup>th</sup> (J17) and June 21<sup>st</sup> (J21) earthquakes. This includes faults within and around the South Iceland seismic zone (SISZ), as well as within the rift zone on Reykjanes Peninsula (RP). Thousands of smaller earthquakes followed J17 and J21, induced either by seismic waves propagating from the two, or by the slower propagating change in stress field, resulting from the large (roughly 1m) slips on their 12.5-16.5 kilometer long faults. The resulting map is a significant input to the detailed hazard map, which will be prepared in the project, as closeness to active faults is critical for the estimation of ground motion due to earthquakes in South Iceland. The map is also a necessary input for models of stress field changes in time and space.

### **Methodology and scientific achievements related to workpackages including contributions from partners**

Roughly nineteen thousand microearthquakes recorded by the SIL seismic network between June and December 2000 and interactively analyzed, have been relatively relocated using the multi-event relocation method described in the first periodic report (Stefansson et al., 2004). Approximately half of them occurred outside the two main faults. This analysis increases the location accuracy to such a degree that individual fault patterns become resolvable.

The study area, southwest Iceland, was divided into 15 partly overlapping boxes (see map in figure 1) for analysis; two of these include the M=6.5 faults and fall under WP 4.1. Faults and clusters have been identified in all boxes. Most faults strike close to north and show a dominant right-lateral slip direction, most often accompanied by a normal component, as commonly observed in the SISZ. In the Western Volcanic Zone (WVZ), north-east fault directions are more common, but right-lateral motion is still the dominant slip direction. In many areas, fault strikes occasionally deviate from the normal trend of the area and more easterly directions can be observed. These are predominantly left-lateral strike-slip faults with a small normal component.

A trend towards shallower activity is observed in geothermal areas. This is most distinctively seen in the vicinity of the Geysir geothermal system, north of the SISZ. Box A, including the area, was divided into three sub-boxes according to the clustering of activity. The histogram in figure 1 shows the different depth distribution in the three boxes. Box A01 includes the cluster in the geothermal area and nearest vicinity, box A02 includes clusters of activity to the north and box A03 to the west. The shallowest earthquakes occur mostly at 1-3 km depth just south of the Geysir geothermal area, while the activity concentrates at 4-10 km depth towards the north and west.



Depth distribution in boxes A01, A02 and A03

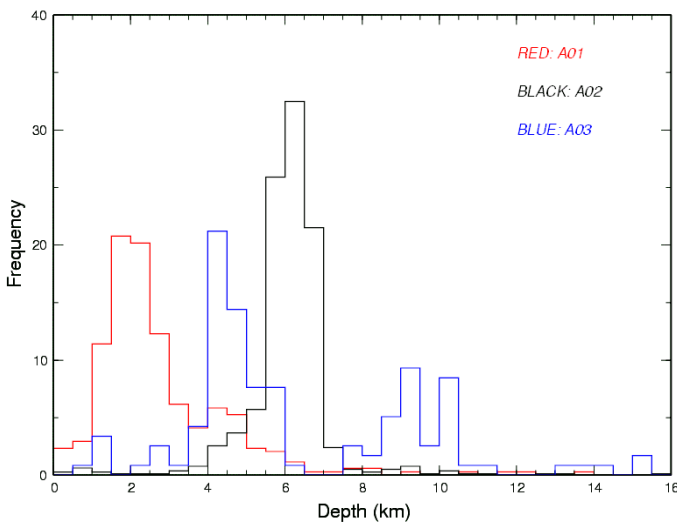


Figure 1. A map of southwestern Iceland, showing the division of the area into the fifteen boxes, A-O. Triangles denote station locations. Box A, including the Geysir geothermal area, was further divided into three sub-boxes. The histogram on the left shows the different depth distribution in the three sub-boxes. The activity is distinctively the shallowest closest to the geothermal area, and deepens towards the north and the west.

The thinnest crust in SW-Iceland (10-15 km) is found beneath the western RP. From there the crust thickens to the east below the SISZ, where crustal thickness of 20-22 km has been estimated (Allen et al., 2002; Bjarnason and Menke, 1993; Kaban et al., 2002; Tryggvason et al, 2002; Vogfjörð et al., 2002 and Weir et al., 2001). Figure 2 shows the different depth distribution for boxes covering the RP, Hengill and western SISZ, and further through the SISZ, including the J17 and J21 faults. At the westernmost part of the RP (boxes B and C), earthquakes mostly occur at depths between 5.5 and 7.5 km. Similarly, the activity further to the east in box F peeks at a similar depth interval, and also at a greater depth, or roughly 9 km. The boxes in between, D and E, include geothermal areas close to lake Kleifarvatn, which may well explain why most events occur at shallower (3-6 km) depths there. Further to the east, the activity is mostly concentrated in the uppermost part of the crust, in the 1.5-6 km depth range, in boxes H, I and K, but deepens towards the coast, in box G. Further east in the SISZ, activity deepens towards the Holt fault (box O) and the distinct activity along its bottom can be seen between 8 and 10 km. It is interesting to notice the deepening

seismicity south of the SISZ, in box J, where the crust is thinner, and the shallower activity in the easternmost box, M, where the crust is expected to be the thickest. A possible explanation is that box J is further away from the Volcanic Zones, and thus the crust is cooler there, while box M is very close to the active volcano Hekla, where the crust is supposedly getting warmer. According to Allen et al. (2002) an S-wave velocity minimum is found beneath Hekla in the 5-10 km depth range.

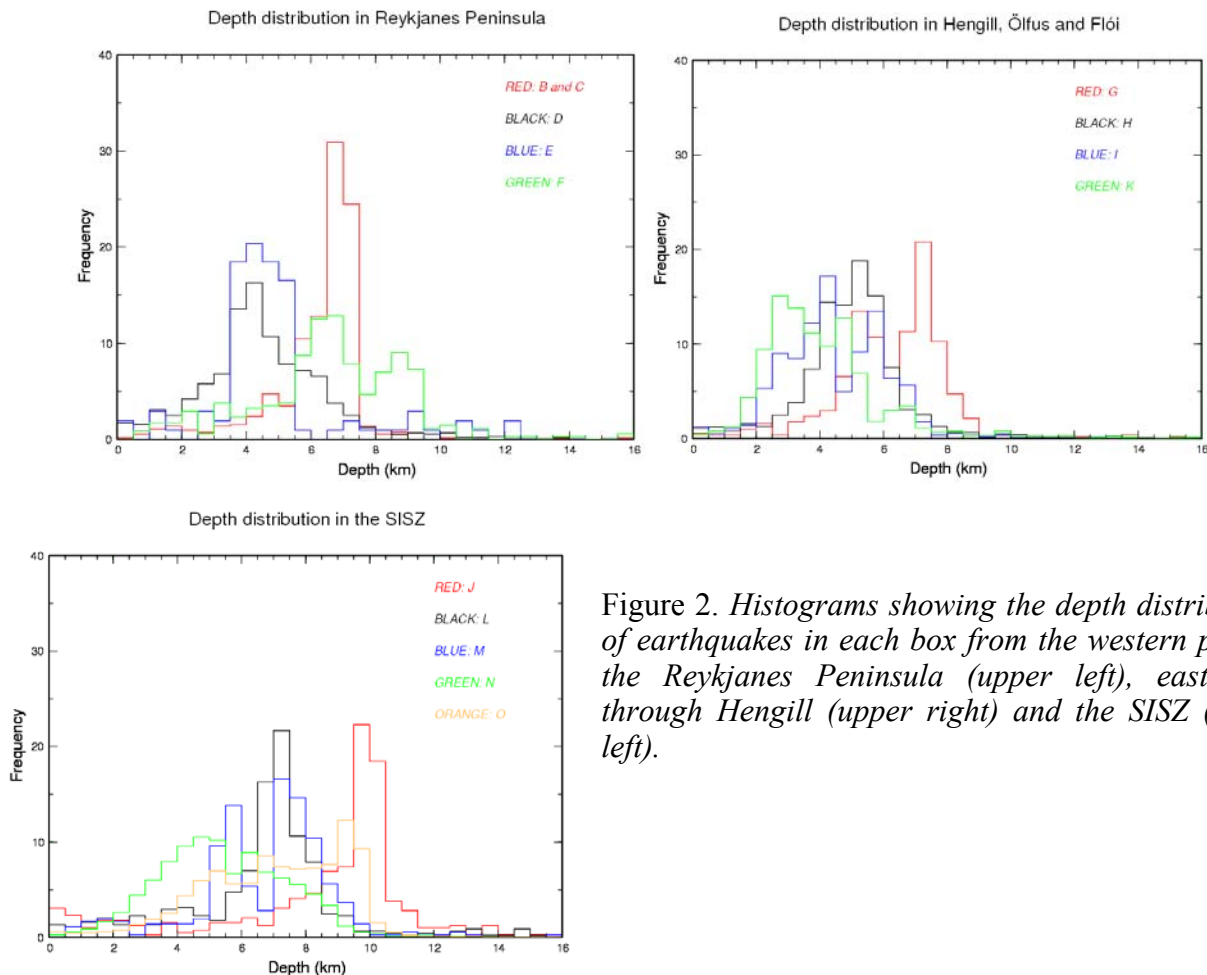


Figure 2. Histograms showing the depth distribution of earthquakes in each box from the western part of the Reykjanes Peninsula (upper left), eastwards through Hengill (upper right) and the SISZ (lower left).

## Socio-economic relevance and policy implication

A detailed map of subsurface faults, along with surface features mapped in the Reykjanes Peninsula (WP 5.2) and the SISZ (WP 4.3), will be an important contribution to the refinement of a tectonic map and for the mapping of the stress field in southwest Iceland. The fault map may also have great value for geothermal power companies and water suppliers in southwest Iceland, as it reveals subsurface faults not seen before. The fault map can possibly define the plumbing system delivering fluid into the geothermal systems in the Hengill-Hellisheiði area and Geysir, as well as flow paths of cold water feeding water wells.

## Discussion and conclusion

The increased aftershock activity following the June 2000 events illuminated innumerable faults and clusters in southwestern Iceland, which have now been mapped. Many of the large historical faults in the SISZ were active, but in most cases only separate patches on each one were illuminated. These can in many cases be linked by use of surface fault maps provided in WP 4.3. The fault

mapping with the aftershocks has also proven invaluable in determining the fault dimensions of the two dynamically triggered M~5 events on RP on June 17th, although the aftershock distribution on these faults is not contiguous. Determination of their mechanism, using only wave form data, has proven problematic.

### **Plan and objectives for the next period**

A report on fault mapping for workpackages 4.1 and 5.1 is in print. An article about fault mapping and the correlation between sub-surface faults and mapped surface faults is in preparation.

### **Abstracts**

Hjaltadóttir, S., Vogfjörð, K. and Slunga, R., Relative locations of earthquakes in SW-Iceland, Summer school on Tectonic-Magmatic Interaction, 31 August - 8 September, 2003, Geysir, South Iceland, p. 18, Nordic Volconological Institute report 0303, Reykjavik, Iceland, 2003.

Hjaltadóttir, S., Vogfjörð, K. and Slunga, R., Einarsson, P., Stefánsson, R., Relative locations of microearthquakes and mapping subsurface faults in southwest Iceland (in Icelandic). Science Symposium (Raunvísindafing), Askja, University of Iceland, 16-17 April, 2004. p. 75.

Hjaltadóttir, S., Vogfjörð, K. S. 2004. Relative event locations and mapping of faults in southwest Iceland (in Icelandic). Geoscience Society of Iceland, Spring meeting 2004. p. 54-55.

Hjaltadóttir, S., K. S. Vogfjörð, R. Slunga, 2005. Mapping Subsurface Faults in Southwest Iceland Using Relatively Located Microearthquakes. Geophysical Research Abstracts, Vol. 7, 06664, 2005.

Hjaltadóttir, S., K. S. Vogfjörð, R. Slunga, 2005. Fault Patterns in the South Iceland Seismic Zone Revealed by Double-Difference Mapping of Microearthquakes. Abstract submitted to AGU for the Fall Meeting in San Fransisco, December 2005.

### **References**

Allen, R. M., G. Nolet, W. J. Morgan, K. Vogfjörð, M. Netles, G. Ekström, B. H. Bergsson, P. Erlendsson, G. Foulger, S. Jakobsdóttir, B. Julian, M. Pritchard, S. Ragnarsson, and R. Stefansson, 2002. Plume driven plumbing and crustal formation in Iceland, *J. Geophys. Res.*, 107 (B8) 101029/2001JB000584.

Bjarnason, I. Th. and W. Menke, 1993. Tomographic image of the Mid-Atlantic Plate Boundary in southwest Iceland. *J. Geophys. Res.*, 98, 6607-6622.

Kaban, M. K., Ó. G. Flóvenz and G. Pálmason, 2002. Nature of the crust-mantle transition zone and the thermal state of the upper mantle beneath Iceland from gravity modeling, *Geophys. J. Int.*, 149, 281-299.

Ragnar Stefánsson, Françoise Bergerat, Maurizio Bonafede, Reynir Böðvarsson, Stuart Crampin, Páll Einarsson, Kurt L. Feigl, Christian Goltz, Ágúst Guðmundsson, Frank Roth, Ragnar Sigbjörnsson, Freysteinn Sigmundsson, Peter Suhadolc, Max Wyss, May 2004: PREPARED - first periodic report. February 1, 2003-January 31, 2004. Icelandic Meteorological Office, report 04014.

Slunga, R., Rögnvaldsson, S. Th., Böðvarsson, R., 1995. Absolute and relative locations of similar events with application to microearthquakes in southern Iceland, *Geophys.J.Int.*, 123, 409-419.

Tryggvason, A., S. Th. Rögnvaldsson and O. G. Flovenz, 2002. Three-dimensional imaging of the P- and S-wave velocity structure and earthquake locations beneath southwest Iceland, *Geophys. J. Int.*, 151, 848-866.

Vogfjörð, K. S., G. Nolet, W. J. Morgan, R. M. Allen, R. Slunga, B. H. Bergsson, P. Erlendsson, G. Foulger, S. Jakobsdóttir, B. Julian, M. Pritchard, S. Ragnarsson, 2002. Crustal profiling in Iceland using earthquake source arrays, AGU Fall meeting, Abstract S61C-1161, San Francisco, California, 6-10 December, 2002.

Weir, N. R. W., R. S. White, B. Brandsdóttir, P. Einarsson, H. Shimamura, H. Shiobara and the RISE Fieldwork Team, 2001. Crustal structure of the northern Reykjanes Ridge and Reykjanes Peninsula, southwest Iceland, *J. Geophys. Res.*, 106, 6347-6368.

## **WP 5.2 Mapping and interpretation of earthquake rupture in the Reykjanes peninsula and other surface effects there and in the SISZ**

**Author: Amy Clifton**

The objectives of the work package were to identify distant faults (on the Reykjanes peninsula) whose movement was triggered by the 17 June, 2000 earthquake in the South Iceland lowland, map the extent of surface rupture along these distant faults and other surface effects (rock fall and slope failure) in the entire area of SISZ and the Reykjanes peninsula, and characterize the faults along which motion was triggered in order to determine future predictability of minor fault movements.

A GIS database was established for the entire Reykjanes Peninsula. A new fault and fracture map was generated from a combination of field mapping and mapping from georeferenced digital air photos. Other layers incorporated into the GIS as separate layers include earthquake location point data, digital geologic map data, resistivity data and GPS vector data. Thematic layers showing slope and aspect have been generated within the GIS. The fracture map shows clearly that faults and fissures are unevenly distributed across the Reykjanes Peninsula and that the stress field across the peninsula from west to east is non-uniform. It also appears that strike-slip faults are more numerous than previously recognized and that these faults are either longer or extend farther to the north than previously recognized. When earthquakes are plotted over the fault map it can be seen that earthquake swarms are often occurring at the tips of mapped surface fault traces along strike-slip faults, indicating that these faults are still active and pose a potential hazard. A number of these swarms occurred in the weeks preceding the 4 June 1998 Hengill earthquake and again in the weeks preceding the 17 June 2000 earthquakes. Further study may allow us to use this information to better predict where larger earthquakes will occur.

A manuscript characterizing surface rupture along the 17 and 21 June 2000 faults in South Iceland has been published. Conclusions stated in the manuscript were that rupture occurred in large part along pre-existing structures, that surface rupture geometry was controlled by shallow crustal structure, and that the June 2000 earthquakes were of lower magnitude than other more recent historic earthquakes in South Iceland. Considerable progress has been made in identifying the surface characteristics of seismogenic faults on the Reykjanes Peninsula. An examination of earthquake hypocenters on the central part of the peninsula shows that their spatial distribution parallels the trend of mesoscale topographic features which had not previously been recognized as faults. Additional data from a M 5 earthquake in August 2003 provides support for this conclusion.

Cooperation is ongoing with partners at the IMO. The completed fault map has been added to the Bráðavá database.

## **WP 5.3 Study of the strong ground motion, acceleration and intensities of the two large earthquakes**

**Authors: Símon Ólafsson and Ragnar Sigbjörnsson**

### **Objectives**

The ground motion at a site due to an earthquake can be considered a convolution of source, path and site effects. A study of seismic hazard is not complete without considering site effects that can considerably increase the destructiveness of the ground motion. The main objective of the work, in WP 53, in this reporting period (months 25-30) was to study site effects in South Iceland by using recorded ground acceleration in the June 2000 earthquakes.

### **Methodology and scientific achievements**

The method applied to the acceleration records from the earthquakes in South Iceland does not require a reference site as the transfer function is calculated from the horizontal to vertical component ratio from a single recording. This method has been called 'Nakamura's method' or the H/V or HVR (horizontal-to-vertical ratio) technique. A parametric model describing the site amplification of vertically propagating S-waves is also fitted to the ground motion records. This method can be utilized for modelling site effects when realistic ground motion is simulated. This method can both be applied to records of microtremors and earthquakes. A detailed report of the work is given in the following deliverables:

- **Report:** *Site effects in South-Iceland based on strong ground acceleration.*
- **Abstract:** *Stochastic modelling of ground motion in Iceland.* Accepted abstract for 8NCEE (100<sup>th</sup> Anniversary Earthquake Conference) in San Francisco, April 18-20, 2006. (Abstract no: 1490). Work on paper in progress (Paper due Oct. 15, 2005).

The report contains a survey of the different methods that are used to estimate site effects. It also mentions the limited prior studies of site effects in the study area. A description is given of the computation of the H/V ratio from the acceleration records. The predominant period of ground motion and spectral amplification is computed from the records. Response spectra are also computed from the records and a study made of its shape in relation to design spectra in seismic codes (NHERP and Eurocode 8). A parametric site response model has been fitted to the acceleration records. This site response model describes vertically propagating S-waves and is can be applied to simulation of ground motion for sites that cannot be classified as rock-sites.

### **Socio-economic relevance and policy implication**

Large earthquakes have the potential to bring on casualties and great economic loss due to the damage and even collapse of structures. It is of great relevance towards mitigating earthquake risk to study ground acceleration in large earthquakes and develop mathematical models that describes the ground motion. These models make it possible to estimate in a probabilistic framework the earthquake loading that structures must be able to withstand in large earthquakes. This makes it possible to improve the basis for rational earthquake resistant design. A study of site effects is important due to the fact that they can dramatically increase the destructive potential of ground motion by amplifying the seismic waves for periods of motion where structures are especially vulnerable.

## **Discussion and conclusion**

The Nakamura method can be used to classify the sites with respect to the level of amplification that the seismic waves will be subjected to when they travel through the softer layers on their way from bedrock to the surface. This is possible because theoretically there is a direct link between the frequency of the largest peak of the H/V, the thickness of soil layers and the velocity of the seismic waves. In order to obtain thickness it is necessary to have a good idea of the velocity profile of the S-waves in the top layers beneath each site. The best way to establish this profile is by studying data from boreholes. Other methods to estimate the velocity profile include studying the propagation of seismic waves from explosions and SASW (Spectral Analysis of Surface Waves). Unfortunately very few data concerning velocity profiles exist for South Iceland. Alluvial deposits can also be overlain by lava-rock making the geological structure rather complicated. These are some of the problems that exist regarding the modelling of site effects and needed further study.

## **Plan and objectives for future research**

For further study of site effects it would be important to obtain better estimates of the S-wave velocity profile in the top 100 m of the surface layers. Drilling boreholes is very expensive. Other methods are, however, less expensive. It would therefore be very important in the future to perform such measurements at the sites of the stations that measured the acceleration in the June 2000 earthquakes. In further studies it would also be useful to obtain estimates of H/V ratios using microtremor measurements.

## WP 5.4 Reevaluation of the historical earthquakes in light of the new observations

**Author: Páll Halldórsson**

The aim of the project is to reevaluate magnitudes, locations and possible fault sizes for historical events in South Iceland seismic zone back to the year 1700. Historical earthquakes are defined here as events which neither magnitude nor location are based on measurements. In fact we are dealing with 10 events between 1700 and 1900 in the South Iceland seismic zone, where  $M \geq 6$ .

The method was to estimate the size of the destruction zone of each earthquake and compare the intensities with the intensities of the earthquakes in the year 2000. In this study the main damaging zone is defined as the zone containing farms where almost all houses (>90%) collapsed. The new estimates are based on reevaluation of historical documents. The reevaluation of the earthquake in the year 1734 was not possible because of lack of information.

The size of the destruction zone of each event was estimated:

Event	Destruction-zone [km <sup>2</sup> ]
1706	81
1732	261
1734	
1784-1	983
1784-2	359
1896-26. ág.	466
1896-27. ág.	162
1896-5. sept.-1	222
1896-5. sept.-2	43
1896-6. sept.	53

For the location the center of the zone was used, for the magnitude the size of it and for the fault length the shape of the zone.

The results are shown in the following table:

Event	New location		Older location		Magnitudes		Fault length [km]
	Lat.	Long.	Lat.	Long.	New	Old	
1706	63,95	20,18	64,0	21,2	6,3	6,0	6
1732	63,99	20,05	64,0	20,1	6,5	6,7	(25)
1734	63,90	20,80	63,9	20,8	6,8	6,8	
1784-1	64,00	20,40	64,0	20,5	7,0	7,1	18
1784-2	63,95	20,86	63,9	20,9	6,8	6,8	11
1896-26. ág.	63,95	20,15	64,0	20,2	6,8	6,9	(23)
1896-27. ág.	64,00	20,25	64,0	20,1	6,5	6,7	13
1896-5. sept.-1	63,93	20,50	64,0	20,6	6,5	6,5	7
1896-5. sept.-2	63,93	20,98	63,9	21,0	6,0	6,0	4
1896-6. sept.	63,95	21,18	63,9	21,2	6,0	6,0	4

## **WP 5.5 Hydrogeological changes associated with the June 2000 earthquakes**

**Author: Ágúst Guðmundsson**

### **Objectives**

The main objectives during the reporting period were as follows:

a) To make field studies in the Hengill Central Volcano to improve our understanding of fluid transport in seismically active geothermal fields, particularly in view of the loading of this volcano through stress transfer from the South Iceland Seismic Zone (SISZ) prior to the June 2000 earthquakes. This fieldwork aims partly at testing models developed in papers by Gudmundsson and Brenner (2003) and Gudmundsson (2005) on the effects of the SISZ on the nearby volcanoes, and how these effects (particularly seismicity and ground deformation, such as in Hengill in the years 1994-2000) can be used as precursors to large earthquakes in the SISZ.

These new studies were made in June-August 2005 (although financed by Prepared only to the end of July). Complementary field studies were also made on the deeply eroded magma chamber and related geothermal field in the Tertiary Geitafell Volcano in Southeast Iceland. This extinct volcano and its geothermal field are used as analogies for the Hengill Volcano and its geothermal field at the crustal depth of about 2 km.

b) To write the main results of the project work up as manuscripts for publication in international journals. Here the main work during this period has had to do with summarising and writing up, first, work on fault slip, similar to that which occurred on the strike-slip faults that slipped during the 17 and 21 June in South Iceland. Particular focus was on the fault displacement (slip), since this parameter is of fundamental importance for understanding fault effects on crustal fluid (such as geothermal water) transport. This work has been submitted as a paper by Gudmundsson and Geyer to Geophysical Research Letters. Secondly, the focus was on related work on the infrastructure, fluid transport processes, and loading by the South Iceland Seismic Zone of the nearby central volcanoes (composite volcanoes). This work has been submitted as papers to Journal of Geodynamics, Earth-Science Reviews, and the Geological Society of London Special Publications.

c) To present the main new results at international conferences. The main conferences attended during this period were the EGU meeting in Vienna in April and AGU meeting in New Orleans in May. The list of presentations and abstracts indicates the topics presented.

### **Methodology and scientific achievements**

1. *Field data.* The new field data from Hengill include more than 2044 joints and small-scale shear fractures (faults), 970 mineral veins, and some 60 large normal faults. These data will, it is to be hoped, allow us to understand better the relationship between the stress fields associated with the SISZ and those generating the earthquake swarms and doming in the Hengill Volcano in the period 1994-2000, that is, prior to the June 2000 earthquakes. The new data should also provide vital information on how permeability is maintained in geothermal fields in central volcanoes in Iceland and, in particular, how permeability is related to seismic activity in such volcanoes. It is well known that nearly all fracture-related permeability in geothermal fields is maintained through seismogenic faulting, such as in the SISZ. In the Hengill Volcano, however, the permeability, and the geothermal fields and springs, are related to two types of faults: (1) the large normal faults that form the main grabens, and (2) strike-slip faults, that is, the NNE-trending dextral and ENE-trending

sinistral faults, of the same type as occur in the SISZ. Many of the 2044 measured joints and small-scale shear fractures are thought to be such strike-slip systems.

2. *Numerical models.* Here the main progress has involved further analysis, and writing up of, the numerical results obtained in 2004 on strike-slip fault development. The main results of these models concern fault displacement as a function of (a) the mechanical properties of the damage zone, and (b) mechanical properties of the surrounding rocks, particularly the hyaloclastite mountains and other “soft inclusions”. The main results, some of which are now incorporated in the submitted papers listed below, may be summarised as follows:

- (i) When the fault tip is nearby, or inside, a hyaloclastite mountain, the slip, for given loading conditions and fault geometry, is much larger than when the tip is far away from the mountain.
- (ii) In models where hyaloclastic mountains are absent but the damage-zone thickness around the fault increases with time, the maximum displacement ( $u$ ) on a fault of a given length and with a constant loading condition, gradually increases. Thus, for rupture (trace) length ( $L$ ), the ratio  $u/L$  gradually decreases with time, so that the slip in individual earthquakes in relation to the rupture length increases with time.
- (iii) Even as the fault slip in individual earthquakes increases, the displacement (slip) profile remains similar as regards shape. Thus, for this type of loading, and with gradually increasing damage-zone thickness, the displacement profile remains a smooth, convex curve with a maximum slip at the fault centre.

3. *Borhole analysis.* The main work of the subcontractor Icelandic Geosurvey (Isor) has been televiwer logging, made in several wells in the SISZ and its vicinity. The main focus was on determining the state of stress in the SISZ and its surroundings. A total of 7 wells, with a cumulative depth of 6500 m, have been logged. The results are being processed at the time of writing, but appear very promising and likely to add to our understanding of the state of stress in the SISZ. More details are given in the formal Isor report which follows as an Appendix.

### **Socio-economic relevance**

The work made in this package has great socio-economic relevance, in particular in the following fields (both as regards South Iceland and in general):

- Earthquake hazard analysis
- Earthquake risk analysis
- Fracture-generated and maintained permeability and transport of crustal fluids (gas, oil, groundwater, geothermal water)
- Understanding and using geothermal reservoirs
- Interaction between volcanic and seismogenic zones
- Understanding volcanic unrest and hazards
- Volcanic risk analysis.

### **Discussion and conclusions**

Apart from some delays in the televiwer studies of the subcontractor (Isor), and the decision (by EU) that the year 2003 should not being part of the project period for the contractor (Göttingen), the work in this package progressed as planned. The work has already resulted in many new ideas and models concerning the mechanics of seismogenic faulting in the SISZ and the related fluid transport. In particular, the effects of mechanical heterogeneities and layering on faulting and fluid transport appear to be of fundamental importance for understanding the mechanics of earthquakes,

and associated changes in geothermal fields and permeability, in the SISZ. At the time of writing results are being obtained from borehole studies as to the state of stress in the SISZ – results that will be of fundamental importance for understanding and forecasting earthquakes in the SISZ.

## WP 5.6 Paleo–stress fields and mechanics of faulting

**Authors: Françoise Bergerat and Jacques Angelier**

### 1. Objectives

The main purpose of the WP 5.6 is the description of the stress field and understanding of the mechanical behaviour of the South Iceland active seismogenic zone (SISZ). In that way, our first aim was to determine how the stresses are distributed along the active faults and their evolution, using the earthquake data base of IMO. In a second time, to recognise the parameters which could control the nature and the distribution of the surface rupture traces induced by major earthquakes, we carried out field measurements of recent (plio-quadernary) faults and a detailed GPS mapping along selected parts major historical active faults. All these works deal with analysis of faulting in terms of geometry and mechanics, based on both the inversion of focal mechanisms of earthquakes and of fault slip data analysis, and the analysis of surface deformations associated to major earthquakes.

### 2. Methodology and scientific achievements

The main methodologies used in WP 5.6 are:

- Inversion of fault slip and of double-couple earthquake focal mechanisms (from the SIL network) data to obtain the recent (Plio-Quaternary) and the present-day stress tensors.
- Analysis of surface features of faults (mapping and geometrical analysis)
- Numerical modelling (distinct-element, finite-element)

A last field work has been carried out in the South Iceland Seismic Zone, 16<sup>th</sup> May – 1<sup>st</sup> June, 2005 (F. Bergerat, J. Angelier and M. Bellou) for (1) completing fault slip data collection in the SISZ, (2) additional measurements of push-up structures along some historical faults such as Selsund and Leirubakki faults.

### Fault slip data measurements and analyses

The study of fault slip data, during the PREPARED project, has been focussed on selected areas where the brittle mechanisms can be reconstructed from both the geological and seismological observations, between Hengill to the West to the Hvolsvöllur area to the East. The synthesis of all the brittle tectonic analyses carried out in this area, before and during the project, allowed to reconstruct the different stress regimes that prevailed in the SISZ area during the last 2-3 millions years. These results based on systematic inversion of about 1660 fault slip data, collected in 40 sites, have been compared with the stress regimes obtained from focal mechanisms of earthquakes. They indicate that there are four main regimes, with NW-SE (Fig. 1), NE-SW, N-S and E-W (Fig. 2) extension directions, respectively. All these regimes display inhomogeneous data sets, related to extensional and to strike-slip faulting. The dominating stress regime (NW-SE extension) is in agreement with both the general behaviour of the SISZ as a left-lateral transform zone and the opening of the rift segments. The three other regimes reflect stress permutation, dyke injection and maybe partly decoupling. The results of the focal mechanisms of earthquakes show a similarity in terms of stress directions. However the proportion of strike-slip faulting *versus* normal faulting is different for geological and seismological data, revealing an evolution from rifting to transform motion since the end of Pliocene.

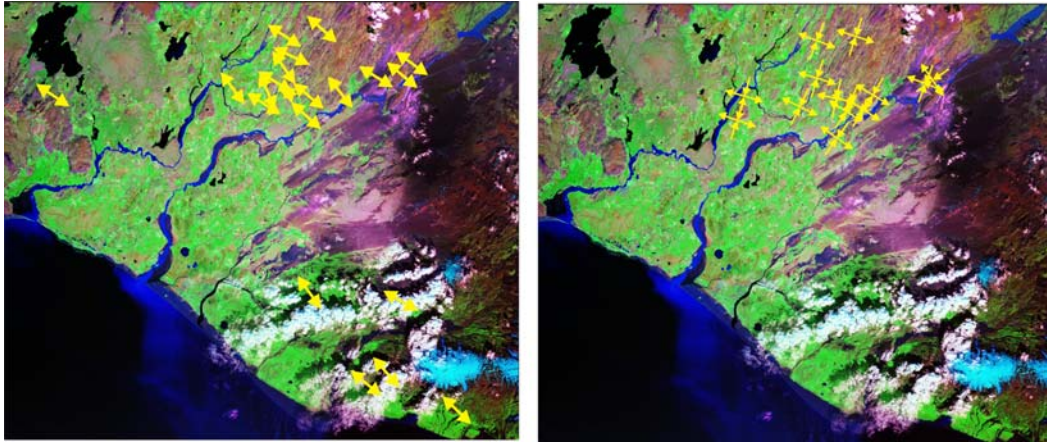


Figure 1. *The major regime: NW-SE extension, from normal (on the left) and strike-slip (on the right) faulting*

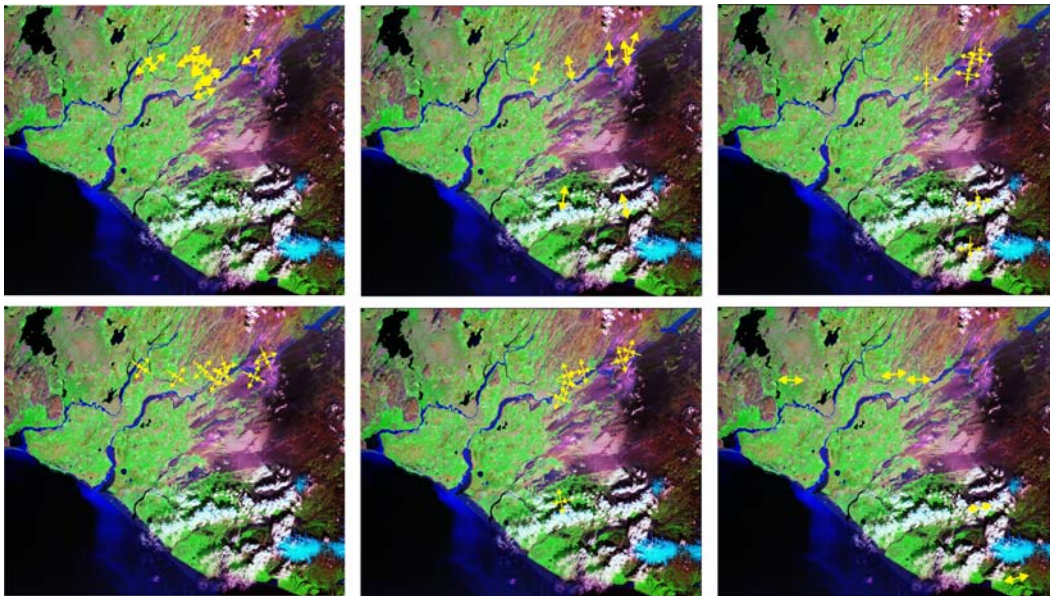


Figure 2. *The minor regimes: NE-SW, N-S and E-W extensions, from normal faulting (upper line) and strike-slip faulting (lower line)*

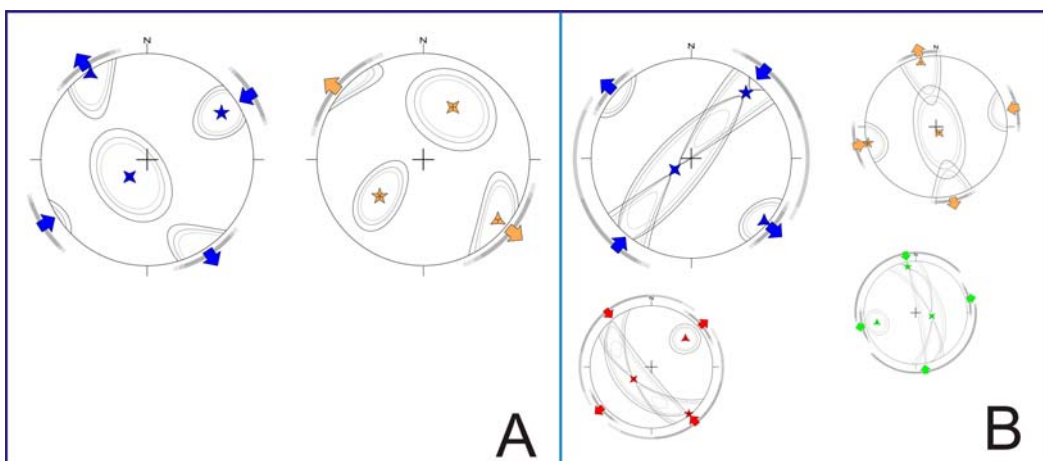


Figure 3. *Inversion of focal mechanisms of earthquakes: A - Example of  $\sigma_1/\sigma_2$  stress permutation in the central part of the SISZ, B - Different proportions of the four seismo-tectonic regimes in the eastern part of the SISZ (example for strike-slip faulting)*

## Present stress distribution and evolution in the South Iceland Seismic Zone

The aim of this work was to determine the volumes in which exists a homogeneous stress tensor and consequently determine the best fitting stress tensor in order to define an accurate state of stress around a major fault. In this study we present the results for the fault activated by the June 21<sup>st</sup> 2000 earthquake (M=6.6). To perform stress tensor inversion we use ZMAP6, a new tool for analyses of seismicity patterns (Wiemer et al., 2001).

The data used are:

- Period of time: From 1999/01/01 to 2000/12/31;
- 25090 nodal planes = 12545 focal mechanisms of double couple type;
- $0 \leq M_L$ .

To obtain the evolution in space and time of the stress tensor we consider:

- 1999/01/01 – 2000/06/17 (before the seismic crisis)
- 2000/06/17 – 2000/06/21 (Seismic crisis)
- 2000/06/21 – 2000/12/31 (after the seismic crisis)

Firstly, we have carried out some comparison between the Angelier's stress tensor inversions and the Michael's stress tensor inversions methods (1987), in order to define a confidence level to interpret the stress tensor variations correctly.

In a second time, we have drawn variance value maps and carried out stress tensor inversion in the South-western part of the Hestfjall Fault to illustrate the stress variations in space and time.

1/ The study of the variance value map, in order to define the best fitting stress tensor, give us significant results for the stress tensor determination according to the Angelier's method :

- for  $\sigma \leq 0.1$  only 8%- 15% of the data set are rejected for the stress tensor determination program (Angelier, 2002);
- for  $0.1 \leq \sigma \leq 0.2$  we have 24%- 40% of the data set are rejected;
- for  $0.2 \leq \sigma$ , 50% of the data set, and may be more at different location, are exclude from the stress tensor calculation.

2/ The variance value maps (Fig. 4) show us an evolution in space and time of the stress tensor all along the South Iceland Seismic Zone and particularly along the Hestfjall Fault. When we compute some stress inversions (Fig. 5) we noticed that this evolution point out a significant evolution of the stress axes directions along the N-S strike of the fault but also with depth.

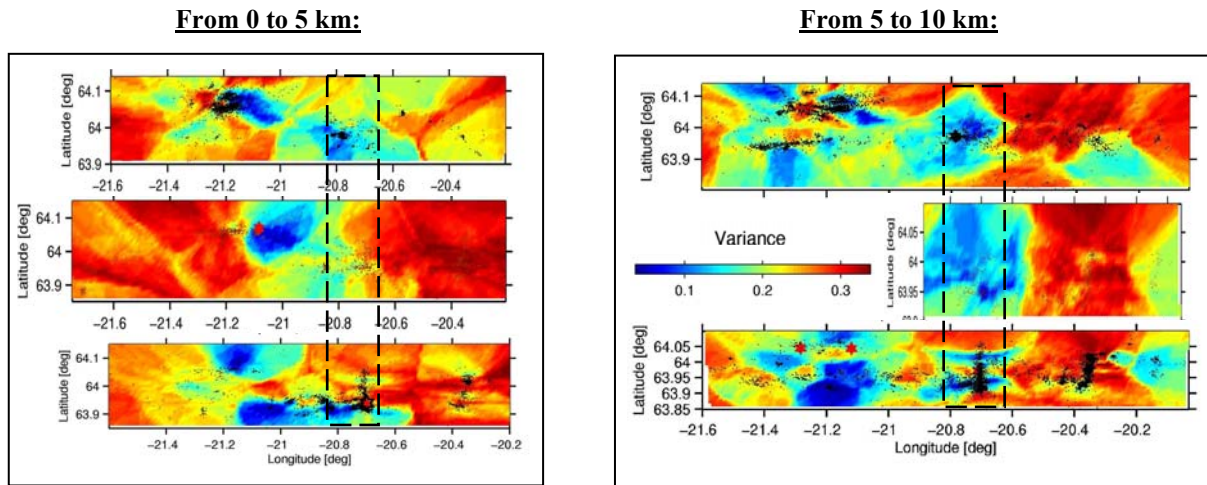


Figure 4. Variance value maps. On the left: Variance value maps obtained considering the first five kilometres of the crust, on the right, we consider a depth between five and ten kilometres. From the top to the bottom we illustrate the three periods of time (before the seismic crisis, the seismic crisis, and after the seismic crisis, respectively). The dashed lines delimitate the area of the Hestfjall fault. The white quadrangle shows the area in which the stress tensor inversion were realised.

Actually, these results show:

- A modification of the state of stress in the south western part of the Hestfjall Fault occurs after the earthquake of June 21st 2000.
- We notice a larger deviation of the stress between 5 to 10 km ( $\sim 40^\circ$ ), instead of  $\sim 20^\circ$  above.

0-5 km		Az.	Pl.	5-10 km		Az.	Pl.
Before	$\sigma_1$	43	4	Before	$\sigma_1$	52	6
	$\sigma_3$	132	8		$\sigma_3$	144	12
During	$\sigma_1$	50	5	During	$\sigma_1$	45	18
	$\sigma_3$	138	13		$\sigma_3$	130	13
After	$\sigma_1$	23	2	After	$\sigma_1$	12	19
	$\sigma_3$	113	7		$\sigma_3$	105	7

Figure 5. Stress tensor inversion carried out with the Angelier's method (2002). As for the figure 4, we consider the three periods of time (before, during and after the seismic crisis) and the two different depths (between 0-5km in the table situated on the left, and between 5-10km in the table on the right). We realise the stress tensor inversion for the Southwestern part of the Hestfjall Fault (See white quadrangle in figure 4).

By combining different methods of stress tensor computation, we are able to define a stress tensor inversion as accurate as possible, thanks to the determination of the volumes of uniform stress. This method allow us to point out a significant deviation in depth of the stress tensor, that may be imputed to an effect of the pore pressure beneath five kilometres depth or to a rheological contrast in the rheology.

### **Socio-economic relevance**

This study contributes to a better understanding of earthquake processes and mechanisms in the SISZ. Associated with the other studies carried out with the other WP of the PREPARED project, the WP 5.6 is socially and economically important for Iceland and other seismic areas.

### **Discussion and conclusion**

The study of recent and present day brittle deformations (fault slip data and focal mechanisms of earthquakes), as well as the analysis of surface traces of historical major faults, allow a better understanding of the mechanics of earthquakes. Combining these different elements highlights the crustal process leading to large earthquakes.

### **Plan and objectives for the next period**

The PREPARED project is now finished, but we plan to continue our collaboration with some of the PREPARED colleagues – at least in a informal way – especially in the focal mechanisms of earthquakes analysis and the numerical modelling domains. On the other hand we will carry out the preparation of papers to be published in international journals.

## **WP 6 Modelling and parameterizing the SW Iceland earthquake release and deformation processes**

### **Objectives**

Modelling and parameterizing the strain build-up and strain release in the SW Iceland earthquake zones on basis of all available relevant multidisciplinary data.

### **Methodology and scientific achievements related to workpackages including contribution from partners**

WP6 is based on inputs from progress and results of WP6.1 and WP6.2, as well as results of other workpackages parameterizing or modelling earthquake processes on basis of various observations of the year 2000 earthquakes as well as on older observations and modelling of earthquake processes in the zone, especially from the PRENLAB projects.

Intensive fusion work has been ongoing within WP6 during the last 6 months period, culminating in the the EGU special PREPARED session in Vienna and following special PREPARED meeting after the conference, as well as in the July 12 and July 21 meetings in Reykjavík.

### **Socio-economic relevance, policy implication and plans for the future**

The new understanding for earthquake release provides new possibilities for providing earthquake warnings ahead of earthquakes. Although some of this new understanding has already become useful in the Icelandic warning procedures, much work awaits in building alerts and visualizing tools to apply this new understanding in full.

### **Discussuion and conclusions**

An innovative outcome of the modelling fusion work is that high pore pressure values can effectively migrate from below the brittle-ductile transition to shallower depths in crustal conditions prevailing in the SISZ, in response to strain changes. This can explain various geophysical observations within the seismic zone. Such fluid-rock interaction which can be observed by microearthquakes can then be used to monitor redistribution of stress in the nucleation phase of the earthquake. This understanding is thus a significant basis for the PREPARED approach to warnings ahead of earthquakes. Thus the fusion work has been going from observations to modelling and then back to new understanding of the observations and thus created a new basis for alerts and visualizing of earthquake premonitory processes (Stefánsson et al. 2005c).

### **Deliverable**

Stefánsson, R., M. Bonafede, F. Roth, Þ. Árnadóttir, P. Einarsson & G.B. Guðmundsson 2005. Modelling and parameterizing the Southwest Iceland earthquake release and deformation process. *Icelandic Meteorological Office - Report*. In press.

## WP 6.1 Earthquake probability changes due to stress transfer

Authors: Sandra M. Richwalski and Frank Roth

### Introduction

The probabilistic approach to determine seismic hazard assumes that earthquakes occur randomly in space and time. Contrary to this, several authors have found evidence that an event may trigger or prevent a subsequent one by changing the shear or Coulomb stress at the site of this subsequent event (for an overview over the field see e.g., *Harris, 1998, Harris, 2000, or Freed, 2005*). Hence, stochastically speaking, the likelihood of the next event is conditionally increased or decreased. In the South Iceland seismic zone (SISZ) this was found to be true for the two large earthquakes in June 2000 (e.g., for co-seismic triggering: *Árnadóttir et al., 2003 and 2004*; for poro-elastic post-seismic triggering: *Jónsson et al., 2003*).

The SISZ is a 70 to 80 km long and 10 to 15 km wide zone taking up the transform motion forced upon southern Iceland by the opening of two offset branches of the mid-Atlantic ridge (Fig. 1). The western branch continues on land as the Reykjanes Peninsula oblique rift zone. West of the SISZ lies the Western Volcanic Zone (WVZ) and east of it the Eastern Volcanic Zone (EVZ). There is no clear expression of an actual E-W trending transform fault and the SISZ is at an oblique angle with the neighbouring ridges. Damaging earthquakes (i.e.  $M_s \geq 6$ ) in the SISZ occur fairly regularly at intervals between 45 and 112 years (*Einarsson et al., 1981*) and often as a series of events with time lags of generally only a few days between them. Generally, the first event in a series is the most eastward one, the subsequent events occur farther and farther west in the SISZ. All earthquakes occur as NS-oriented right-lateral strike-slip events.

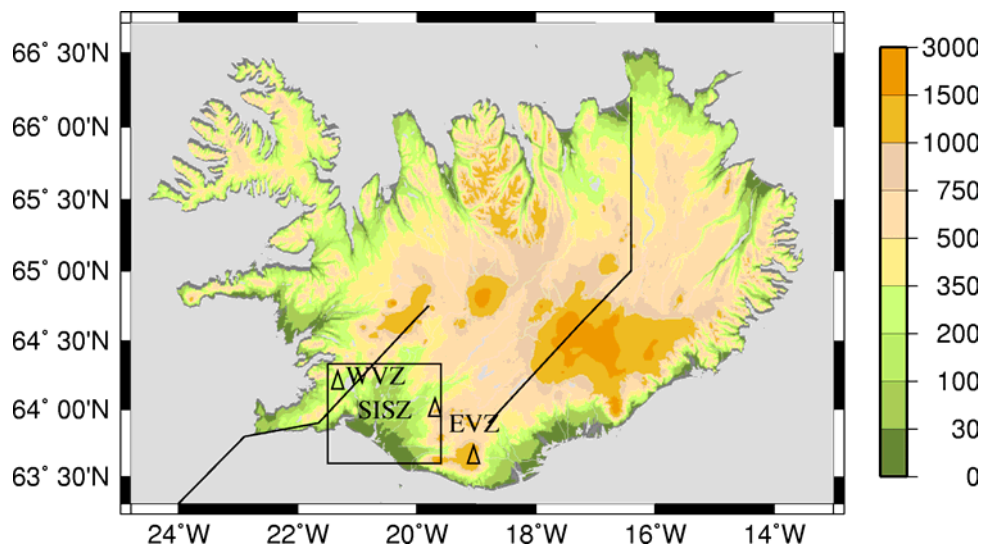


Figure 1. Topographical map [height in m] of Iceland. Western (WVZ) and Eastern Volcanic Zone (EVZ) are indicated. The black lines represent the branches of the mid-Atlantic ridge. The triangles show the position of the volcanoes Hengill, Hekla, and Katla (from west to east). The box represents the map section of southern Iceland presented in Figure 2.

Although the knowledge about the past events is far from complete (only the last three major events have been recorded instrumentally), the regularities observed so far, i.e., multiplicity of events (sub-series), east-west migration of events belonging to one sub-series, and average recurrence time of sub-series, suggest a triggering mechanism. It seems obvious to assume that stress build-up by plate

motion as well as stress changes caused by volcanic eruptions and seismic events, but also lateral inhomogeneities and the variation in crustal thickness determine the magnitude, location, and time of the impending event.

Therefore, *Roth* (2004) modelled the temporal evolution of the shear stress field by superimposing the background stress field caused by rift opening and the stress field changes induced by 13 events from 1706 to 2000. He applied an elastic half-space model. He concluded that the respective pre-seismic stress levels at the location of the impending events were generally high enough for triggering and fairly stable, also when varying the size of the rupture planes. Inside a sub-series, a mainshock-aftershock pattern became apparent. *Roth* (2004) explained inconsistencies by the incomplete knowledge about the events: Slight shifting of rupture planes might change the modelled pre-stress levels significantly in areas of inhomogeneous stress distributions. Due to the model being elastic, no post-seismic relaxation processes could be taken into account. These processes however have an influence on the stress distribution.

Encouraged by the results of *Árnadóttir et al.* (2003, 2004) and *Jónsson et al.* (2003) and by the findings of *Roth* (2004) we tried to find evidence for stress triggering for all or at least most of the 13 strong events, which occurred in the SISZ since 1706. Here, the lower crust and mantle were considered visco-elastic and, in addition to the steady stress increase of the stress field due to plate motion and seismic events, stress changes caused by relaxation were taken into account.

## **Modelling method**

Based on dislocation theory *Wang et al.* (2003) developed software for computing the elastic deformation, strain, and stress field produced by slip on a surface in a layered half-space model. The software was then extended to allow for modelling a mixed elastic/inelastic layered half-space model (*Lorenzo Martín et al.*, 2002; *Wang et al.*, 2005). This visco-elastic-gravitational extension can be used to model post-seismic creep processes. The software is composed of two parts, the first is called PSGRN and computes the Green's functions of three fundamental double-couple point sources at pre-defined depths; PSCMP finalizes the output by linear combination of discrete sources on the fault plane(s). Slip on the rupture surface can be chosen non-uniformly. Geographical coordinates can be used for input and output, but all internal computations are carried out in model coordinates.

The stress field was evaluated at 101 grid points in NS- and at 141 grid points in EW-direction, which corresponds to a grid spacing of about 1x1 km.

## **Data**

*Roth* (2004) summarised information from several authors to obtain information about the location and magnitude of 13  $M \geq 6$  events in the SISZ since 1706. Table 1 shows the values he used in his elastic half-space model.

Table 1. 13  $M \geq 6$  events inside the SISZ after Roth (2004). Note:  $M_S$  has been estimated by Halldórsson (pers. comm., 2004) by calibrating the damage area of events prior to the 1912 event to the reported damage area of this event and by using its recorded surface wave magnitude.

Date	$M_S$	Lat.°N	Long.°W	L [km]	W [km]	$U_0$ [m]
1706	6.0	64.0	21.2	10	7	0.30
1732	6.7	64.0	20.1	22	14	0.77
1734	6.8	63.9	20.8	25	14	0.96
14.08.1784	7.1	64.0	20.5	35	14	1.90
16.08.1784	6.7	63.9	20.9	22	14	0.77
26.08.1896	6.9	64.0	20.2	28	14	1.20
27.08.1896	6.7	64.0	20.1	22	14	0.77
05.09.1896	6.0	63.9	21.0	10	7	0.30
05.09.1896	6.5	64.0	20.6	18	14	0.48
06.09.1896	6.0	63.9	21.2	10	7	0.30
06.05.1912	7.0	63.9	20.0	32	14	1.50
17.06.2000	6.5	64.0	20.4	16	14	0.90
21.06.2000	6.4	64.0	20.7	18	14	1.10

*Einarsson* (pers. comm., 2004) conducted field campaigns for mapping the surface expression of faults in the SISZ. He found evidences that some locations of the faults differ from the so far published ones. He also estimated the increasing width of the rupture zone (from the surface down to the brittle-ductile transition) from the maximum depths of hypocentres published by *Stefánsson et al.* (1993). This width increases from 6 km in the western to 13 km in the eastern part of the SISZ.

Table 2. 13  $M \geq 6$  events in the SISZ after *Einarsson* (per. comm., 2004)

Date	$M_S$	Lat.°N	Long.°W	W [km]	$M_0$ [ $10^{19}$ Nm]
20.04.1706	6.0	63.98	21.19	6	0.1
07.09.1732	6.7	63.97	20.04	13	1.4
21.03.1734	6.8	63.97	20.83	7	2.0
14.08.1784	7.1	63.97	20.48	10	5.6
16.08.1784	6.7	63.97	20.94	6	1.4
26.08.1896	6.9	63.99	20.13	12	2.8
27.08.1896	6.7	63.97	20.26	11	1.4
05.09.1896	6.0	63.98	20.99	6	0.1
05.09.1896	6.5	63.99	20.58	9	0.7
06.09.1896	6.0	63.98	21.19	6	0.1
06.05.1912	7.0	63.94	19.95	13	3.5
17.06.2000	6.5	63.97	20.36	10	0.7
21.06.2000	6.4	63.98	20.72	9	0.6

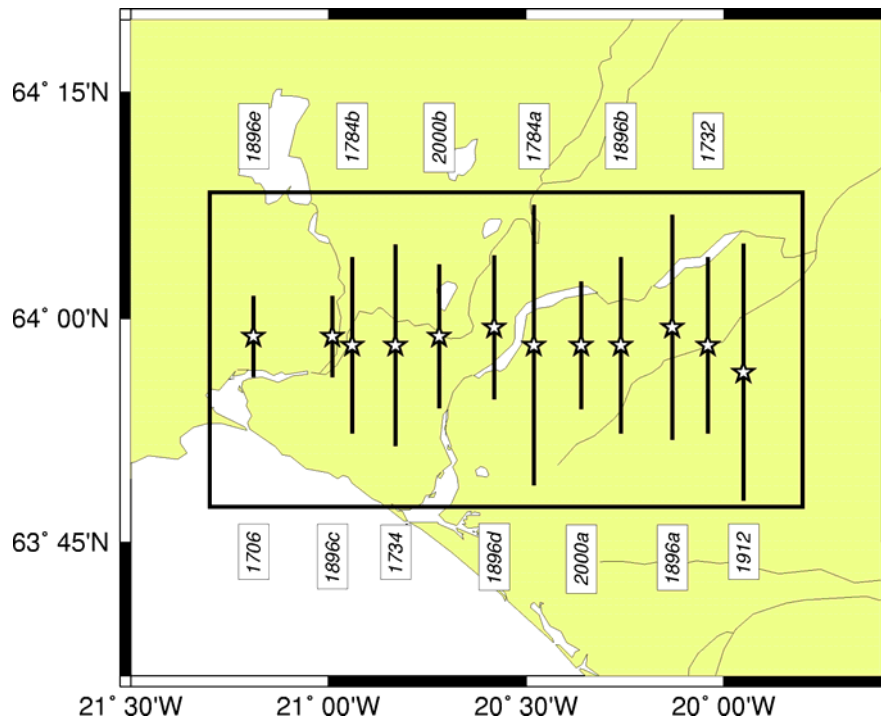


Figure 2. The South Iceland Seismic Zone with epicentres of 13  $M \geq 6$  earthquakes from 1706 to 2000. Epicentre locations correspond to values given in Table 2, rupture lengths to values given in Table 1.

## Model

Starting from the model of Roth (2004) shown in Table 1, we successively changed the coordinates according to Einarsson (pers. comm., 2004; Table 2). The final model for the location of the events is shown in Table 3. Although the computation of the scalar moment had been done by Einarsson taking  $M_S$  values for  $M_w$  ones in the relation  $M_w = 1.5 \log M_0 + 6.0$ , we used these values to compute the co-seismic slip  $U_0$ . The shear modulus value of 39 GPa given in Roth (2004) is rather high compared to values found in the literature (e.g., Stefánsson *et al.*, 1993: 34 GPa; Pedersen *et al.*, 2003: 30 GPa), but is used in absence of further constraints. No information on the total length of the ruptures was provided by Einarsson (pers. comm., 2004), therefore the values in Table 1 (Roth, 2004) were taken. Since fault planes solutions are available only for the two events in 2000 (Dziewonski *et al.*, 2001), all earlier events are modelled as vertical strike-slip events.

Table 3. Final model for the location and slip of the 13 events.

Date	$M_S$	Lat.°N	Long.°W	L [km]	W [km]	$M_0 [10^{19} \text{ Nm}]$	$U_0 [m]$
20.04.1706	6.0	63.98	21.19	10	6	0.1	0.43
07.09.1732	6.7	63.97	20.04	22	13	1.4	1.26
21.03.1734	6.8	63.97	20.83	25	7	2.0	2.93
14.08.1784	7.1	63.97	20.48	35	10	5.6	4.10
16.08.1784	6.7	63.97	20.94	22	6	1.4	2.72
26.08.1896	6.9	63.99	20.13	28	12	2.8	2.14
27.08.1896	6.7	63.97	20.26	22	11	1.4	1.48
05.09.1896	6.0	63.98	20.99	10	6	0.1	0.43
05.09.1896	6.5	63.99	20.58	18	9	0.7	1.11
06.09.1896	6.0	63.98	21.19	10	6	0.1	0.43
06.05.1912	7.0	63.94	19.95	32	13	3.5	2.16
17.06.2000	6.5	63.97	20.36	16	10	0.7	1.12
21.06.2000	6.4	63.98	20.72	18	9	0.6	0.95

Crustal velocities of the model are shown in Figure 3 for S- and P-waves. The shear modulus of 39 GPa is reached at a depth of about 6 km, values in the upper crust are much lower (down to 11 GPa). The transition from lower crust to mantle is fixed at 24.5 km, an average value for the SISZ according to *Menke (1999; see Figure 4)*.

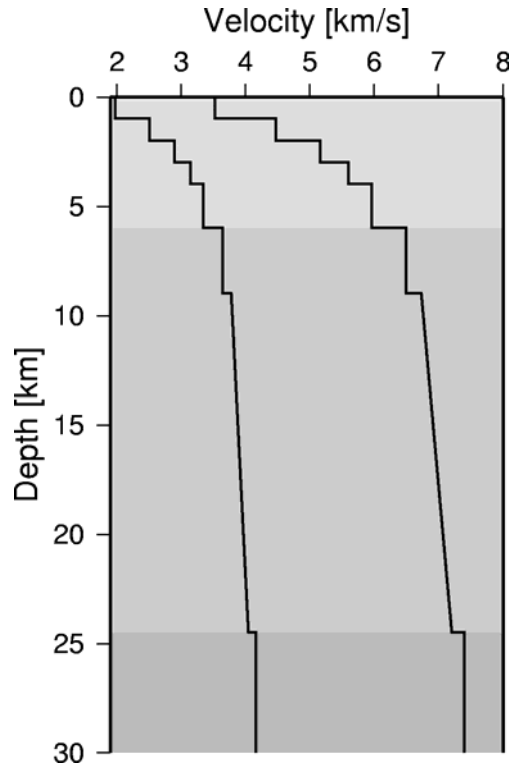


Figure 3. Velocity depth model from the South Iceland Lowland (SIL) project for routinely locating earthquakes in the region (*Stefánsson et al., 1993*). The light grey area represents the elastic upper crust with a density of  $2500 \text{ kg/m}^3$ . Below is the visco-elastic lower crust ( $3060 \text{ kg/m}^3$ ). Its viscosity is set to  $10^{18} \text{ Pas}$  in the fast-relaxing model and  $10^{19} \text{ Pas}$  in the slower-relaxing model. The visco-elastic mantle (dark grey) has the same viscosity and a density of  $3150 \text{ kg/m}^3$ . Density values are taken from *Menke (1999)*.

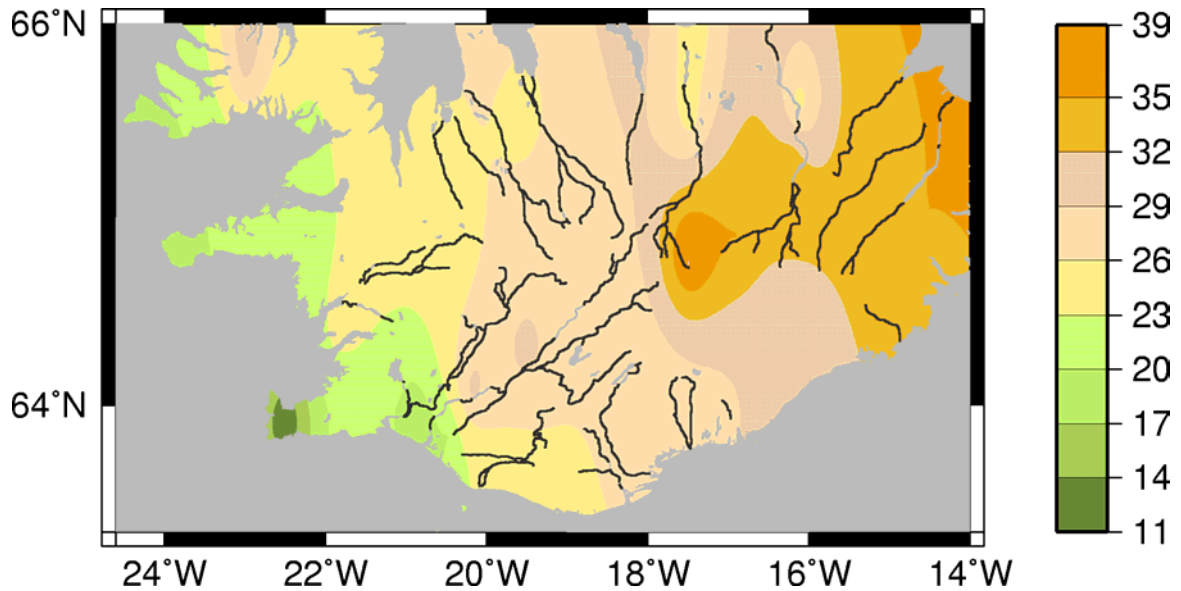


Figure 4. *Depth of the Moho after Menke (1999). For the SISZ an average crustal thickness 24.5 km was estimated.*

Viscosity estimates for the lower crust and mantle in Iceland range from  $10^{18}$  Pas to  $5 \times 10^{19}$  Pas (Jónsson *et al.*, 2003, and references therein). Figure 5a shows the shear stress imposed by the 1706 event for several time intervals until 2000. The profile crosses the rupture at 5 km depth. The results are shown for a model with a viscosity of  $10^{18}$  Pas, therefore, relaxation occurs very fast. Figure 5b shows the relaxation for a model with viscosity of  $10^{19}$  Pas. In the second case the inelastic material reacts much slower and stress changes can be expected until many years after the event. We used the latter viscosity in the final model.

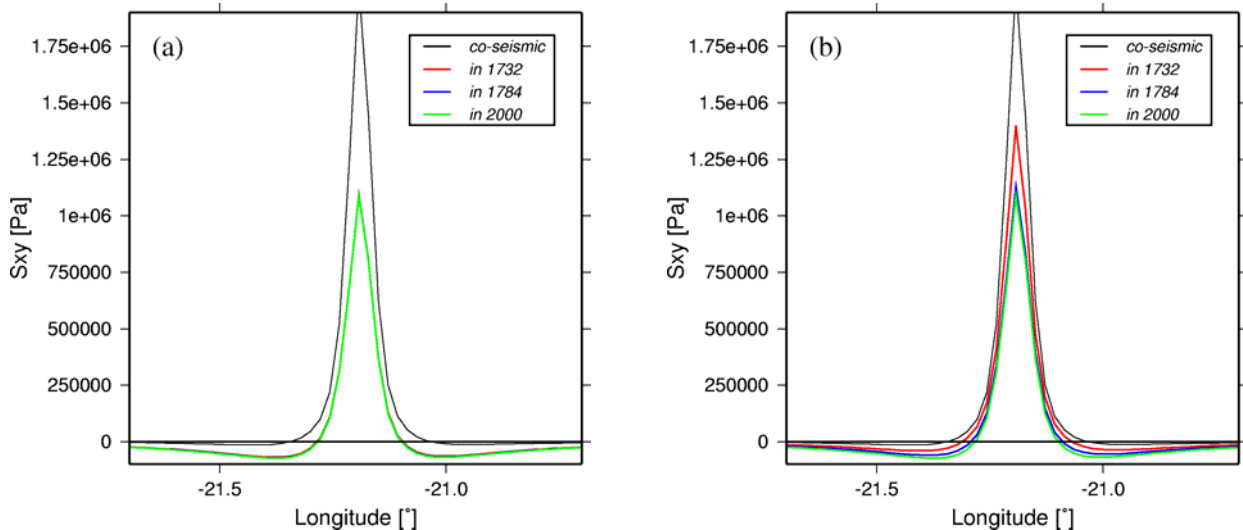


Figure 5. *Comparison of shear stress at 5 km depth along epicentral latitude ( $63.98^\circ$ ; i.e. perpendicular to strike direction) relaxed by the event of 1706 and its time-dependent variation between the fast-relaxing model with high viscosity (a; note that red and blue curves have almost the same values as the green one) and the slower-relaxing model with smaller viscosity in the lower crust and mantle (b).*

## Analysis of the modelling results

Horizontal shear stress changes: To study the temporal variation of the shear stress field in the SISZ, we followed Roth (2004). Regarding the background model (starting model in 1706) Roth (2004) had accounted in his elastic half-space modelling for the stress fields of the rifts neighbouring the SISZ. Since rift opening was not yet implemented in the visco-elastic software at the time of our calculations, we developed a background model similar to his, hereby using a EW-running pure strike-slip event (due to the rift opening component being small, we assume this approximation adequate). The background stress field was scaled such that its value at the location of the event of 14 August 1784 was not higher than the stress released by this event. Starting from this simplest assumption of a background stress field in 1706, we summed up the stress field produced by further tectonic loading in the inter-seismic times and superimposed the stress fields caused by the individual events.

We evaluated the shear stress changes at a depth of 5 km, which could be an average hypocentral depth throughout the SISZ. We computed the average shear stress along the rupture before and after each event.

Coulomb stress changes: We computed the Coulomb stress changes at 5 km depth on NS oriented strike slip faults using a Skempton parameter of 0.5 and a coefficient of friction of 0.75 (Árnadóttir *et al.*, 2003). We evaluated what percentage of the total rupture trace showed a positive Coulomb stress change or even values above 0.01 MPa, a value generally considered the threshold for Coulomb triggering (e.g. Harris, 1998, and references therein).

## Results

Regarding the uncertainties of all input parameters, the results should not be interpreted in an absolute sense. The magnitude of stress depends on e.g. the slip on the rupture surface, the shear modulus, and the viscosity. Without calibration of the modelling results with measured values, only the distribution of stresses should be considered. And this distribution is subject to uncertainties in the location of the events.

### Horizontal shear stress changes

As described in Section 5, we successively accounted for the contribution of the individual events and a background stress field. Figures 6 through 8 show a comparison for the final shear stress field in 2004 between different centring of the background field. Clearly, 64.0° N produces the result that looks most balanced. Therefore, in the following only results using this centring are shown and interpreted.

Figure 9 shows the evolution of the shear stress field. Clearly, the field in 1706 is too homogeneous. Roth (2004) considered the time up to and including 1784 a tuning phase. From that time on we find a balanced distribution between areas of positive and negative stress. It should be noted that small events continuously slightly modify the stress in the SISZ locally, but are not considered here. In comparison with the elastic modelling results of Roth (2004) the visco-elastic relaxation tends to smooth out the distribution of stresses such that small patches of low stress in high stress areas (and vice versa) vanish with time. Due to the parallel location of the events and the consequential similarity of their stress patterns (lobes) the shear stress generally increases in E-W direction over time (increase of red areas), while in N-S direction it decreases (blue).

Figure 10 shows the averaged pre-stress levels at each rupture for elastic (upper two rows) and visco-elastic modelling (lower two rows). The values along the ruptures were summed up at the

corresponding grid points; values were interpolated between neighbouring grid points in EW-direction if necessary. Each individual panel is scaled to the maximum of the average pre- or post-seismic stresses along the rupture (indicated at the top). This maximum is generally higher for the visco-elastic models. With exception of the two events in 2000, the stress increase and decrease during time is very similar for the elastic and the visco-elastic modelling results. The shear stress component along the slip direction of the earthquakes reaches its absolute maximum in only 6 out of the 12 cases (earthquakes of 1732, 1734, 1784a, 1896a, 1896c and 1986e) before the subsequent event in case of elastic models (cf. Tab. 4). For inelastic models the ratio is 7 out of 12 (1732, 1734, 1784a, 1896a, 1896c, 1986e and 2000b). However, this means that in the elastic (visco-elastic) model the shear stress has reached its maximum well before the event in 6 (5) of these cases (Table 4). Therefore, triggering should have occurred already earlier, i.e. by the time of the first shear stress maximum.

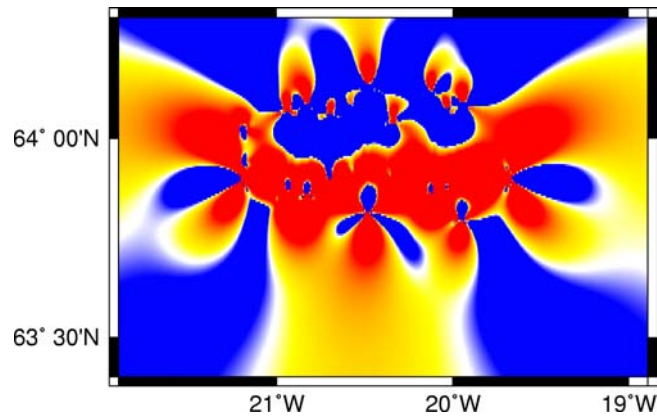


Figure 6. *The final shear stress distribution in 2004. The background field was placed at 63.9° N.*

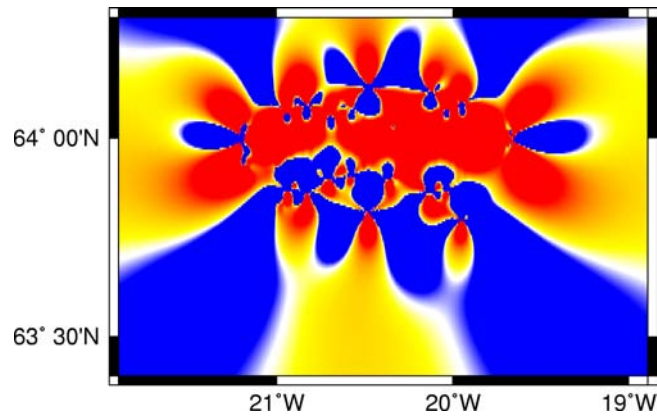


Figure 7. *The final shear stress distribution in 2004. The background field was placed at 64.0° N. This configuration was then used for the calculations.*

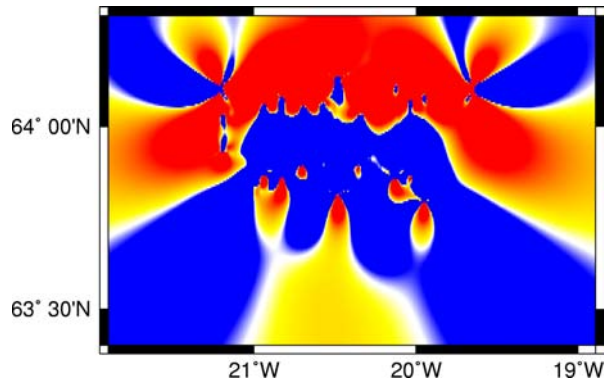


Figure 8. *The final shear stress distribution in 2004. The background field was placed at 64.1° N.*

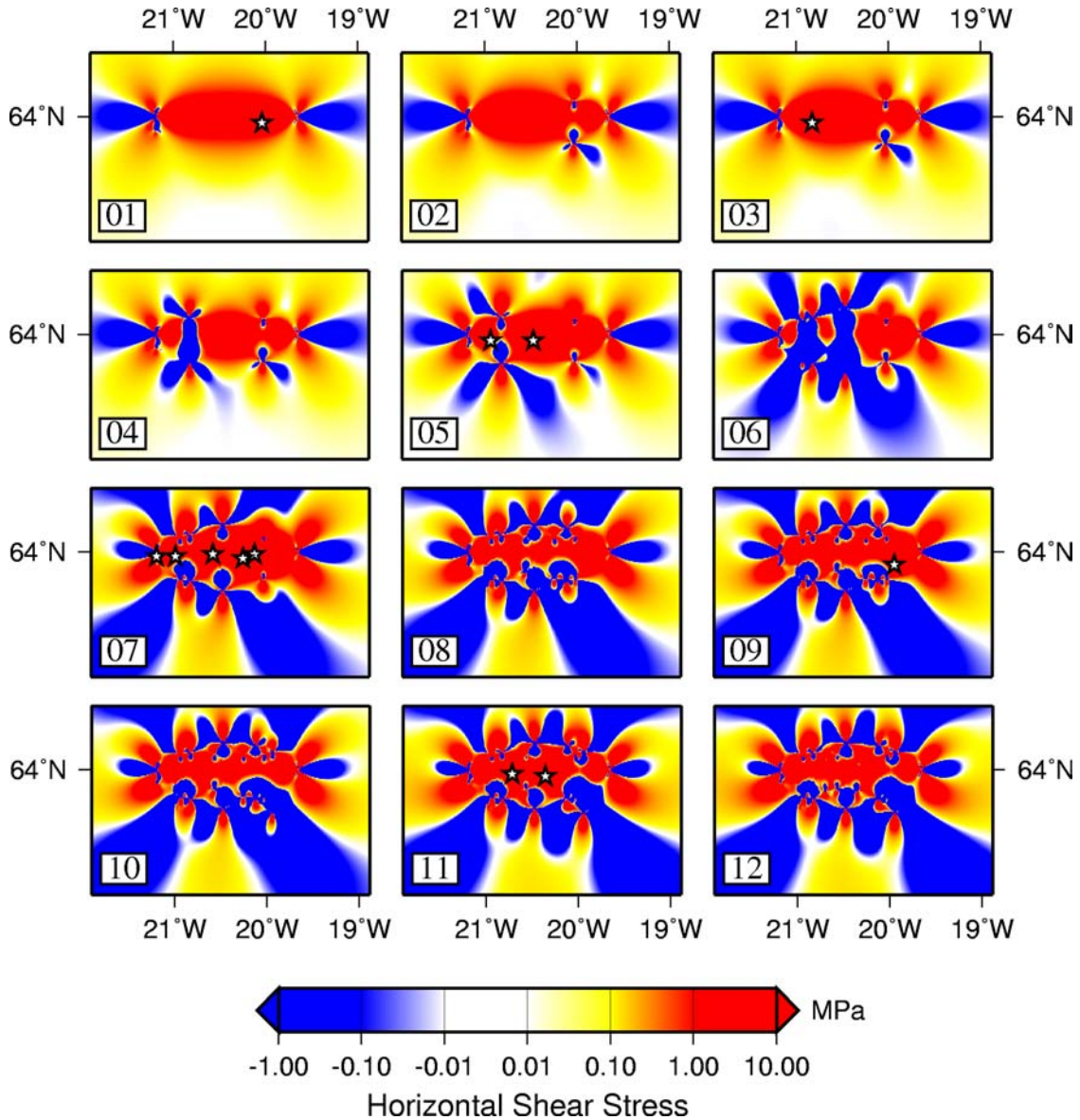


Figure 9. *Temporal evolution of the horizontal shear stress field for the visco-elastic layered earth model. The background field is centred at 64.0° N. Panel #01 shows the situation after the 1706 event. With exception of panel #02 (situation after the 1732 event), successive panels always show the pre and post seismic stress field belonging to the events in 1734 (#03/#04), 1784 (#05/06), 1896 (#07/#08), 1912 (#09/#10), and 2000 (#11/#12). The location of impending events is indicated by stars.*

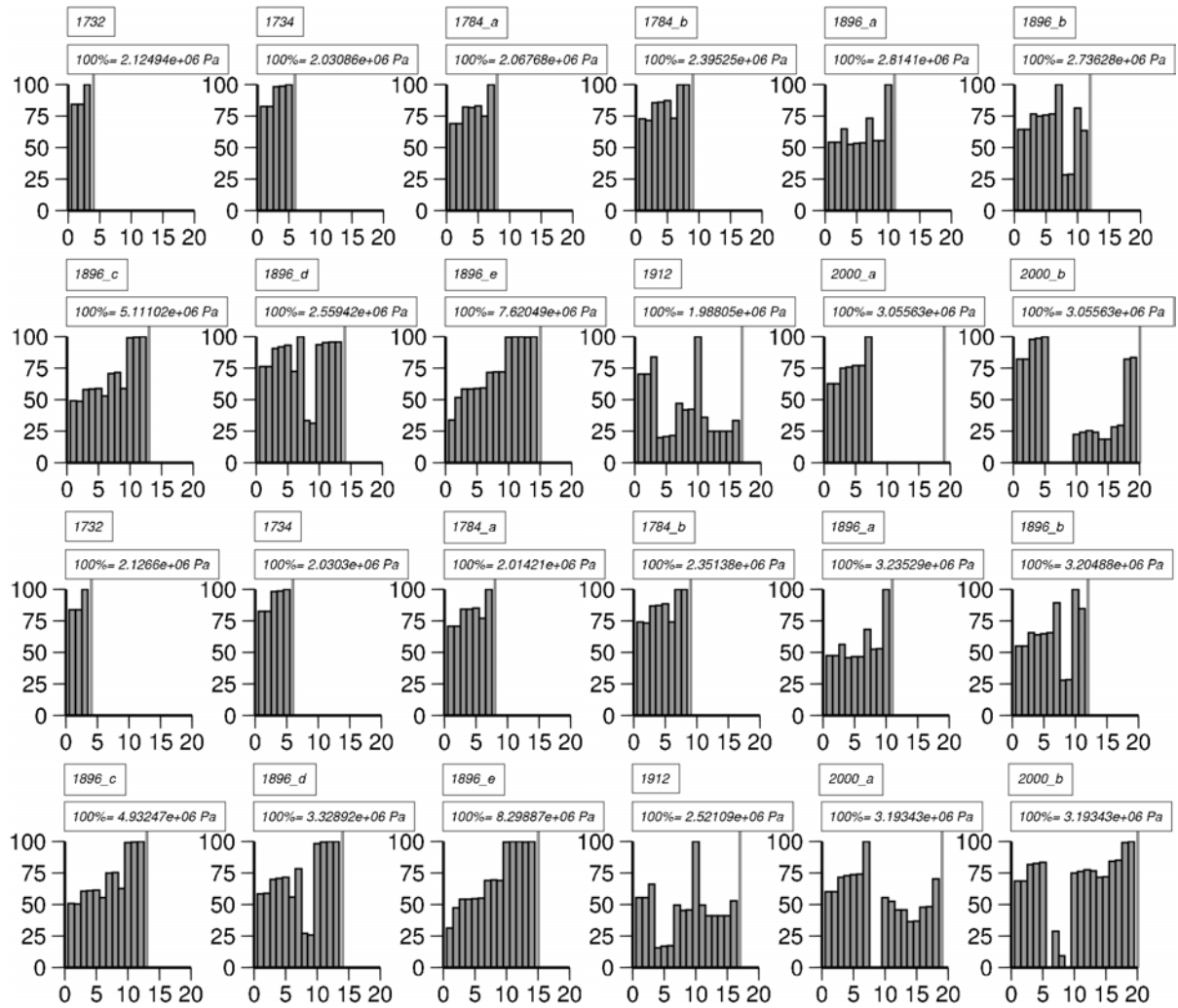


Figure 10. Comparison between elastic (upper two rows) and visco-elastic (lower two rows) modelling results for shear stress evolution, centring the background field at  $64.0^\circ$  N. The 20 bars display the respective values due to the events: 1(1706), ..., 20(2000\_b). The stress field was evaluated before and after each event (for events occurring within one year the inter-seismic time was assumed to be zero and post- and pre-event stress levels can be assumed to be equal, e.g. post 1784\_a and pre 1784\_b; this results in 19 different values). The maximum of the average shear stresses indicated on top of each individual figure corresponds to 100%.

Table 4. Evaluation of the stress level at the rupture plane of the triggered event (Fig. 10). \* This refers to single events (1912) and 1<sup>st</sup> events of sub-series (1732, 1784a, 1896a, 2000a).

Criterion	Elastic model		Visco-elastic model	
	Success ratio	Events meeting the criterion	Success ratio	Events meeting the criterion
High, i.e. $\geq 50$ % of maximum for that rupture	10 / 12	1732, 1734, 1784a, b, 1896a, b, c, d, e, 2000b	12 / 12	all
Maximum since 1706	6 / 12	1732, 1734, 1784a, 1896a, c, e	7 / 12	1732, 1734, 1784a, 1896a, c, e, 2000b
Maximum for 1 <sup>st</sup> events only*	3 / 5	1732, 1784a, 1896a	3 / 5	1732, 1784a, 1896a

## Coulomb stress changes

Figures 11 through 13 display three different ways to compute the contribution of the individual events to the Coulomb stress changes (CFS) found along the rupture of the event under consideration: considering each event as an individual event (Fig. 11), summing up successively the co- and postseismic effect of all events (Fig. 12), and selectively summing up events, which happened in a short time span (i.e. in sub-series; Fig. 13). Inter-seismic stress changes, i.e. by plate tectonics, were not considered in all scenarios.

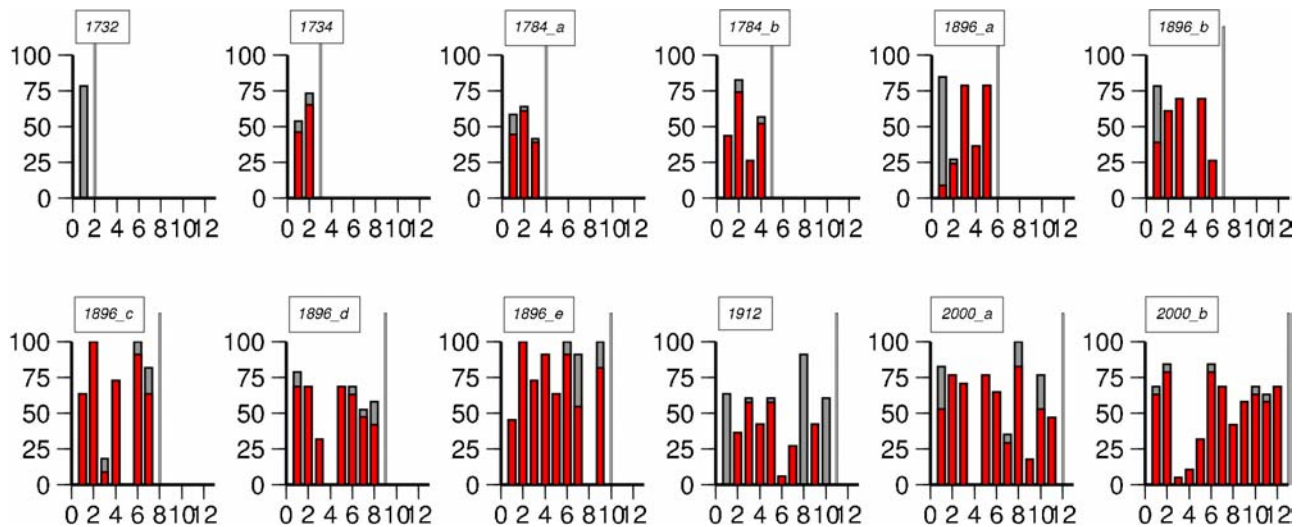


Figure 11. *Percentage of the rupture plane at 5 km depth of the event indicated showing positive Coulomb stress (grey) and values above the threshold of 0.01 MPa (red). The Coulomb stress change is evaluated for each event independently.*

Considering in each case the stress transfer by the preceding event only (Figure 11, Table 5), in 9 out of the 12 cases the CFS was positive on at least 50 % of the rupture plane of the coming event (1732, 1734, 1784b, 1896a, 1896c, 1896d, 1896e, 1912 and 2000b), but only in 6 of the cases (1734, 1784b, 1896a, 1896c, 1896e and 2000b) it was above the usually assumed trigger threshold of 0.01 MPa (e.g., *Reasenber and Simpson, 1992; Hardebeck, 1998*), which is a very low value just at the level of strong air pressure changes associated with the passage of thunderstorms.

The only positive finding is a correlation in so-called sub-series. In these cases, not the 1st but the succeeding events seem to be triggered by CFS in 6 out of 7 cases (1734, 1784b, 1896c, 1896d, 1896e and 2000b); the 1896d event shows on 50 % of the rupture plane positive Coulomb stress, but less than 50 % is above 0.01 MPa. In summary, for the sub-series we can therefore speak of mainshock-aftershock triggering.

To complete the statistics, we considered delays as well. In the SISZ strong events often occur as pairs or small clusters during the same day and in a time-span of up to 18.5 months (Sept. 1732 and March 1734; Aug. 14 and 16, 1784; Aug. 26, 28, Sept. 5 (2 events) & Sept. 6, 1896; June 17 and 21, 2000). If we neglect the events in these sub-series, we obtain a recurrence interval of 59 years for strong events (series). If we investigate the delay of events by a preceding stress decrease in our CFS analysis (in the shear stress analysis we added the plate tectonic stress changes, so that the summed stress value indicates already the effect of delays and advances), we find - as far as 1st events of sub-series are considered - that the events in 1896a and 2000a are delayed by 53 and 29 years, respectively, with respect to an average recurrence interval of 59 years (Table 6). Even

though the stress transfer in the two cases is not negative, indeed it is at least low from 1912 to 2000a. However, the stress transfer is high from 1784 to 1896a, where it should be low, and it is low from 1896 to 1912, where it should be high. We have tested these potential effects assuming different criteria, coined “hard” to “soft” in table 6.

Table 5. *Coulomb stress changes (for both the co-seismic and co- plus post-seismic stress changes) at the rupture plane of the triggered event. Here, only pairs of triggering and triggered events are considered. The results of the elastic and the inelastic model differ but not essentially with respect to the criteria applied here. \* This refers to single events (1912) and 1<sup>st</sup> events of sub-series (1732, 1784a, 1896a, 2000a). † This is trivial as it is the first triggered event in the whole series.*

	$\Delta\text{CFS} > 0 \text{ MPa}$		$\Delta\text{CFS} \geq 0.01 \text{ MPa}$	
	Success ratio	Events meeting the criterion	Success ratio	Events meeting the criterion
At $\geq 50$ % of the rupture plane	9 / 12	1732, 1734, 1784b, 1896a, c, d, e, 1912, 2000b	6 / 12	1734, 1784b, 1896a, c, e, 2000b
Maximum since 1706	2 / 12	1732 <sup>†</sup> , 1734	1 / 12	1734
At $\geq 50$ % of the rupture plane of 1 <sup>st</sup> events* only	3 / 5	1732, 1896a, 1912	1 / 5	1896a
At $\geq 50$ % of the rupture plane inside clusters only	6 / 7	1734, 1784b, 1896c, d, e, 2000b	5 / 7	1734, 1784b, 1896c, e, 2000b

Table 6. *Time delays (advances) for events due to stress decrease (increase) by Coulomb stress changes (for both the co-seismic and co- plus post-seismic stress changes) on different fractions of the rupture planes at 5 km depth. The results of the elastic and the inelastic model differ, but not essentially with respect to the criteria applied here.*

	Event	Timing	CFS-criteria met				
			hard	→	soft		
		“-“ early “+” late (in years)	$\Delta\text{CFS} > 0.01 \text{ MPa}$ at $\geq 50$ %	$\Delta\text{CFS} > 0$ at $\geq 50$ %	$\Delta\text{CFS} > 0.01 \text{ MPa}$ at $> 0$ %	$\Delta\text{CFS} > 0$ at $> 0$ %	
1 <sup>st</sup> events only (average recurrence time 58.8 years)	1732	-32.4	no	yes	no	yes	
	1784a	-6.9	no	no	yes	yes	
	1912	-43.2	no	yes	no	yes	
				$\Delta\text{CFS} < -0.01 \text{ MPa}$ at $\geq 50$ %	$\Delta\text{CFS} < 0$ at $\geq 50$ %	$\Delta\text{CFS} < -0.01 \text{ MPa}$ at $> 0$ %	$\Delta\text{CFS} < 0$ at $> 0$ %
	1896a	+53.2	no	no	yes	yes	
2000a	+29.3	no	yes	yes	yes		

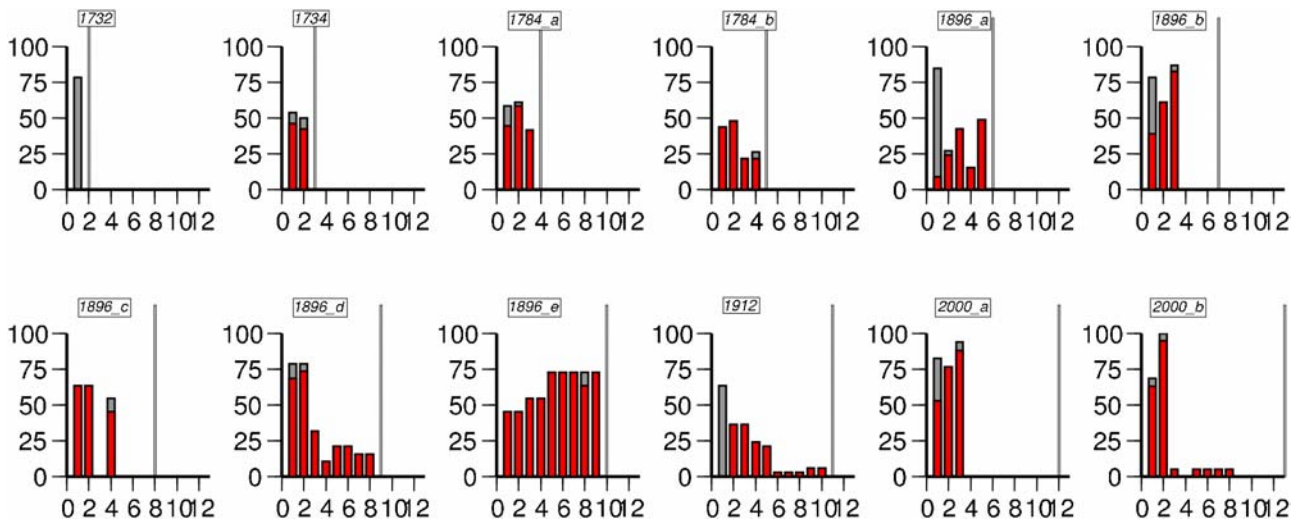


Figure 12. Same as Figure 11, but shown is the cumulative effect of all preceding events.

When summing up successively the effect of all events (Figure 12) most events show a decrease in percentage of the fault being above the threshold level due to stress release by neighbouring events. This indicates that tectonic loading of the SISZ due to rift opening is needed to push the rupture plane partly above the threshold.

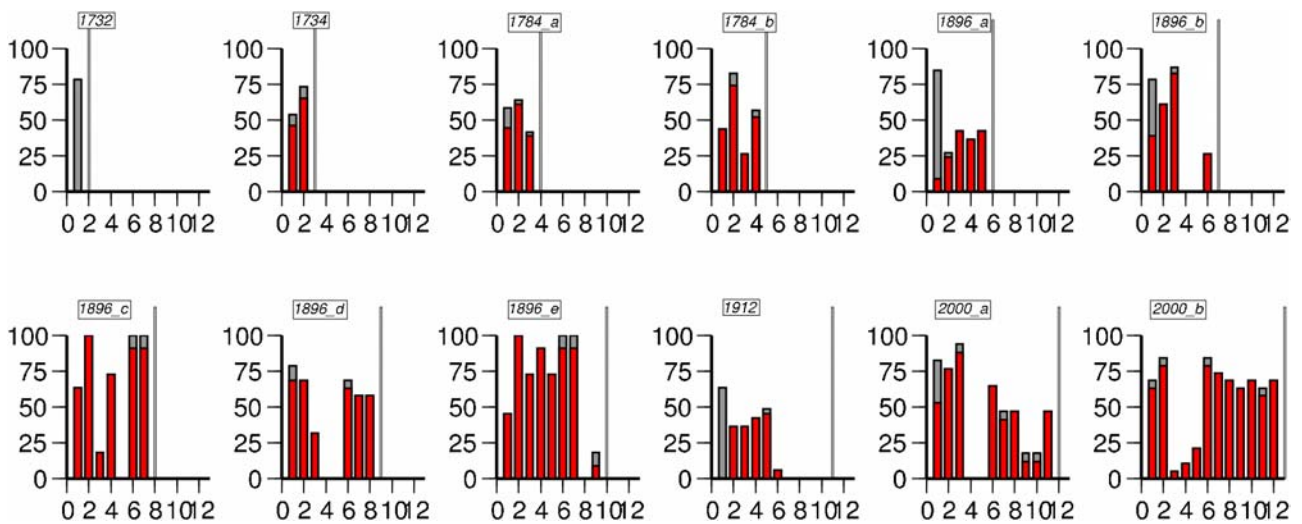


Figure 13. Same as figures 11 and 12, but events have been summed up only, if they happen in the same sub-series. The 12 bars display the respective values due to the events 1706, 1732, 1732+1734, 1784\_a, 1784\_a+b, 1896\_a, 1896\_a+b, 1896\_a+b+c, 1896\_a+b+c+d, 1896\_a+b+c+d+e, 1912, 2000\_a.

A mixture of the two previous approaches is presented in Figure 13. Here, only events happening inside a sub-series are summed up.

## Discussion and Conclusions

Computing shear stress and Coulomb stress changes in the SISZ did not lead to definite conclusions regarding the time and location of the next event. Uncertainties in the model parameters (e.g. location of the historical events, rupture history, viscosity, knowledge about events prior to 1706, i.e. background stress field) as well as the simple approach used (e.g. 1D crustal structure, disregard of stress transfer due to volcanic activity) complicate the evaluation of the results. Generally, the

modelling showed that it is impossible to constrain the stress field such that the impending event can only occur at its known location. There are always large areas in which stress levels seem to be high enough to trigger an event.

Therefore, we restricted the interpretation of the modelling results to the known locations. But even in this case, the modelling of the evolution of the shear stress field showed that regarding absolute stress levels the maximum is only reached in 50% of the cases right before the event. Regarding Coulomb stress changes, contrasting three different models – independent triggering, successive summing and selective summing – the following conclusions can be drawn: Tectonic loading is certainly necessary to prepare the mainshock (the first event inside a sub-series). Subsequent events of such a sub-series might be regarded as being triggered by this first event. However, the spatial distribution of the events can again not be explained by our modelling. The observed migration of subsequent events towards the west might be correlated with the thinning of the crust towards the west (Fig. 4). Additional 2D modelling might allow for testing this hypothesis. Regarding an interaction between earthquake and volcanic activity *Gudmundsson and Saemundsson (1980)* statistically analysed 82 eruptions and 44 seismic events for mutual influence and found a weak but significant relationship: volcanic activity leads the seismic one. They explain it partly by triggering effects (local), but postulate a common cause, namely plate motion.

Certainly, having better and more detailed information about previous events and subsurface parameters will lead to better modelling results. However, the SISZ cannot be considered a region with mature faults, which rupture with a certain recurrence interval. Rather, as shown by detailed mapping of seismicity around the two 2000 events (WP 2 of PREPARED, see First Periodic Report, p. 10), foreshocks appeared on an old fault rotated 30-40° to the south with respect to the direction of later seismicity. 17 days before the June 17 earthquake, seismicity started to rotate into the direction of the mainshock and seismicity on the older fault disappeared. Furthermore, events in the SISZ appear parallel to each other. Successful Coulomb stress change reports come mainly from areas, where there is one mature main through going fault (e.g. North-Anatolian Fault Zone, San Andreas Fault Zone), while secondary faults branch off or run only partly in parallel.

Summarising, we can state that strong events in the SISZ are presumably not triggered by preceding events but could rather occur randomly with the stress provided by plate tectonics. Under these unfavourable circumstances (too many assumptions) and with the modelling results at hand it is presently unreasonable to derive meaningful conclusions from computing the changes in occurrence probability of future earthquakes for the SISZ. Concerning the sub-series, we may surely assume that another strong event is probably ahead (4 in 6 cases) during the next months.

## References

- Árnadóttir, T., Geirsson, H., and Einarsson, P., 2004, Coseismic stress changes and crustal deformation on the Reykjanes Peninsula due to triggered earthquakes on 17 June 2000, *J. Geoph. Res.* **109**, B09307, doi: 10.1029/2004JB003130.
- Árnadóttir, T., Jónsson, S., Pedersen, R., and Gudmundsson, G.B., 2003, Coulomb stress changes in the South Iceland Seismic Zone due to two large earthquakes in June 2000. *Geoph. Res. Lett.* **30**, 1205, doi: 10.1029/2002GL016495.
- Einarsson, P., Björnsson, S., and Foulger, G., 1981, Seismicity pattern in the South Iceland Seismic Zone. in: *Earthquake Prediction – An International Review*, Simpson, D.W. and Richards, P.G. (eds.), Maurice Ewing Series 4, AGU.

- Dziewonski, A.M., Ekström, G., and Maternoskaya, N.N., 2001, Centroid moment tensor solutions for April-June 2000. *Phys. Earth Planet. Inter.* **123**, 1-14.
- Freed, A. M., 2005, Earthquake triggering by static, dynamic, and postseismic stress transfer. *Ann. Rev. Earth Planet. Sci.* **33**, 335-367.
- Gudmundsson, G. and Saemundsson, K., 1980, Statistical analysis of damaging earthquakes and volcanic eruptions in Iceland from 1550-1978. *J. Geoph.* **47**, 99-109.
- Hardebeck, J. L., Nazareth, J.J., and Hauksson, E., 1998, The static stress change triggering model: Constrains from two southern California aftershock sequences. *J. Geoph. Res.* **103**, 24427-24437.
- Harris, R.A., 1998, Introduction to special section: Stress triggers, stress shadows, and implications for seismic hazard. *J. Geophys. Res.* **103**, B10, 24347-24358.
- Harris, R. A., 2000, Earthquake stress triggers, stress shadows, and seismic hazard. *Current Science* **79** (9), 1215-1225.
- Jónsson, S., Segall, P., Pedersen, R., and Björnsson, G., 2003, Post-earthquake ground movements correlated to pore-pressure transients. *Nature* **424**, 179-183.
- Lorenzo Martín, F., Wang, R., and Roth, F., 2002, The effect of input parameters on visco-elastic models of crustal deformation. *Física de la Tierra* **14**, 33-54.
- Menke, W., 1999, Crustal isostasy indicates anomalous densities beneath Iceland. *Geoph. Res. Lett.* **26**, 1215-1218.
- Pedersen, R., Jónsson, J., Árnadóttir, T., Sigmundsson, F., and Feigl, K.L., 2003, Fault slip distribution of two June  $M_w$ 6.5 earthquakes in South Iceland estimated from joint inversion of InSAR and GPS measurements. *Earth Planet. Sci. Lett.* **213**, 487-502.
- Reasenber, P. A. and Simpson, R. W., 1992, Response of regional seismicity to the static stress change produced by the Loma Prieta earthquake, *Science* **255**, 1687-1690.
- Roth, F., 2004, Stress changes modelled for the sequence of strong earthquakes in the South Iceland Seismic Zone since 1706. *PAGEOPH* **161**, 1305-1327.
- Stefánsson, R., Böðvarsson, R., Slunga, R., Einarsson, P., Jakobsdóttir, S., Bungum, H., Gregersen, S., Havskov, J., Hjelme, J. and Korhonen, H., 1993, Earthquake prediction research in the South Iceland Seismic Zone and the SIL project. *Bull. Seism. Soc. Am.* **83**, 696-716.
- Wang, R., Lorenzo Martín, F., and Roth, F., 2003, Computation of deformation induced by earthquakes in a multi-layered elastic crust – FORTRAN programs EDGRN/EDCMP. *Computers & Geosciences* **29**, 195-207.
- Wang, R., Lorenzo Martín, F., and Roth, F., 2005, A semi-analytical software PSGRN/PSCMP for calculating co- and post-seismic deformation in a layered viscoelastic-gravitational half-space, *Computers & Geosciences*, accepted for publication.

## **WP 6.2 Model stress in the solid matrix and pressure in fluids permeating the crust**

**Authors: Maurizio Bonafede and Maria Elina Belardinelli**

### **Objectives**

WP 6.2 addresses three major objectives through theoretical modelling: (1) Modelling of fault complexities in the SISZ employing crack models in layered elastic media (D98); (2) Lithosphere-asthenosphere interaction under the SISZ, taking into account viscoelastic constitutive relationships and intrusive events across rheological discontinuities (D99); (3) Fault instability in the SISZ, taking into account poro-elastic constitutive relationships (D100); (4) triggered seismicity and the interaction between the two large earthquakes of year 2000 in the SISZ (D101). These objectives include interaction with WP 5.1, WP 5.2, WP 5.5, WP 5.6, WP 6, WP 6.1.

### **Methodology and scientific achievements related to workpackages including contributions from partners**

#### **D98 – Original mathematical solutions for crack models in trans-tensional environment**

No further development during last semester.

#### **D99 – Crack models in viscoelastic media**

Previously obtained solutions (PRENLAB project) for elementary dislocations in layered media have been generalized to the viscoelastic case (Maxwell rheology). The solutions (for mode I, II and III dislocations) describe the stress relaxation following fault rupture or fluid-filled intrusion. The expressions have been used to model tensile, dip-slip and strike-slip cracks and analyze the interaction of more realistic structures with layering interfaces.

Results show that homogeneous and inhomogeneous media differ mostly in proximity of the layer interface. There, with a time scale depending on the elastic parameters and on the viscosity, stresses tend to concentrate on the elastic side while relaxing on the viscoelastic one.

In Fig. 1 an example for the crack profile and the evolution of the shear stress on crack plane is shown. The boundary between the elastic and the viscoelastic media is at  $z = 0$ . The instantaneous rigidities of the two media were chosen equal (30 Mpa) in order to enhance the effects of viscosity ( $10^{18}$  Pa s). A stress drop of 3 MPa for  $t = 0$  (solid line in the right panel) causes the opening of an elliptical crack (left panel). After  $t = 2$  months (dotted line) and  $t = 4$  months (dashed line) the stress evolves. For  $z < 0$ , in the viscoelastic domain, stress relaxes. For  $z > 0$ , in the elastic domain, stress increases, with a peak close to the transition boundary. The increase in shear stress is expected to cause a concentration of aftershocks in proximity of the brittle-ductile transition, with a different statistic depending on the distance from it. Spatial and temporal variation of aftershock occurrence could then give information on the rheology of the buried media and on the co-seismic stress drop.

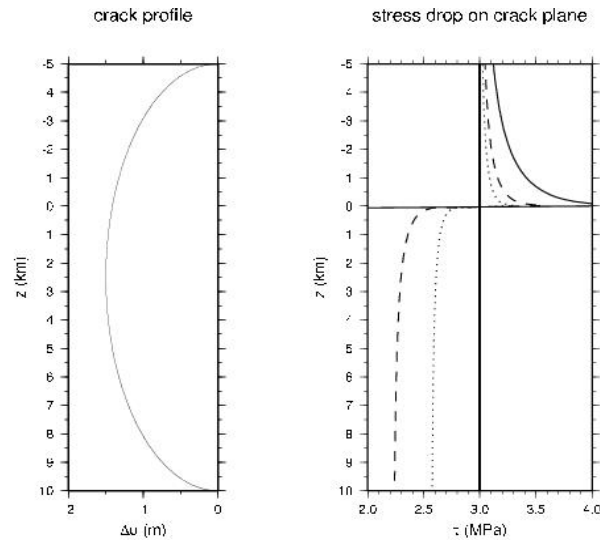


Figure 2. (a) Crack profile for a strike slip fault crossing a layer interface at  $z=0$ . The two media have the same rigidity but the lower one is viscoelastic. (b) Solid line: shear stress for  $t=0$ . Dotted and dashed line: shear stress for  $t = 2$  months and  $t = 4$  months.

## D100 - Crack model in poroelastic media

We analyzed the effects of fluids trapped within deep rocks, which come suddenly into contact with shallower fractured regions, modifying their temperature, pressure, permeability and stress conditions. In particular, we computed the solutions of a set of two coupled equations for heat and pressure transfer in compressible thermo-poro-elastic fluid-saturated media, which become suddenly connected with an hot and pressurized fluid reservoir. The model employed is 1D and it is constituted by a layer  $0 < z < b$ , which, before the connection, has pressures and temperatures characterized by a constant gradient. A reservoir, which occupies the half space  $z < 0$ , characterized by a lithostatic pressure  $P_0$  and a temperature  $T_0$ . At the time  $t=0$  the reservoir is connected with the medium and the fluid migrates upward in response to the overpressure and temperature excess at the boundary. In  $z=b$  pore pressure is kept at the hydrostatic value.

We concentrated our attention on basaltic rocks and on water as the fluid constituent. The fault zone permeability model is assumed to be composed of layers of intact porous rock with a constant intrinsic permeability  $K_r$ , alternated with layers characterized by a periodic distribution of interacting fractures whose opening depends linearly on the overpressure within. The effective permeability of the whole system depends on the pressure and on three geometrical parameters of the model: the horizontal and vertical distances between the centers of two near dislocations  $D$ , and  $d$  and their length  $h$ . During the final semester, we examined the role of parameters appearing in the pressure-dependent permeability model. If the fault zone is fully pervaded by fractures (i.e. if the layers of intact porous rock have vanishing thickness  $d=h$ ), the effective permeability increases, following pressure increase, by orders of magnitude with respect to the intrinsic permeability  $K_r$ : if  $K_r=10^{-16}m^2$  the overpressure causes minor permeability increases; if  $K_r=10^{-17}m^2$ , the effective permeability increases up to 40 times  $K_r$ , over a significant extension of the fault zone; if  $K_r=10^{-18}m^2$ , the increase is up to 400 times over most of the fault zone, and so on. Accordingly, the pressure migration becomes more and more rapid with respect to intact rock.

## CASE IV - $K_r = 10^{-17} \text{ m}^2$ - $d=h$

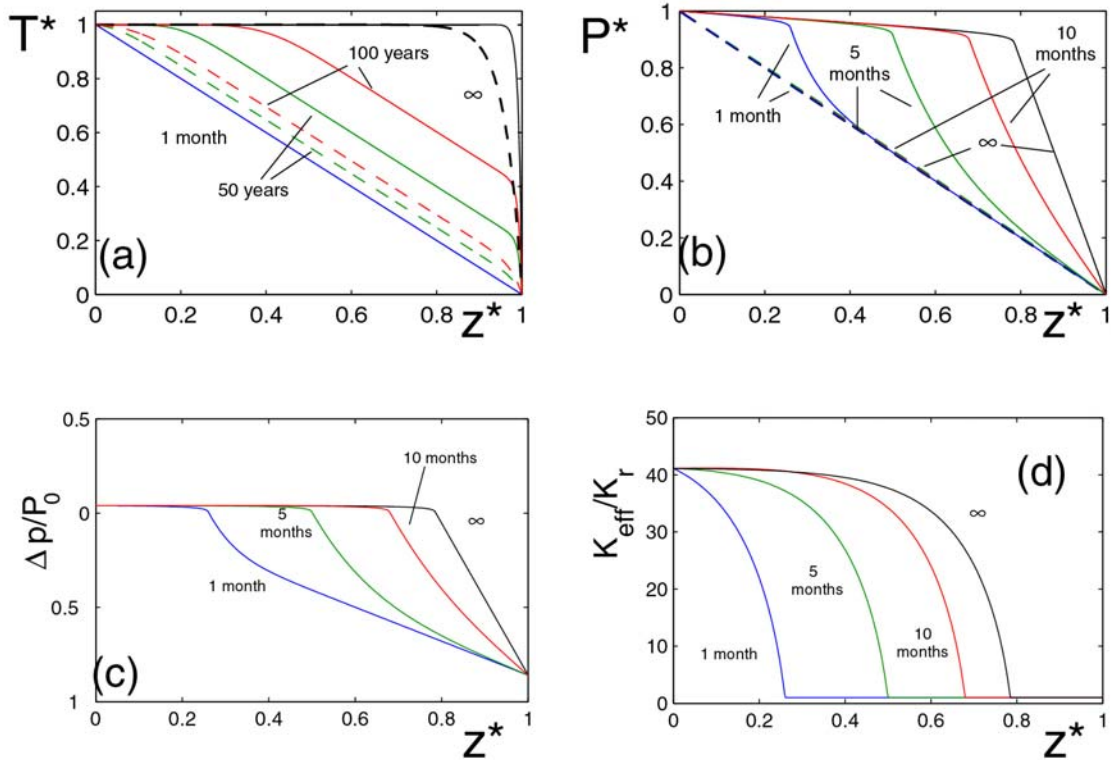


Figure 1. *Temperature (a) and pressure (b) in a fully fractured ( $d = 2l$ ) transition layer of basalt, with thickness  $b = 1 \text{ km}$ , intrinsic permeability  $K_r = 10^{-17} \text{ m}^2$ , assuming uniform-gradient initial conditions. The deviatoric stress is  $10 \text{ MPa}$ . The overpressure within the dislocations (c) brings near lithostatic pore pressure values throughout most of the layer. The effective permeability  $K_{\text{eff}}$  increases up to 40 times  $K_r$ . Parameters of the permeability model:  $D = h = 0.01 \text{ m}$ . Dashed lines in (a) and (b) show the solution for constant permeability. Symbols:  $T^* = T/T_0$ ,  $P^* = P/P_0$ ,  $z^* = z/b$ . CASE IV refers to temperature and pressure conditions thought to be appropriate for the seismogenic depth in the SISZ.*

We considered also the role of the thickness  $b$  of the transition layer: by increasing  $b$  from  $1 \text{ km}$  to  $3 \text{ km}$  the effective permeability increases and near lithostatic pressures pervade the transition layer to a greater extent.

### **D101 - Article and report on triggered seismicity in terms of dynamic fault interaction**

Even at large distance from the epicenter compared to the fault dimension, earthquakes can perturb the state of stress of other seismogenic faults. Our study of two events occurred in the Reykjanes Peninsula at the passage of seismic waves generated by the June 17-th, 2000 earthquake allowed us to investigate conditions for the effect to occur in the framework of a rate- and state- dependent fault rheology assumed for the perturbed faults. We found that low values of effective normal stress can favour this kind of events. More recently, we extended this finding to another early event occurred in near field conditions, for a suitable value of the strike assumed for the perturbed fault. We also verified that conditions to have dynamic triggering at the passage of seismic waves in the location of the two events in the Reykjanes Peninsula are not in contrast with the observed, five

minutes delayed event occurred in the same region, but further away from the mainshock. (Paper submitted for publication on Journal of Geophysical Research).

### **Socio-economic relevance and policy implication**

D98 and D99 – Understanding the detailed processes in which surface fractures develop, in connection with seismic faulting at depth, has important implications for seismic risk analyses in fault regions. Similarly, the role played by viscoelastic relaxation at depth may help understanding the post-seismic evolution of seismicity, particularly in regions with high geothermal gradient, like the SISZ.

D100 – The role played by fluids in the preparatory stage of an earthquake, as described by this modelling, has important implications in understanding the overall seismicity pattern in the SISZ, both in the long term and in the short term, and also provides a conceptual scheme within which precursory  $R_n$  anomalies can be interpreted. In the framework of this model, other hydro-geochemical parameters may be considered to monitor fault regions approaching seismic failure.

D101 – We have verified that earthquakes in the SISZ can trigger other earthquakes even at several tens of kilometres from the mainshock. This is important in order to establish time-dependent probability of future earthquakes. Furthermore, seismic risk studies cannot be based on conventional attenuation laws only.

### **Discussion and conclusion**

**D100** The results obtained from the effective permeability model show that high pore pressure values can efficiently migrate from below the brittle-ductile transition to shallower depths. The effect is more important for rocks characterized by low intrinsic permeability. These solutions show that episodes of fluid migration can increase the pore pressure up to lithostatic values and then decrease substantially the instability threshold of a fault region, with obvious seismogenic implications.

**D101** Our most recent results confirm that a rate- and state-dependent fault rheology is able to explain a wide temporal spectrum of triggering effects and that high pore pressure values in fault regions are in favour of short term triggering, even at large distances from the fault.

### **Plan and objectives for the future**

Collaboration with IMOR, GFZ and IPGP will probably continue beyond the end of the project. Submission of papers concerning the results of this project to peer-reviewed journals. Models obtained in this project will be further developed and applied to other seismic regions, particularly in Italy.

## APPENDIX 1

**Authors: Kurt Feigl and Loïc Dubois**

During this reporting period, CNRS.DTP contributed to the following work packages:

WP	Title	Leader
WP 2.3	Long-term deformation in the South Iceland seismic zone inferred by joint interpretation of GPS, InSAR and borehole strain data	NVI
WP 4.4	Deformation model for the June 2000 earthquakes from joint interpretation of GPS, InSAR and borehole strain data	NVI
WP 6.1	Earthquake probability changes due to stress transfer	GFZ POTSDAM
WP 6.2	Model stress in the solid matrix and pressures in fluids permeating the crust	DF.UNIBO

CNRS.DTP contributed to the deliverables in the work packages listed above, led by other partners. For information on these work packages, please refer to the reports by the leaders of these work packages and the papers cited above.

### **Coupling between hydrological and seismological processes**

We seek to understand how an earthquake can increase seismicity on remote faults. For example, the 1992 Landers earthquake increased seismicity as far away as Yellowstone [Hill, et al., 1993]. The triggering “source” and the triggered “receiver” earthquakes can be separated by distances as large as thousands of kilometers and by time intervals ranging from minutes to months. Although increases in static Coulomb failure stress can explain many triggered events at distances of ~50 km [e.g., King, et al., 1994; e.g., Stein, 1999], they become negligible at larger distances. In contrast, the dynamic stresses generated by seismic waves propagating at ~3 km/s can trigger seismicity at great distances, for example at Wrangell volcano in Alaska after the great Sumatra earthquake of 26 December 2004 [West, et al., 2005]. Yet some earthquakes seem to be triggered by a slower process. For example, one earthquake in Iceland triggered another one 81 hours later on a fault some 16 km distant [Arnadóttir, et al., 2003]. The apparent propagation speed is of the order of 5 km per day, or roughly 5 cm/s, consistent with a rule of thumb that Icelanders have used to explain the impression of “seismicity fronts” moving from east to west across the Southern Iceland Seismic Zone (SISZ).

To evaluate the different processes that underlie these mechanically coupled events, we plot the separation in time and space between source and receiver for each pair of earthquakes found in the literature (Figure 3) and in the Harvard catalog (Figure 4).

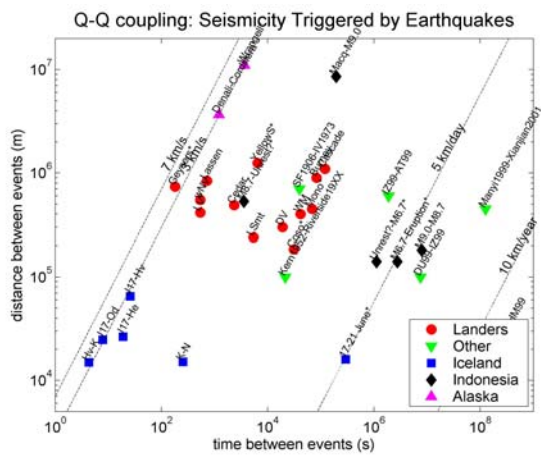


Figure 3. Pairs of triggered earthquakes showing the distance and time between events from the literature. Dashed lines show apparent propagation speeds of P-waves (7 km/s), surface waves (3 km/s), “seismicity fronts” observed in Iceland (5 km/day), and a very slow process (10 km/year). Pairs with asterisks denote pairs with a second, “receiver” event in a volcanic setting. Data from [Hill, et al., 1993; Gomberg, et al., 1998; Gomberg, et al., 2001; Kilb, et al., 2002; Vogfjord, 2003; Vogfjord and Slunga, 2003; Vogfjord and Slunga, 2004; Hjaltadottir, et al., 2005].

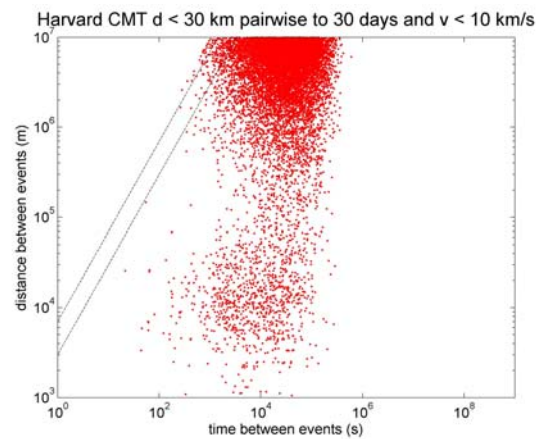


Figure 4. Pairs of earthquakes showing the distance and time between events from the Harvard CMT catalog. Events were selected according the following criteria: depth < 30 km, date between 1997 and 2004, time between events less than 30 days, and apparent propagation speed less than 10 km/s. Dashed lines show apparent propagation speeds of P-waves (7 km/s) and surface waves (3 km/s).

Looking at their apparent propagation speed (in km/s), we see four different categories:

**Slower than 1 km/year.** The only example we could find of such a slow process is the pair formed by the Landers earthquake in 1992 and the Hector Mine earthquake in 1999 that has been attributed to viscous flow in the lower crust and/or upper mantle [Freed and Lin, 2001].

**Faster than 3 km/s.** The few examples in this category occur at distances less than 100 km. These events are probably triggered by the P-wave and/or static stress changes. The standard static Coulomb Failure Criterion seems to provide an adequate explanation.

**About 3 km/s.** The examples in this category show stress transfer at distances over 1000 km. These events are probably triggered by dynamic stresses generated by the Rayleigh wave as it propagates across the receiver fault. Several examples from various tectonic settings have been documented [Hill, et al., 1993; Brodsky, et al., 2000; Gomberg, et al., 2001].

**Slower than 3 km/s.** These pairs of events are not adequately explained by any current model. Either the separation in distance is too long to be explained by static stresses and/or the separation in time is too long to be explained by seismic waves by propagating waves. For example, the Killeifarvartn and Nupshhlidarhals earthquakes (labeled ‘K-N’ in Figure 3) in Iceland were separated by 15 km and 6 minutes [Clifton, et al., 2003; Pagli, et al., 2003; Vogfjord, 2003; Árnadóttir, et al., 2004]. In this case, the earthquake sequence drastically perturbed the hydrological conditions in the surrounding area. The water level in Lake Klevervatn dropped several meters in the months following the earthquake (photo?) as the water flowed out through a fissure (photo?) that presumably opened during one of the earthquakes.

Our current thinking invokes a two-step process to explain this remote triggering. In the first (fast)

step, the seismic wave transfers the stress from the source to the local area around the receiver fault, where it perturbs the hydrological, for example, the pressure of fluids in pores and fissures. In the second (slow) step, fluids flow through the porous media into the nucleation zone of the receiver fault. There, they increase the pore pressure enough to unclamp the receiver fault and trigger a second earthquake. This two-step process can explain both the long length scale and the slow time delay. Since the overall speed is governed by the second, slower (non-linear) process, the apparent rate of propagation is not constant. Indeed, it varies by many orders of magnitude, from  $\sim 100$  m/s to less than  $\sim 1$  mm/s.

## Temporal dependence of aftershocks

Although the poro-elastic model seems to explain deformation observed on time scales of days to weeks, it cannot explain longer time scales. One model that could explain the decay in seismicity over a time scale of 3 years involves brittle creep. Perfettini and his colleagues derive a model of brittle creep in the middle layer of the crust above a subduction zone using rate- and state-dependent friction [Perfettini and Avouac, 2004; Perfettini, et al., 2005]. Similarly, Kato and others simulate post-seismic deformation on a vertical, strike-slip fault with rate- and state- dependent friction overlying a Maxwellian visco-elastic half space [Kato, 2002]. Other studies formulate models along similar lines [Lapusta, et al., 2000; Lapusta and Rice, 2003, 2004]. In its simplest form, rate- and state-dependent friction laws predict a temporal evolution of the form

$$f_{creep}(t) = \frac{c_{creep}}{\log d} \left\{ \log \left[ 1 + d \cdot \left( \exp \left( \frac{t - t_q}{\tau_{creep}} \right) - 1 \right) \right] - \frac{t - t_q}{\tau_{creep}} \right\} \quad (1)$$

where  $c_{creep}$  is a coefficient and  $\tau_{creep}$  is a characteristic relaxation time, of the order of 7 years for Landers. The  $d$  term is an empirical, dimensionless constant that depends on the fault, of the order of  $d \sim 10$  for Landers [Fialko, 2004; Perfettini and Avouac, 2004]. Just after earthquake, at time  $t_q^+$ , the  $f_{creep}$  function has a value of zero. After starting quickly, it reaches 63% of its fully relaxed value at  $t = t_q + 0.5 \tau_{creep}$ . Fitting this function to the time series of the northing coordinate of the continuous GPS station at OLKE, we find a relaxation time of 3 years similar to the decay time for the aftershock seismicity (Figure 5). Although this model reproduces the shape of the time series at one GPS station, it will require additional work to calculate the map of post-seismic deformation recorded by INSAR. Similarly, a curve with the same shape should also fit the temporal evolution of number of aftershocks [Perfettini and Avouac, 2004]. Improving these models is the focus of one of the work packages described below.

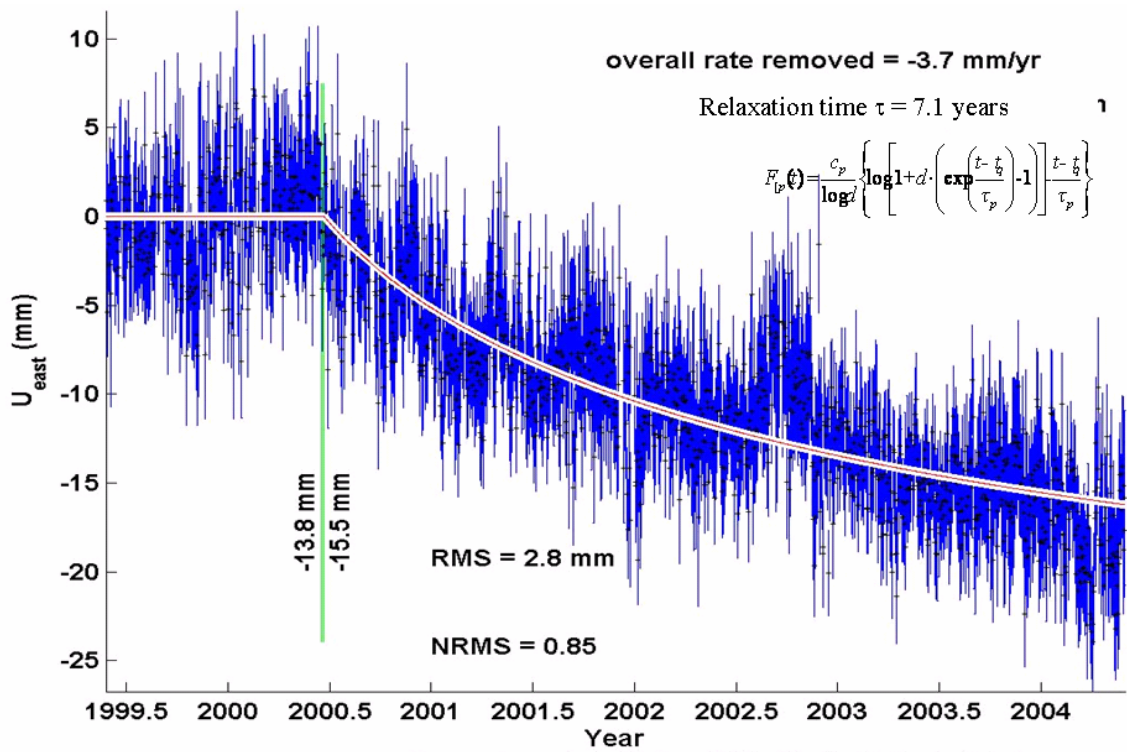


Figure 5. GPS time series for the northing coordinate of station OLKE following the earthquake in June 2000. The curve is described by five parameters: an initial position (arbitrarily set to zero here), two co-seismic offsets at the dates of the earthquakes on 17 and 21 June 2000 (green bars), an overall inter-seismic trend of -3.7 mm/yr (not shown), a relaxation time of 7.1 years and a dimensionless constant  $d = 10$  as described in the text (1) [Dubois, et al., 2005].

## Change in Coulomb failure stress from earthquake of 17 June 2000

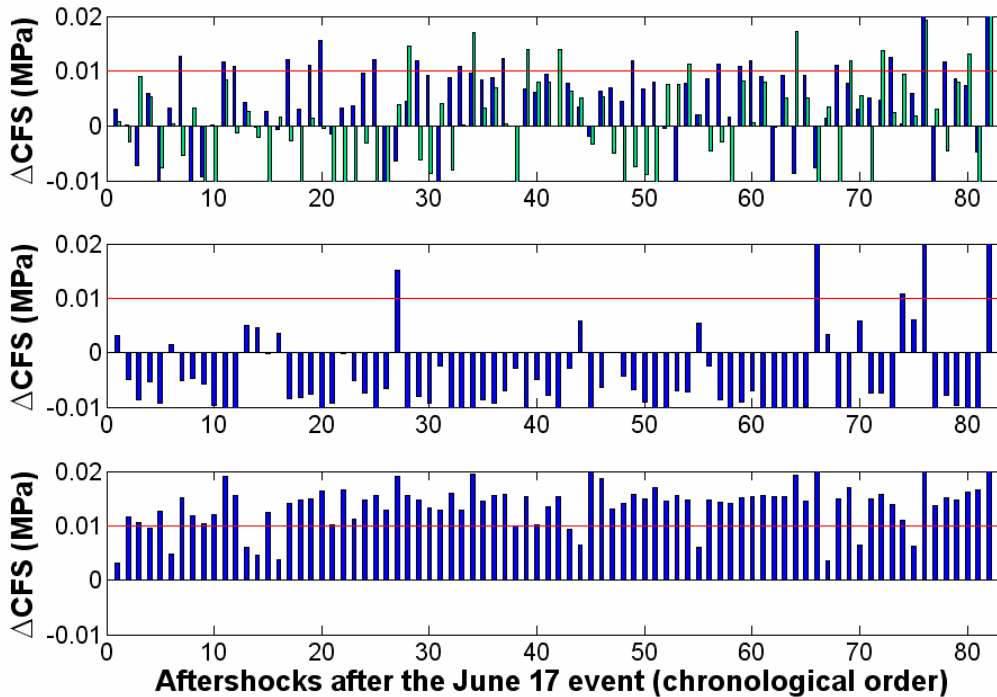


Figure 4. Change in Coulomb Failure Stress (CFS) at the locations of aftershocks between June 17 and June 21, 2000. The last event in the time-ordered series is the June 21 event. The aftershocks have been located by relative relocation method by IMO's scheme, retaining only the events with a fine precision (500 m or less) on the calculated depth. (a) Blue and green bars are the change in CFS calculated on the observed double-couple focal mechanism determined by IMO's scheme. (b) CFS are determined on a right-lateral north-strike vertical fault. (c) CFS are calculated on the optimally oriented fault with a maximum value.

The June 17 event has been simulated with the finite element code TECTON using as input the slip distribution calculated by Pedersen et al. (2003). For this first calculation of the change in Coulomb Failure Stress (CFS) with TECTON, the model for the crust and the mantle is an homogeneous volume ( $\mu = 30$  GPa and  $\nu = 0.28$ ). To use CFS calculations for risk management requires knowing the location (latitude, longitude and depth), orientation (strike and dip), and dimensions (length and width) will. The knowledge of the double focal mechanism is important (Figure 4). Indeed the calculation on a fixed plan or on the optimally oriented fault gives completely different and extreme results. Moreover the change in CFS could be a way to determine the real fault from the double focal mechanism. These results are for the elastic case. The next step to take into account the poro-elastic and other mechanisms for post-seismic deformation. Later, the use of finite element method will enable us to measure the effect of an heterogeneous crust.

## References

- Árnadóttir, T., et al. (2004), Coseismic stress changes and crustal deformation on the Reykjanes Peninsula due to triggered earthquakes on 17 June 2000, *Journal of Geophysical Research (Solid Earth)*, *109*, 09307.
- Arnadottir, T., et al. (2003), Coulomb stress changes in the South Iceland Seismic Zone due to two large earthquakes in June 2000, *Geophys. Res. Lett.*, *30*, doi:10.1029/2002GL016495.
- Brodsky, E. E., et al. (2000), A new observation of dynamically triggered regional seismicity: earthquakes in Greece following the August, 1999 Izmit, Turkey earthquake, *Geophys. Res. Lett.*, *27*, 2741-2744.
- Clifton, A. E., et al. (2003), Surface effects of triggered fault slip on Reykjanes Peninsula, SW Iceland, *Tectonophysics*, *369*, 145-154.
- Dubois, L., et al. (2005), Three-dimensional Finite Element calculations of co- and post-seismic displacement and stress fields for hazard evaluation in the South Iceland Seismic Zone, paper presented at EGU, Vienna.
- Fialko, Y. (2004), Evidence of fluid-filled upper crust from observations of post-seismic deformation due to the 1992 Mw7.3 Landers earthquake, *J. Geophys. Res.*, *109*.
- Freed, A. M., and J. Lin (2001), Delayed triggering of the 1999 Hector Mines earthquake by viscoelastic stress transfer, *Nature*, *411*, 180-183.
- Gomberg, J., et al. (1998), Earthquake triggering by transient and static deformations, *Journal of Geophysical Research*, *103*, 24411-24426.
- Gomberg, J., et al. (2001), Earthquake triggering by seismic waves following the Landers and Hector Mine earthquakes, *Nature*, *411*, 462-466.
- Hill, D. P., et al. (1993), Seismicity remotely triggered by the magnitude 7.3 Landers, California earthquake, *Science*, *260*, 1617-1623.
- Hjaltadóttir, S., et al. (2005), Mapping subsurface faults in southwest Iceland using relatively located microearthquakes, paper presented at EGU General assembly, European Geoscience Union, Vienna.
- Kato, N. (2002), Seismic cycle on a strike-slip fault with rate- and state-dependent strength in an elastic layer overlying a viscoelastic half-space, *Earth, Planets, and Space*, *54*, 1077-1083.
- Kilb, D., et al. (2002), Aftershock triggering by complete Coulomb stress changes, *Journal of Geophysical Research (Solid Earth)*, *107d*.
- King, G. C. P., et al. (1994), Static stress changes and the triggering of earthquakes, *Bull. Seism. Soc. Amer.*, *84*, 935-953.
- Lapusta, N., and J. R. Rice (2003), *J. Geophys. Res.*, *108*.
- Lapusta, N., and J. R. Rice (2004), Earthquake Sequences on Rate and State Faults With Strong Dynamic Weakening, paper presented at AGU Fall Meeting Abstracts, December 1, 2004.

- Lapusta, N., et al. (2000), Elastodynamic analysis for slow tectonic loading with spontaneous rupture episodes on faults with rate- and state-dependent friction, *J. Geophys. Res.*, *105*, 23765 - 23790.
- Pagli, C., et al. (2003), Triggered aseismic slip on the Reykjanes Peninsula, Iceland captured by radar interferometry, *EGS - AGU - EUG Joint Assembly, Abstracts from the meeting held in Nice, France, 6 - 11 April 2003*, abstract #6434, 6434.
- Pedersen, R., et al. (2003), Fault slip distribution of two  $M_S=6.6$  earthquakes in South Iceland from joint inversion of InSAR and GPS, *Earth Planet. Scien. Lett.*, *213*, 487-502.
- Perfettini, H., and J.-P. Avouac (2004), Postseismic relaxation driven by brittle creep: A possible mechanism to reconcile geodetic measurements and the decay rate of aftershocks, application to the Chi-Chi earthquake, Taiwan, *J. Geophys. Res.*, *109*, B02304, doi:02310.01029/02003JB002488.
- Perfettini, H., et al. (2005), Geodetic displacements and aftershocks following the 2001,  $M_w = 8.4$  Peru earthquake: Implications for the mechanics of the earthquake cycle along subduction zones, *J. Geophys. Res.*, *in press*.
- Stein, R. S. (1999), The role of stress transfer in earthquake occurrence, *Nature*, *402*, 605-609.
- Vogfjord, K. (2003), Triggered Seismicity after the June 17,  $M_w=6.5$  Earthquake in the South Iceland Seismic Zone: The first five minutes, *EGS - AGU - EUG Joint Assembly, Abstracts from the meeting held in Nice, France, 6 - 11 April 2003*, abstract #11251, 11251.
- Vogfjord, K., and R. Slunga (2003), Rupture in the South Iceland Seismic Zone forced by magmatic intrusion in the Hengill area, *EGS - AGU - EUG Joint Assembly, Abstracts from the meeting held in Nice, France, 6 - 11 April 2003*, abstract #9685, 9685.
- Vogfjord, K. S., and R. Slunga (2004), Fault Mapping in the Hengill Region, SW Iceland by Joint Interpretation of Microearthquake Distribution and Collective Focal Mechanisms, *AGU Fall Meeting Abstracts*, *51*, 05.
- West, M., et al. (2005), Periodically Triggered Seismicity at Mount Wrangell, Alaska, After the Sumatra Earthquake, *Science*, *308*, 1144-1146.

## APPENDIX 2

Author: Grímur Björnsson, Iceland Geosurvey

### Introduction

The following short report describes televiwer logging activities, carried out by Iceland Geosurvey (Ísor) on the behalf of University of Göttingen, Germany. The logging is a part of the EU-PREPARED contract where University of Göttingen is one of the primary partners. The logging was carried out in a few wells in the S-Iceland seismic zone, and in three wells in the vicinity. Isor was namely able to integrate the PREPARED logging activities into other projects in the area, thereby generating more well logs than initially anticipated. Figure 1 show location of wells where televiwer logging took place. Two wells are still pending, in Kaldárholt and Thykkvibaer.

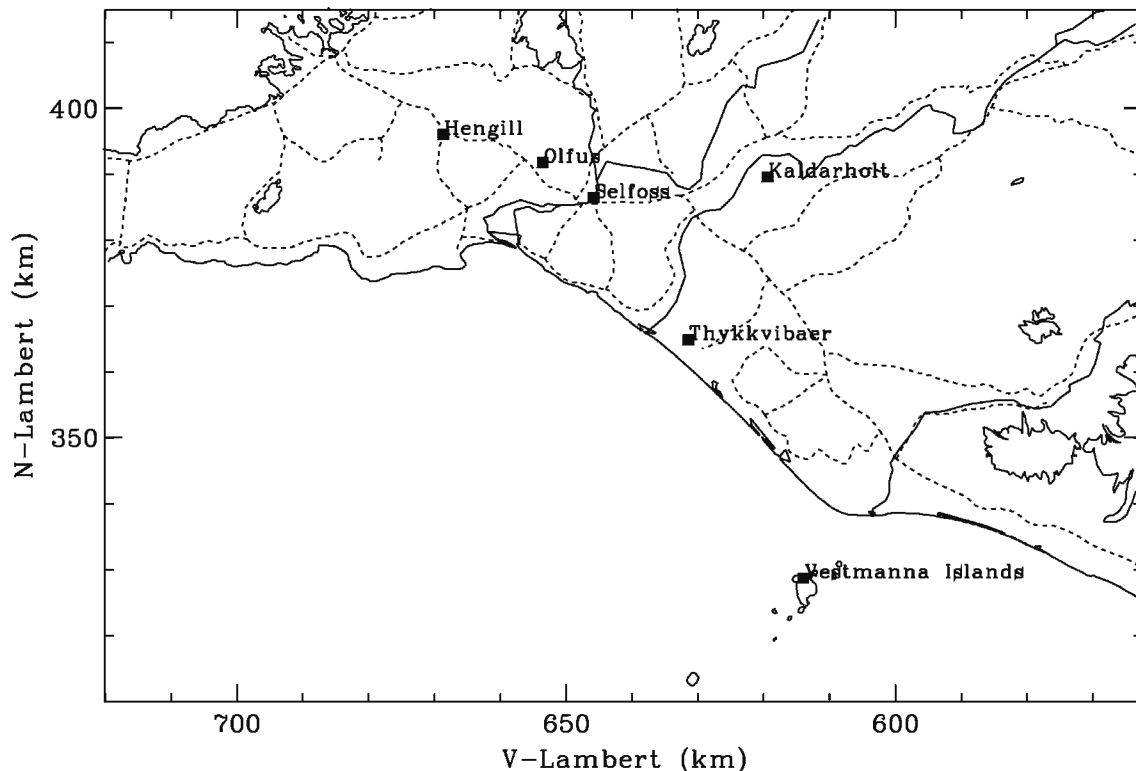


Figure 6. Well sites in and near the S-Iceland seismic zone where televiwer images have been collected.

The televiwer applied is made by Robertson Geologging. Tool is acoustic and images wells by frequent sound ticks and a rotating mirror in tool nose. The DSP chip of tool measures first arrival time of each sound pulse and its attenuation. Up to 360 shots are possible for one revolution of the mirror and mirror makes 3-6 revolutions per second. Tool is therefore able to image wellbores at high resolution but downside is then slow logging speed (1-3 m/min). Another obstacle in the logging has to do with well temperatures. By default, Robertson manufactures tools with 70 °C maximum tolerance. At this temperature exiting features arise in well images, in particular tensile fractures along the wellbore. These orientate parallel to the direction of maximum principal stress and are generated by cooling stresses during drilling. Isor has cooperated with Robertson to upgrade the tool temperature limit to 100 °C. This caused a delay in the logging activities but in return allowed for deeper logs in the S-Iceland seismic zone than initially considered possible in this project.

## Scope of work and progress

The scope of the present work was defined in the subcontract between Isor and University of Göttingen as:

Acquisition of new field data, by operating a logging truck, a televiewer and 2 logging specialists in wells within the South-Iceland seismic zone. The wells in question are the same as have been monitored previously for waterlevel changes after the two large quakes. By carefully studying these wells, we hope to retrieve information on the nature of well feedzones (fractures/interbeds), detect tensile fracturing originated from cooling, thus determining the greatest horizontal stress at the time of drilling, and check for the existence and orientation of well breakouts.

Interpretation of the new field data: Determine dip and strike of existing fractures, interbeds, tensile fractures and breakouts in the wells. Correlate this data to the existing well data-base of Isor, in order to better define conceptual models of the hydrothermal reservoirs in question. Summarize the new information into tables and maps, such as orientation of the horizontal stress field in the South Iceland seismic zone.

Combine the hydrological data, collected after the two quakes, to the nature of well feedzones. Come up with an estimate of the immediate hydraulic response of wells due to stress changes induced by the two quakes. Tabulate these data and make available to those who model numerically the source mechanism of the quakes. These data will serve as a constraint to the source mechanism models.

Discuss/synchronize the results from above with other participants in the Prepared project.

At this point in time, the bulk of the work has been completed, i.e. collection of field data. One day of field work is though still ahead, where a brand new well in Kaldarholt will be imaged and orientation of possible cooling fractures compared to the orientation logged in nearby wells, drilled prior to the year 2000 quakes in S-Iceland. Preliminary on-site interpretation also has been carried out and interesting features in well images correlated with possible feedzones and fractures in wells. For example we observe that most feedzones correlate with steeply dipping fractures in the bedrock. Table 1 gives an overview of the logging activities carried out for Prepared and also some local district heating companies in the region.

Table 4. *Overview of televiewer logging activities.*

Well ID	Well name	Logging depth (m)	Logging date	Location
73381	HB-01	1425	2003-01-20	Vestmanna islands
73417	HH-08	1700	2005-04-14	Vestmanna Islands
83323	KH-34	441	2005-03-22	Kaldarholt
83324	KH-35	538	2005-03-21	Kaldarholt
97251	SO-01	723	2005-03-22	Sog, Olfus
96591	HN-01	1100	2005-05-04	Hengill, Threngsli
87439	HT-10	600	2005-05-04	Selfoss
Total	7 wells	6500 m		

## Continuation of work

The televiewer imaging data available at present provide a comprehensive data base on features in wells that relate to stress field and faulting history of the S-Iceland seismic zone. Bulk of the project is near completion and awaits only drilling of a new well that makes comparison of pre- and post-quake stress fields possible. Interpretations consists of replotting the image data and determine dip and strike of faults and interbeds seen in well images. The interpretation has already been initiated.

For example the Kaldarholt data has been given to a student of the United Nations University Geothermal Training Programme in Iceland. Isor is also building expertise at its Akureyri subdivision. Finally, experience gained during project helped in making the STREP proposal HITI that was submitted to EU recently and focuses on the development of high temperature logging tools.

## APPENDIX 3

### SIL Data Status Report

**Authors: Gunnar B. Guðmundsson, Kristín S. Vogfjörð and Bergþóra S. Þorbjarnardóttir**

#### Outline of SIL history

The SIL seismic system was designed and installed in the South Iceland Lowland in 1989-1990 and was fully operational in automatic mode in June 1991. In 1994 the system was expanded to the northeastern part of Iceland and has been gradually covering larger parts of Iceland since 1996 (see Appendix 4.1). During 1991-2000 some 170,000 events were recorded and processed.

#### Data Processing

All waveform file headers, 2.303.129 in all, were checked and corrected where necessary. The events were then reanalyzed with the latest version of the focal mechanism programs. This version still underestimates magnitudes of events greater than  $M_{lw} = 4$ . Some doublets may still remain in the data, but known explosions have been removed.

In some instances -9.99 may appear in the magnitude columns of data from the initial years. This signifies that no waveform data was found. In future releases some of these events may be eliminated.

#### SIL data files

Table 1: SIL data files

SIL data file	Format	Number of eq	Delivery date
1991_07-1995_12.v01m	m	46150	May 2003
1991_07-1995_12.v00f	f	46119	May 2003
1996_01-1996_12.v01m	m	16276	August 2003
1996_01-1996_12.v01f	f	16275	August 2003
1997_01-1997_12.v01m	m	~ 37142	September 2003
1997_01-1997_12.v01f	f	~ 37142	September 2003
1998_01-1998_12.v01m	m	~ 33542	September 2003
1998_01-1998_12.v01f	f	~ 33542	September 2003
1999_01-1999_12.v01m	m	13980	August 2003
1999_01-1999_12.v01f	f	13978	August 2003
2000_01-2000_12.v01m	m	23482	August 2003
2000_01-2000_12.v01f	m	23469	August 2003

Detection thresholds have varied through the time of network operation and sometimes during major earthquake swarms, they have been increased in order to enable the system to keep up. This occurred for example in the year 2000 earthquake swarms, between June 20 and September 1. This of course decreased the number of detected events.

## Appendix

### SIL stations

Table 2: SIL station history

Station id	Latitude degrees	Longitude degrees	Elevation km	Up yyyy-mm-dd	Down yyyy-mm-dd
bj hau gyg sau hei mid	63.94590 63.96851 64.28107 63.98983 64.19978 63.65833	-21.30258 -19.96471 -20.21483 -20.41519 -21.23604 -19.88573	0.057 0.072 0.119 0.074 0.162 0.132	1989-08-15 1989-12-08 1989-12-10 1989-12-12 1989-12-13 1989-12-21	
asm sol	63.83361 63.92896	-20.61474 -20.94357	0.022 0.030	1990-01-03 1990-01-03	
aku	65.68611	-18.09950	0.024	1991-10-06	1994-11-22
skh kri	63.45347 63.87810	-19.09453 -22.07646	0.070 0.146	1992-08-28 1992-11-05	2003-01-29
snb gra gil lei sig gri	63.73637 65.91760 66.07734 66.40665 66.13229 66.54152	-18.63068 -17.57855 -16.35131 -16.48957 -18.91483 -18.00951	0.245 0.024 0.134 0.041 0.010 0.036	1993-02-10 1993-10-21 1993-10-23 1993-10-24 1993-10-26 1993-12-08	
asb hla	64.74818 65.94441	-21.32535 -18.38724	0.094 0.037	1994-08-01 1994-11-24	
kra grs kud hve hrn skr kro san kal ren	65.69474 65.63811 64.32059 64.86979 66.11000 64.56014 64.09806 64.05601 63.94761 65.64699	-16.77783 -16.12409 -21.87472 -19.56661 -20.12252 -18.38647 -21.11976 -21.57013 -17.68698 -16.90591	0.437 0.378 0.028 0.640 0.015 0.858 0.147 0.208 0.078 0.338	1996-02-13 1996-02-15 1996-06-26 1996-08-29 1996-08-30 1996-10-01 1996-10-08 1996-10-14 1996-10-19 1996-11-03	1996-11-01
haf nyl grv vog vos	64.04257 63.97368 63.85716 63.96967 63.85279	-21.91870 -22.73792 -22.45583 -22.39285 -21.70357	0.070 0.007 0.052 0.007 0.008	1997-01-16 1997-02-06 1997-02-23 1997-02-23 1997-04-12	2000-06-21 2003-01-30
vat sva ada	64.18664 65.33691 65.01879	-18.91768 -17.25454 -15.57452	0.573 0.403 0.443	1998-04-20 1998-07-14 1998-09-09	

Table 2: SIL station history

Station id	Latitude degrees	Longitude degrees	Elevation km	Up yyyy-mm-dd	Down yyyy-mm-dd
fag	63.87478	-16.65364	0.027	1999-05-06	
hvo	63.52610	-18.84781	0.196	1999-10-19	
hed	66.08080	-17.30975	0.075	2000-09-25	
na	66.16069	-17.84750	0.013	2000-11-08	
bre	66.12336	-17.90967	0.041	2000-11-17	
grf	64.40656	-17.26713	1.710	2001-05-10	
esk	63.52503	-19.45080	0.095	2001-10-04	
kvo	65.71392	-16.88130	0.572	2003-06-23?	

**m-format**

Table 3: m-format

Columns	Remark
1- 8	Date of event in yyyyymmdd
10-19	Origin time of event in hhmmss.sss
20-28	Latitude of event in degrees
29-38	Longitude of event in degrees
40-45	Depth of event in km
47-51	Local magnitude $M_{lw}$ calculated from seismic moment according to (1)
53-57	Local magnitude $M_l$ calculated from amplitude and distance according to (2)
59-60	Number of stations supplying arrival times
62-63	Number of P arrival time picks
65-66	Number of S arrival time picks
69-70	Number of polarities
73-76	Accuracy in origin time, in seconds
78-82	Accuracy in latitude, in degrees (1 std. dev. confidence interval)
84-88	Accuracy in longitude, in degrees (1 std. dev. confidence interval)
92-94	Accuracy in depth, in kilometers (if =0.0, then depth is fixed)
98-101	rms error of time residuals in arrival time picks, in seconds
104-108	Smallest distance to recording station, in kilometers
110-114	Largest azimuthal gap between recording stations, in degrees
116	Velocity model used in location (1=SIL, 2=Northern, 3=Iceland)

(1)	$m = \log_{10}(M_o) - 10$		
	$M_{lw} = m$	if	$M_{lw} \leq 2.0$
	$M_{lw} = 2.0 + (m - a) * 0.9$	if	$2.0 < M_{lw} \leq 3.0$
	$M_{lw} = 3.0 + (m - a - b) * 0.8$	if	$3.0 < M_{lw} \leq 4.6$
	$M_{lw} = 4.6 + (m - a - b - c) * 0.7$	if	$4.6 < M_{lw} \leq 5.4$
	$M_{lw} = 5.4 + (m - a - b - c - d) * 0.5$	if	$5.4 < M_{lw} \leq 5.9$
	$M_{lw} = 5.9 + (m - a - b - c - d - e) * 0.4$	if	$5.9 < M_{lw} \leq 6.3$
	$M_{lw} = 6.3 + (m - a - b - c - d - e - f) * 0.35$	if	$6.3 < M_{lw}$

$a = 2,$	$b = 1/0.9,$	$c = 1.6/0.8,$	$d = 0.8/0.7,$	$e = f = 1$
----------	--------------	----------------	----------------	-------------

For reference see:

Ragnar Slunga, Peter Norrman, Ann-Christine Glans, 1984: Seismicity of Southern Sweden. - Stockholm : Försvarets Forskningsanstalt, July 1984. - 106 p. (FOA report ; C2 C 20543-TI).

Fig. 3 page 79: The theoretical  $M_L$  (Wood-Anderson) –  $M_O$  relation adjusted vertically to fit the  $M_L(W)$  estimates of the earthquakes 1979–81 studied by Slunga (1982).

**Note: Seismic moment of events  $\geq 4$  may be severely underestimated.**

(2)	$M_l = \log_{10}(amp) + 2.1 * \log_{10}(dist. - in - km) - 4.8$
-----	---

where amplitude is estimated in a 10 second window around the S arrival.

**f-format**

Table 4: f-format

Columns	Remark
1- 8	Date of event in yyyyymmdd
10-19	Origin time of event in hhmmss.sss
20-28	Latitude of event in degrees
29-35	Latitude error in degrees
36-45	Longitude of event in degrees
46-52	Longitude error in degrees
53-60	Depth of event in km
61-66	Depth error in km
67-73	Local magnitude $M_{lw}$ calculated from seismic moment according to 4.2(1)
74-79	Corner frequency in Hz
80-84	Fault radius in m
85-91	Stress drop in Mpa
92-99	Peak slip in mm
100-104	Strike - plane a
105-109	Dip - plane a
110-114	Slip - plane a
115-119	Strike - plane b
120-124	Dip - plane b
125-129	Slip - plane b
130-133	Polarity number
134-138	Number of amplitudes used
139-145	Percentage of all mechanisms which are acceptable